Universitat Politècnica de València

Departamento de Comunicaciones

Doctoral Thesis

Microwave Filters in Planar and Hybrid Technologies with Advanced Responses

Sandra Marín Martínez

Advisors

Dr. Jorge D. Martínez Pérez (Universitat Politècnica de València)
Dr. Vicente E. Boria Esbert (Universitat Politècnica de València)

September 2022, Valencia

Thesis submitted to the Departamento de Comunicaciones,
in partial fulfillment of the requirements for:
Título de Doctor en Ingeniería de Telecomunicación
por la Universitat Politècnica de València.

Resumen

La presente tesis doctoral tiene como principal objetivo el estudio, diseño, desarrollo y fabricación de nuevos dispositivos pasivos de microondas, tales como filtros y multiplexores con respuestas avanzadas para aplicaciones de alto valor añadido (i.e. comerciales, militares, espacio); orientados a distintos servicios, actuales y futuros, en sistemas inalámbricos de comunicación.

Además, esta investigación se centrará en el desarrollo de filtros encapsulados de montaje superficial y con un elevado grado de miniaturización. Para ello, se propone investigar distintas técnicas que consigan respuestas muy selectivas o con unas características exigentes en rechazo (mediante la flexible introducción de ceros de transmisión), así como una excelente planaridad en banda (aplicando técnicas tales como la mejora del Q o el diseño de filtros con pérdidas, *lossy filters*), obteniendo de este modo respuestas mejoradas, con respecto a soluciones conocidas, en los componentes de microondas desarrollados.

De forma general, la metodología seguida se iniciará con una búsqueda y conocimiento del estado del arte sobre cada uno de los temas que se acometerán en esta tesis. Tras ello, se establecerá un procedimiento de síntesis que permitirá acometer de forma teórica los objetivos y especificaciones a conseguir en cada caso. Con ello, se establecerán las bases para iniciar el proceso de diseño, incluyendo co-simulación circuital/electromagnética y optimización que permitirán, en última instancia, implementar la solución planteada en cada caso de aplicación concreto.

Finalmente, la demostración y validez de todas las investigaciones realizadas se llevará a cabo mediante la fabricación y caracterización experimental de distintos prototipos.

Resum

La present tesi doctoral té com a principal objectiu l'estudi, disseny, desenvolupament i fabricació de nous dispositius passius de microones, com ara filtres i multiplexors amb respostes avançades per a aplicacions d'alt valor afegit, (comercials, militars, espai); o-rientats a oferir diferents serveis, actuals i futurs, en els diferents sistemes sense fils de comunicació.

A més, aquesta investigació es centrarà en el desenvolupament de filtres encapsu-lats de muntatge superficial i amb un elevat grau de miniaturització. Per a això, es proposa investigar diferents tècniques que aconsegueixin respostes molt selectives o amb unes característiques exigents en rebuig (mitjançant la flexible introducció de zeros de transmissió), així com una excel·lent planaritat en banda (aplicant tècniques com ara la millora de l'Q o el disseny de filtres amb perdues, *lossy filters*), obtenint d'aquesta ma-nera respostes millorades, respecte solucions conegudes, en els components de microones desenvolupats.

De forma general, la metodologia seguida s'iniciarà amb una recerca i coneixement de l'estat de l'art sobre cadascun dels temes que s'escometran en aquesta tesi. Després d'això, s'establirà un procediment de síntesi que permetrà escometre de forma teòrica els objectius i especificacions a aconseguir en cada cas. Amb això, s'establiran les bases per iniciar el procés de disseny, amb co-simulació circuital / electromagnètica i optimització que permetran, en última instància, implementar la solució plantejada en cada cas d'aplicació concret.

Finalment, la demostració i validesa de totes les investigacions realitzades es durà a terme mitjançant la fabricació i caracterització experimental de diferents prototips.

Abstract

The main objective of this doctoral thesis is the study, design, development and manufacture of new passive microwave components, such as filters and multiplexers with advanced responses for comercials, military and space applications; oriented to offer different services, in current and future wireless communication systems.

In addition, this research will focus on the development of surface-mounted encapsulated filters with a high degree of miniaturization. With this purpose, it is proposed to investigate different techniques that achieve highly selective responses or with demanding characteristics in rejection (through the flexible introduction of transmission zeros), as well as an excellent in-band planarity (applying techniques such as the Q enhancement or lossy filters), thus obtaining improved responses, with respect to known solutions, in the developed microwave components.

In general, the followed methodology will begin with a search and knowledge of the state of the art on each of the topics addressed in this thesis. After that, a synthesis procedure will be established, which will allow the achievement of the objectives and specifications in a theoretical way, for each case. With this, the bases will be established to start the design process, with circuital and electromagnetic co-simulations and optimizations that will allow, ultimately, to implement the proposed solution, in every application case, specifically.

Finally, the demonstration and validity of all the investigations will be carried out through the manufacture and experimental characterization of different prototypes.

Contents

5 Conclusions and Future Work   137

A Publications list   143

Bibliography   145

Figure list

Table list

Acronyms

5G	Fifth-Generation.
BW	Bandwidth.
CPWG	Coplanar Waveguide with Lower Ground Plane.
EM	Electromagnetic.
f0	Center Frequency.
FBW	Fractional Bandwidth.
HPF	HighPass Filter.
IL	Insertion Losses.
IMUX	Input Multiplexer.
LPF	LowPass Filter.
LTE	Long Term Evolution.
MUX	Multiplexer.
NRN	Non-Resonating Nodes.
OMUX	Output Multiplexer.
RF	Radio Frequency.
RL	Return Losses.
RCCs	Resistive Cross-couplings.
SIW	Substrate Integrated Waveguide.
SMD	Surface Mounted Device.
SRF	Self Resonance Frequency.
Q	Quality factor.
Qu	Unloaded Q factor.
TZs	Transmission Zeros.

Chapter 1

Introduction

1.1 Motivation

In recent years, wireless communication systems have experienced an important growth and development. This fact has resulted in very demanding requirements and designs for the radio frequency (RF) and microwave devices, being filters one of the key components.

The function of the filter is basically to provide a perfect transmission within a frequency band (i.e. passband) and an infinite attenuation in the rest of the frequencies (i.e. rejection band). Naturally, this behavior is an idealization and any real filter will have deviations related to the use of real components for its implementation. Thus, the wide and high-suppression stopband will be an important requirement in filter design within microwave and RF systems. However, this is hard to achieve due to the inherent higher-order modes of the microwave resonator, which introduces undesired spurious passbands in the stopband and thus, deteriorating the stopband performance. At the same time and despite this, certain applications, such as satellite communications, require filters with specific and stringent characteristics in terms of frequency rejection. An example of this is observed in the filters that surround non-linear devices (e.g. mixers, power amplifiers, etc.), in which their rejection responses have to present high levels of attenuation in a wide range of frequencies out of the filter's passband, in order to eliminate unwanted interferences and generated noise.

Furthermore, microwave filters are present in all applications that share resources in the electromagnetic spectrum. The electromagnetic spectrum is limited and its progressive saturation, together with the development of increasingly sophisticated RF applications,

leads to the demand for microwave circuits with advanced features. Therefore, the current situation requires to obtain highly selective filtering responses to efficiently eliminate noise and potential interfering signals from other services very close in frequency.

In this way, the need to reject certain frequencies leads to the development of filters whose responses exhibit transmission zeros (TZs) at finite frequencies [1], [2]. The TZs, conveniently located in frequency, make it possible to cancel out unwanted signals effectively. In addition, this type of design provides high selectivity and good rejection outside the passband, allowing, for example, a better use of the electromagnetic spectrum (see Figure 1.1) by placing TZs close to the cutoff frequencies of the filters; or to achieve ultra-wide rejection bands (see Figure 1.2), in this case strategically positioning the zeros (location of spurious) within the rejection band of the filter.
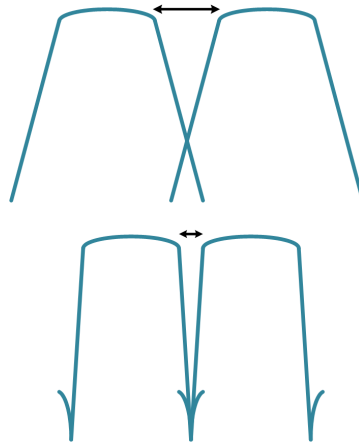
Figure 1.1: Better use of the spectrum by reducing guard bands between channels.
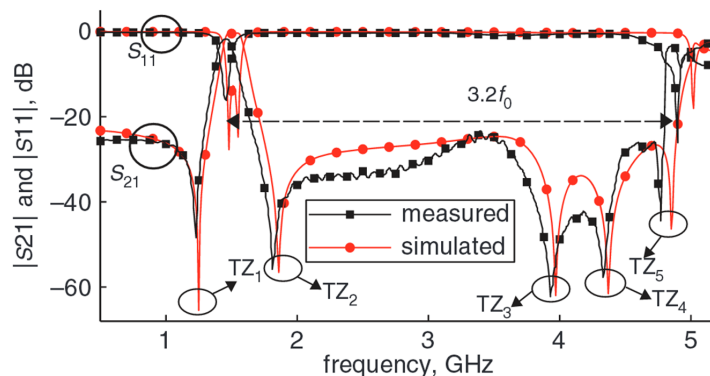
Figure 1.2: Improvement of the rejection band of a bandpass micrsotrip filter by suppressing harmonics [2].

On the other hand, the passband, which allows the transmission of their frequencies, will also require a series of conditions (low losses, planarity, etc.) for the correct

performance of the filter. However, in modern communication systems, miniaturization, compaction and integration of components are pursued together with cost reductions, turning difficult to obtain a high quality factor, Q, at the same time. According to this commitment, new challenges are posed to lower the manufacturing cost and achieve miniaturization and compact devices, while maintaining optimal levels of electrical performance. For this purpose, planar and hybrid solutions become of great interest, as well as integrated components such as multiplexers.

Nonetheless, losses are inevitable due to the material properties used in the practical realization of the components. Therefore, in order to have a high performance filer response, the Q factor should be maximized either by means of techniques to reduce losses, which usually result in larger devices, that can be tolerated in certain applications; or by means of lossy techniques [3]. The latter ones provide a filtering response equivalent to a high Q filter shape using low Q resonators, increasing in this case the absolute insertion losses (IL), which can also be compensated by an amplifier.

Due to the increasing interest on this type of filter features, the development of techniques for the enhancement of both, the passband and the out of band responses is quite interesting and useful. In this manner a simple, multifunctional method, applicable to different topologies and structures for the introduction of transmission zeros is proposed, as well as different solutions for the improvement of the passband characteristics in a filter. In addition, the degree of flexibility in the described techniques in this work allows the tuning capacity easily, which is very promising and attractive for new applications (e.g. 5G, LTE, satellite payloads) that demand the integration and coexistence of multi-standard or multiband operations in a single device. They will provide more functionality, higher efficiency and flexibility in frequency spectrum usage.

All these mentioned aspects have caused a growing interest in the development of high frequency filters and components with improved and advanced responses for RF and microwave applications, being this the framework of this doctoral thesis.

1.2 State of the Art

In this section, the state of the art of three main topics related to the work that has been performed in this thesis is going to be presented. Firstly, a review about different solutions, in planar technologies, to obtain filters with wide stopbands is described. Then, an overview of the design of filters with TZs and pseudo-elliptic responses is presented. And finally, an outline of the bibliography related with techniques for implementing advanced filtering responses is provided.

1.2.1   Filters with Wide Stopbands

The rejection band characteristics of a filter are of vital importance in certain applications. A wide spurious-free band with good attenuation levels is a typical requirement in bandpass filters designs, used for example in frequency conversion applications with image frequency rejection in satellite communications. These filters are also needed for the correct operation of components such as diplexers or multiplexers for Small User Terminals, where reception and transmission channels are far apart in frequency, and the spurious responses of the low-frequency channels can disturb the proper performance of these devices. To meet these requirements, and improve the out-of-band response, several techniques can be found in the literature.

The use of some well-known topologies such as the interdigital topology or the combline structure allow to improve the filer's out of band response regarding to another conventional structures (e.g. hairpin filter in Figure 1.3). The interdigital topology presents spurious resonances only at odd multiples of the center frequency, f_0, (Figure 1.3). In the case of combline structures by reducing the length of the resonator, the first spurious band can be shifted away from the passband. However, by using these structures exclusively, it is not possible to achieve the requirements demanded in the aforementioned applications.
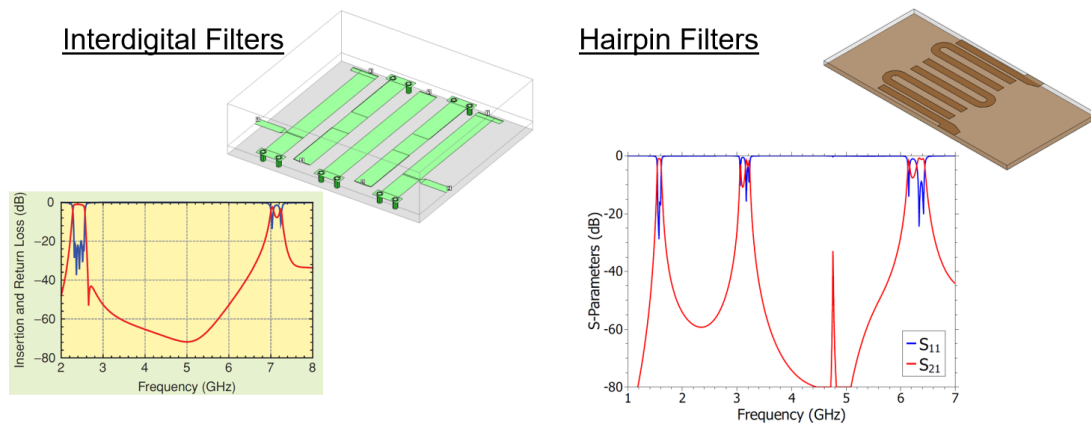
Figure 1.3: Spurious resonances in well-known bandpass filter microstrip topologies. Left: Interdigital bandpass filter structure centered at 2.44 GHz, the spurious passband at roughly $3 \cdot f_0$ [4]. Right: Hairpin bandpass filter structure centered at 1.575 GHz, the spurious passband at roughly $2 \cdot f_0$.

Other proposed solutions consist on modifying the filter structure integrating lowpass [5] or bandstop [6] responses, as seen in Figure 1.4. The basic idea consists of introducing lowpass structures within bandpass topologies. By adjusting lowpass filter cutoff frequencies, harmonic resonances are attenuated, while maintaining in-band performances. The same idea is developed in [6] but including bandstop structures integrated
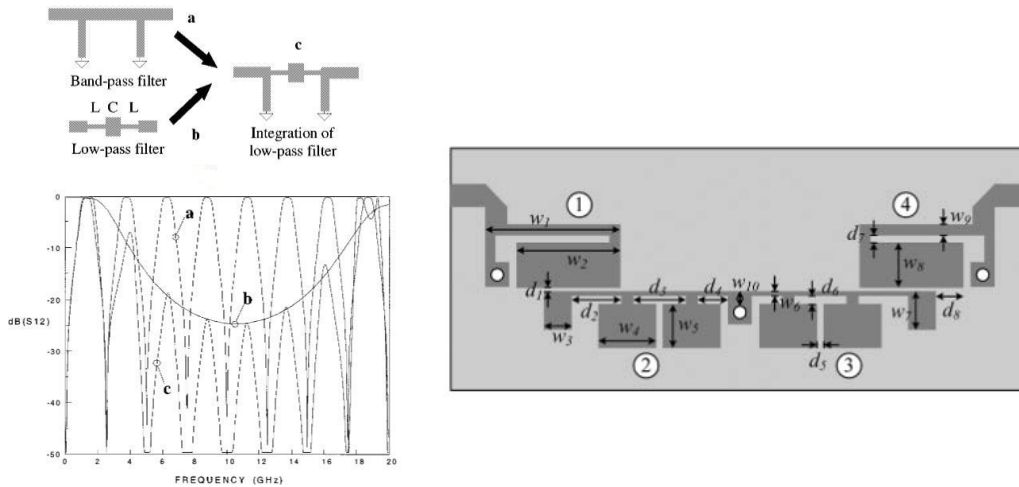
Figure 1.4: Modification of the bandpass filter structure integrating lowpass or bandstop responses: Left: semi-lumped lowpass filter cells into a $\lambda/4$ shunt-stubs bandpass topology [5]. Right: bandstop filter cells into a $\lambda/4$ length stepped impedance bandpass topology [6].

with a bandpass stepped-impedance topology. In [7] the method proposed is based on electromagnetic band-gap concepts and coupled-mode theory in non-uniform periodic structures featuring a sinusoidal perturbation. By applying a continuous modulation pattern to the coupled-line sections following a sinusoidal law, the undesired spurious passband can be eliminated providing the perturbation period is properly adjusted.

Other proposals, however, consist on loading parallel coupled-line filters [8], open-loop structures [9], or cascaded LPF-HPF type wideband bandpass filters [10] with open-stubs, where the high-order harmonic frequencies are suppressed by choosing different stub lengths (Figure 1.5).
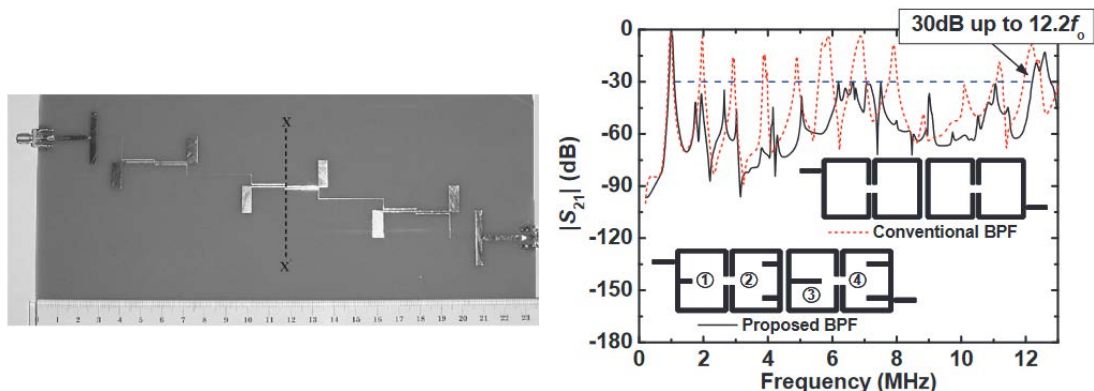
Figure 1.5: Solutions based on the use of open stubs to get a wide stopband. Left: Parallel coupled line topology [8]. Right: Open-loop structure [9].

Lastly, the introduction of TZs within the filter stopband is also carried out in [11], achieving wider and enhanced out of band response by means of a gap spacing and the width of two coupled metals between two capacitors in a lumped filter implementation.

As we have seen, these methods are usually linked to a specific filter topology and, therefore, are not broadly-applicable. The technique proposed in this thesis, on the other hand, can be used in any structure, since it does not depend on the filter topology in order to be implemented.

1.2.2   Introduction of TZs and Highly-Selective Responses

In recent decades, the microwave field has experienced a great evolution thanks to advances on different areas. In filter design area, one of them has been the introduction of TZs in the insertion loss response. Highly selective responses are a must in several wireless communication systems. Filters with elliptic or quasi-elliptic response allow to provide an enhanced rejection without increasing the filter order, and therefore, obtaining a more compact filter in size and with less losses. Several techniques for implementing highly selective filters have been presented in the literature.

One of the most broadly used methods, for the insertion of attenuation poles at finite frequencies, is based on introducing cross-couplings between non-adjacent resonators [12]. In cross-coupled filters, different paths for the EM signal from the input to output ports are provided. Depending on the signal phase, the multipath effect can generate finite TZs for enhanced selectivity [13], improving rejection at desired frequencies, or real-axis zeros (i.e. real axis of the complex frequency plane) to improve the passband delay characteristics, or even both types simultaneously [14].

Clearly, the characteristics of the coupling network will determine the number of TZs and their positions. Different dispositions of the coupling networks are presented [16]: conventional cross-coupling, different paths not interacting and different paths interacting (Figure 1.6). With this regard, planar filters with improved selectivity can be found in [14], [17] and [18]. In [14] a structure with different paths interacting is contemplated, using cascaded quadruplet (CQ) units, but changing the conventional rectangle half-wavelength meander-line microstrip resonator into a trapezoidal resonator, this interaction can be avoided. The S-parameter results of the described design show a flat group delay within the passband and a couple of TZs in the response. In [17] two structures providing two different paths, changed in phase, are described to introduce a TZ. Similarly, in [18] a low-order bandpass filter incorporating a weak signal-interference coupling between the input/output nodes is described to constitute a two-path signal-propagation circuit.
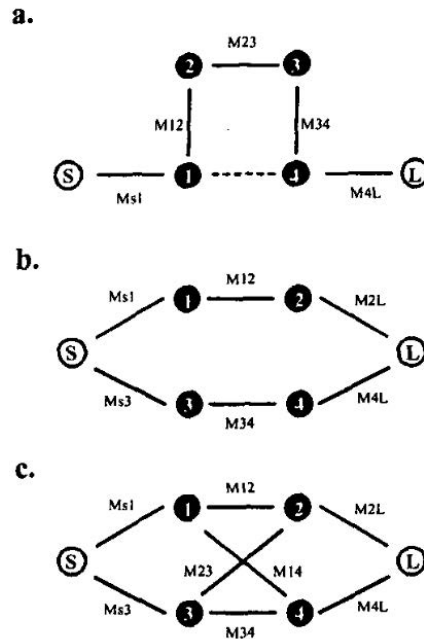
Figure 1.6: Coupling networks of 4-pole filters providing attenuation poles: a) conventional with cross-coupling; b) 2 paths (non-interacting); c) 2 paths (interacting) [16].

As can be seen in these works, the cross-coupling TZs are obtained at the expense of increasing the topological complexity, and sometimes turn to be difficult to perform, due to the strong dependency on the filter structure and also, on the filter technology.

Another approach for generating TZs is the extracted-pole synthesis technique [15]. The TZs are extracted from the transfer function and realized separately with bandstop filters and phase shifters connected to the end of the main coupling filter structure. It can be seen graphically in Figure 1.7. Contrary to the cross-coupling method, this technique implies an increase in area due to the use of phase shifters, but allows to have an independent control of each TZ.

Employing other solutions, such as Dual Behavior Resonator (DBR) topologies [19], is also possible to introduce and control TZs in a filtering response. The DBR is constituted by two dual-behavior stubs (i.e. one bandpass and the other bandstop) in parallel, allowing the independence of the two TZs associated to each stub, as well as the creation of a passband between them. And more recently, alternate circuits based on a distributed implementation of the elliptic filter prototype have been proposed in [20] obtaining also in this way, high rejection and selectivity for the microstrip filter designed.

Most of the former approaches are quite relevant and obtain, from a practical point of view, elliptical and quasi-elliptical responses taking advantage from the topology or the technology used in the filter design. Additionally, in some of these methods the TZs cannot be easily and independently controlled.
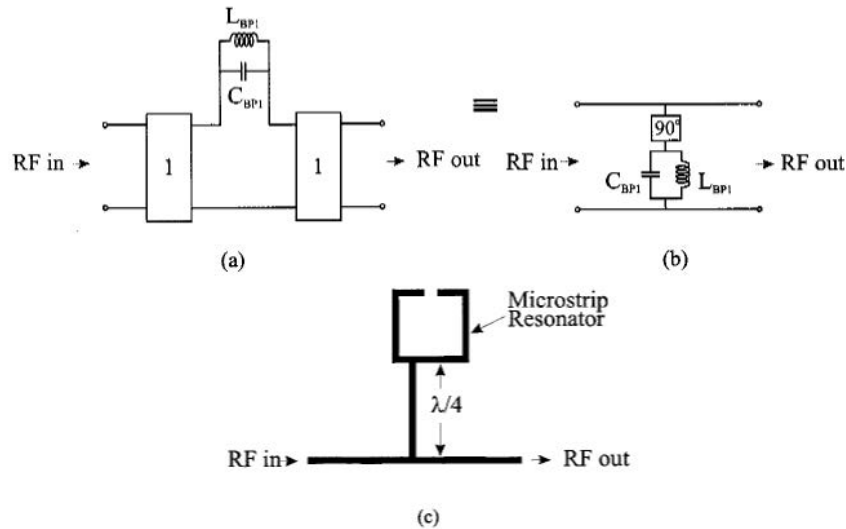
Figure 1.7: Extracted section of the filter for generating TZs [15]. (a) Original-synthesis extracted section. (b) Modified extracted section to a realizable circuit model. (c) Equivalent circuit for microstrip layout using a square-loop resonator.

1.2.3   Implementations of Advanced Filtering Responses

We have extensively reviewed techniques for obtaining advanced filtering responses. Nevertheless, all of them have been related to the improvement of the rejection band characteristics. In this last subsection we will emphasize on reviewing methods to optimize the filter behavior in the passband or globally in the entire response. For this last purpose, techniques for increasing the Q factor have been addressed.

In planar technology, this Q increment is of great relevance, since its own benefits, such as the reduction in size and cost, are directly linked to the Q limitation. For this reason, hybrid technologies solutions will be provided to reach this enhancement in performance.

In this sense, several designs have been developed. In [21] it is presented a bandpass filter in empty substrate integrated coaxial line (ESICL) with the center conductor suspended in air, obtaining a measured Q of 1505 at 15GHz. The structure is composed of 5 layers assembled with metallic screws. Layers 1 and 5 are cover sheets to confine the electromagnetic waves inside the transmission line. Layers 2 and 4 are included to separate the covers from the central line. And the central layer includes the filter resonators and impedance inverters (Figure 1.8). Using air as the main dielectric of the filter instead of another dielectric material produces an increase in the Q factor but also in size with respect to other materials. However, this increase in area is negligible compared to other non-planar technologies such as waveguides. In fact, it represents a good balance

in cost, size and performance between both technologies. Moreover, very cheap dielectric substrate layers could be employed in all layers without involving a high degradation of the filter performance, since is mostly air where is carried out the EM transmission.
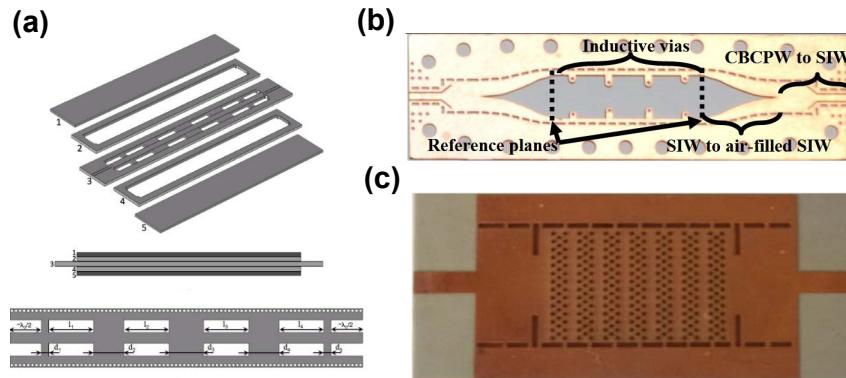
Figure 1.8: Proposed hybrid solutions to obtain enhanced Q filters in planar technologies. (a) Layout of the ESICL [21]. (b) Air-filled SIW structure [22]. (c) PDSIW cavity [23].

This principle of introducing air as dielectric in order to reduce losses and increase the Q-factor has been used by different authors [22]- [24]. In [22] an air-filled SIW bandpass filter using inductive posts at 31 GHz is proposed (Figure 1.8). The Q factor reached in measurements compared to its dielectric-filled counterpart is 706 versus 157. In [23] and [24] the air is added by using arrays of air holes in a SIW resonator, giving Periodically Drilled SIW structures (PDSIW). The consequence is high and low dielectric constant sections within the cavities. The optimal ratio between the two permitivities is studied, getting an increase of the stored energy and the quality factor approximately of 53% with only a 5% increase in size by using this method, in comparison with its standard SIW structure.

Another approach used for enhancing the Q factor is employing active elements. In [25], it is described a design methodology for using negative resistors and increase the Q factor in a planar filter. The provided method is applied to design an active hairpin microstrip bandpass filter, with negative resistors coupled to each resonator to compensate the losses in each one, giving an insertion losses at its center frequency of 0.05 dB.

On the other hand, by using hybrid resonators topologies [26], [27], or through recent advanced fabrication techniques such as 3D printing or additive manufacturing [28], [29], high Q filters are also achieved. The solution described in [26] is based on a compact hybrid resonator composed of a microstrip line and a short-circuit coaxial line integrated with a shielding case, which also leads to better EM performances. In this way, intermediate values of Q (higher than microstrip but lower than coaxial line resonators) are obtained. By properly choosing the length of the microstrip line with regard to the

thickness of the coaxial line (i.e. as a trade off between Q and size), Q values from 600 to 800 are achieved in this hybrid resonator structure. In [27] hybrid acoustic-wave-lumped-element resonator (AWLR) architectures are proposed as fundamental elements of bandpass filters leading Q values of the order of 1000, reaching fractional bandwidths (FBWs) broader than all acoustic waves filters and higher Qs than conventional lumped-element filters. Nonetheless, it is worth mentioning that this type of responses would be still limited to narrow band applications up to 3 GHz. By last, new developments in recent manufacturing processes, have leaded to intermediate solutions, among planar and waveguide technologies, of high Q factors (>1800) and at the same time lighter and smaller than bulky waveguides (See Figure 1.9). Some examples are reported in [28], where a compact Ka-band second order BPF based on hemispherical resonators has been designed and manufactured using a high-temperature-resistant ceramic-filled resin, in a fast and low-cost stereo-lithography-based 3D printing technique, being later metallized by employing electroless copper/silver plating; and in [29] where a new type of additively manufactured coaxial-resonator-based BPFs is reported. Here, the proposed monolithic vertical integration allows for low-losses (Q>1833) and low-weight (11–15 gr).
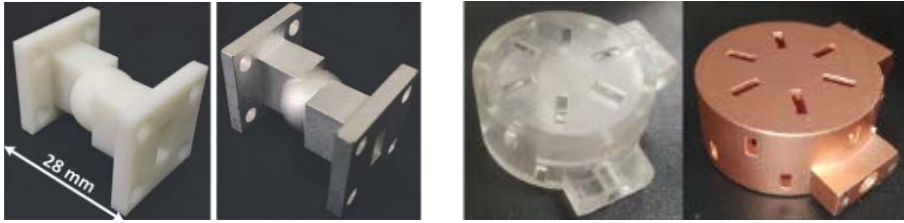
Figure 1.9: Photographs of manufactured prototypes before and after plating using recent techniques: Left: 3D printing [28]. Right: additive manufacturing process [29].

All the techniques seen so far for the Q improvement do not always provide enough Q to meet specifications, or not always are easy to implement in all applications. Hence, when the size requirements lead to a fully planar approach and at the same time, high Q characteristics are demanded for the response, pre-distortion [30]- [34] and lossy [35]- [43] techniques need to be considered. Both approaches are intended to use low Q resonators and make them behave like high Q resonators in order to reduce size. In pre-distortion techniques power is largely reflected to increase in-band flatness rather than absorbed, as it is in lossy techniques.

Losses or the increase in insertion losses (ΔIL) in a filter can be estimated as [36]

$$\Delta IL(\omega) \approx 8.686 \left(\frac{GD(\omega)}{Q_u} \right) \tag{1.1}$$

where GD is the group delay and Q_u is the unloaded Q of the resonators.

Considering a filter with a cutoff frequency of $\omega = 1$ rad/s and with uniform Q among resonators, it can be extracted that the amount of losses will become more significant as the Q_u is lowered, and at frequencies where the GD is large. This is manifested as a rounding of the passband edges and a decrease in maximum stopband attenuation. Since the GD is inversely proportional to bandwidth, these effects become more pronounced in narrow-band filters.

In pre-distortion methods (both, classical [31] and adaptive [32]) the passband equalization is achieved by reflecting energy at frequencies in the middle of the passband, thus increasing the reflection (or Return Losses, RL) so that the IL worsens and IL difference with respect the values at the passband edges is reduced. In this manner, it is possible to ensure good flatness and effective Q-factor performance, but it is required to compensate the poor RL by using non-reciprocal devices such as isolators and circulators at input and outputs ports of the filter. These components contribute to increment footprint and losses. Moreover, for a realizable network in pre-distortion synthesis there would be symmetrical [33] and asymmetrical realizations [31]. For topologies with large number of resonators, the design of asymmetric structures leads to increase the filter sensitivity, as reported in [31], as well as the complexity of the structure.

The pre-distortion methods can be seen in the response shown in Figure 1.10 (taken from [35]), where a comparison between the conventional approach and the classical and adaptive pre-distortion is plotted.

As can be observed in Figure 1.10, the pre-distortion techniques flatten the insertion loss response at expense of deteriorating the return loss. The lossy techniques instead, flatten the response at the passband by absorbing the energy in the desired bands, and in consequence exhibit improved reflection. To do that, additional losses can be introduced either in individual resonators, forming a transversal network with non-uniform Q resonators [36]- [40], or distributed by resistive cross-couplings (RCCs) between resonators and non-resonating nodes (NRNs) [3], [43] or even both, combining heterogeneous loss distribution among resonators and RCCs [36].

In [36] it is firstly described a lossy bandpass filter synthesis with non-uniform Q resonators. From the analysis of the loss distribution in this work, it is deduced that it is preferable to place the lower Q elements towards the outside of the filter, while those of higher Q among the central resonators. However, with this approach the losses are not introduced into the central resonators, thus the flatness improves but it has no effect on the selectivity. To effectively redistribute losses among resonators and improve the filter response, additional use of RRCs and matrix hyperbolic and trigonometric rotations are required. Doing so, the design and manufacture of a 6th-order hybrid filter, using RCCs and multipath loss distribution, is presented as a demonstration of the concept.
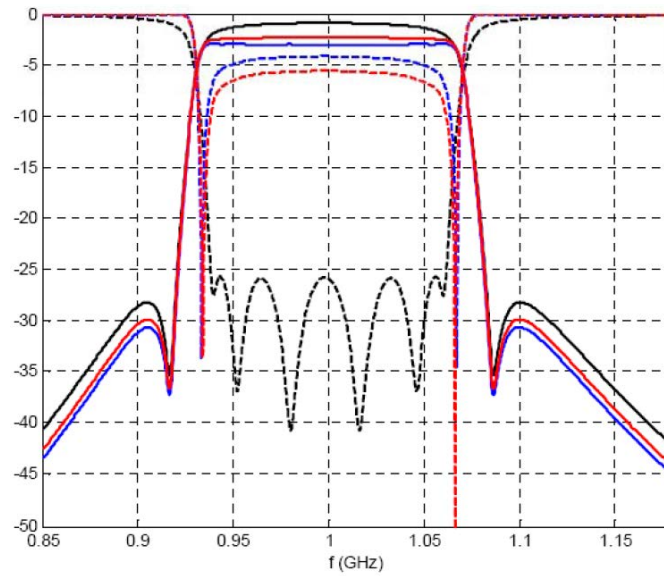
Figure 1.10: Transfer and reflection coefficient for a 6th-order quasi-elliptic filter form with resonators of Q=250 and synthesized using conventional techniques (black line), using classical pre-distortion (blue line) and using adaptive pre-distortion (red line). The solid and dashed lines correspond to the transfer and reflection coefficient respectively [35].

In [37], the same design procedure of lossy filter synthesis was extended, putting focus on the design of parallel connected lossy filters by employing non uniform dissipations only at resonators. The design of a 4th-order filter realized with mixed coaxial and microstrip technology proposed in [37], together with its response, is shown in Figure 1.11.
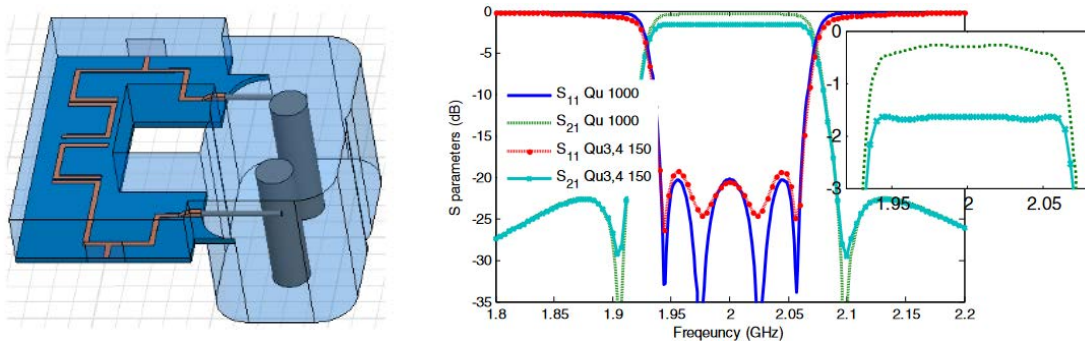
Figure 1.11: HFSS model of the non-uniform Q 4th-order filter with mixed coaxial and microstrip technologies, and its simulated response compared with the design of a conventional uniform Q 4th-order filter using just coaxial technology [37].

In most of the reported works on lossy techniques, filters are implemented using waveguide-cavity resonators or mixed technologies, but only a few of them are fully done

in planar technology. Nevertheless, these fully microstrip-planar designs presented in [36], [38] and [39] normally require RCCs that are difficult to implement. For an easier fabrication, an entire microstrip lossy filter without any resistive coupling, considering an extended doublet configuration as well as a non-uniform Q distribution is described in [40]. In SIW technology, some examples have been proposed too. In [41], a 3rd-order Chebyshev C-band lossy SIW filter with RCCs between non-adjacent resonators and non-resonating nodes is described, applying the synthesis method provided in [42]. Another structure based on SIW technology is proposed in [43]. In Figure 1.12, it can be seen the coupling topology scheme employed in the filter, as well as the coupling matrix and the final implementation. In this case, as shown in Figure 1.12 only the prescribed resistive couplings are added between some resonators, avoiding the use of additional non-resonating nodes and related resistive couplings.
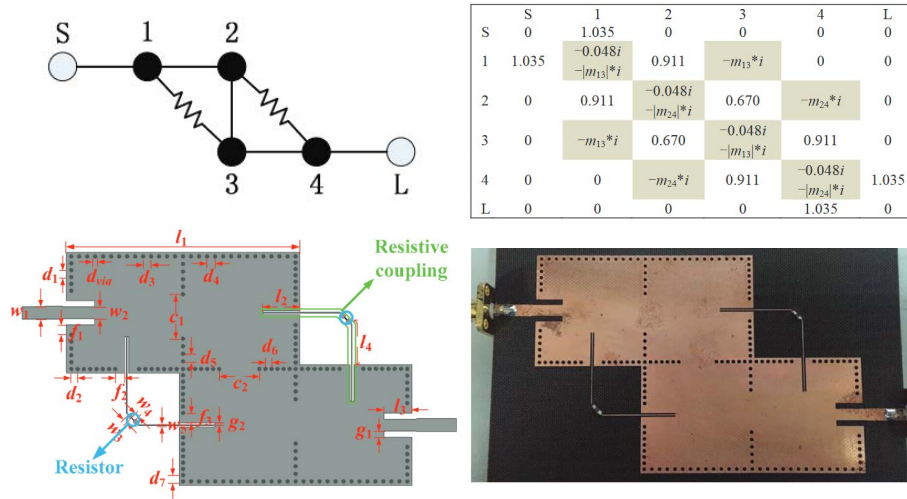
Figure 1.12: 4th-order lossy SIW filter with resistive couplings for flat passband described in [43]. Top: coupling topology scheme and coupling matrix. Bottom: Layout and fabricated prototype.

The resistive couplings between resonators are provided by surface mounted resistors connected with SIW cavities through planar transmission lines, and in consequence there is no reduction in size with regard of a classic SIW topology. In this sense, as can be observed in Figure 1.12, it occurs the opposite. However, a better performance in the response is obtained compared with a conventional SIW as it is depicted in Figure 1.13.

Similarly, in [38] and in [39], SMD resistors have been used for introducing resistive couplings and implement simple hairpin microstrip lossy filters of uniform Q (Figure 1.14). Specifically, in [39] a fair comparison between different lossy approaches is provided considering the same specifications and the same technology (i.e. a 6th-order hairpin filter centered at 3.8 GHz). This study evaluates the classical hairpin filter, with regard the be-
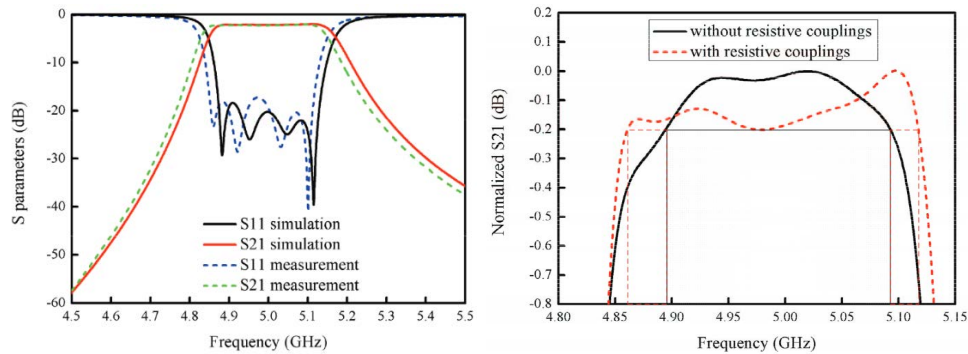
Figure 1.13: Left: Comparison between simulated and measured responses of the 4th-order lossy SIW filter with resistive couplings proposed in [43]. Right: Measured normalized transmission coefficients of the SIW filter without and with resistive couplings.

haviour obtained for the next lossy techniques: transversal lossy filter with non-uniform Q resonators, in-line lossy filters with 2 RCCs and 4 RCCs, and symmetric and asymmetric absorptive lossy filters with 4 RCCs and 2 NRNs. According to the authors' conclusions, the lossy solution presented in [36] with better performance in terms of flatness and selectivity, based on non-uniform Q and RCCs, provides indeed higher performances but has more difficulty in its implementation. Additionally, the input/output junctions between multiple dispersive paths, cause spurious transmission in the stopband. Moreover, this solution shows a higher sensitivity with respect to manufacturing tolerances. Consequently, the best solution chosen for the authors as a good compromise between flatness, insertion loss and feasibility, is the in-line lossy version with 2 RCCs.
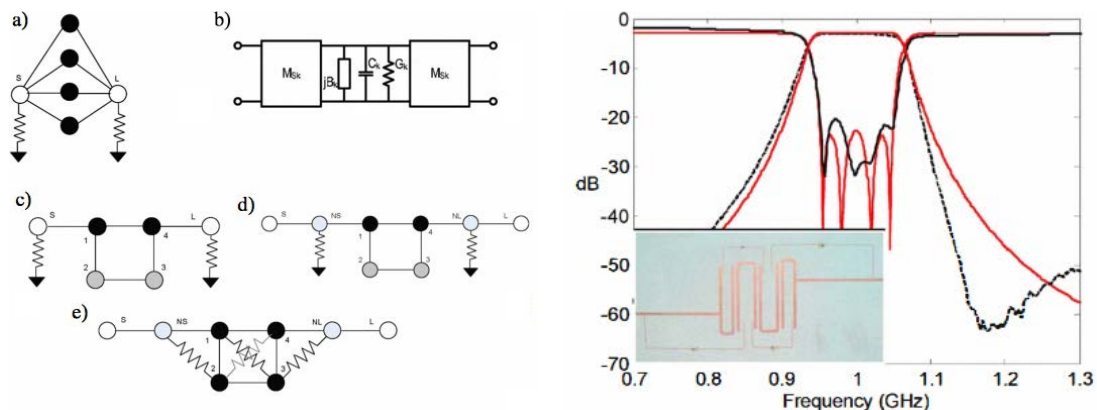
Figure 1.14: Left: Network topology conversion from a lossy transversal scheme (a) to a folded coupling topology with non-resonating nodes after losses distribution (e). Right: S-parameter response and picture of the prototype manufactured. The red solid lines correspond to simulations while the black dashed ones correspond to measurements [38].

A generalized synthesis technique for lossy reciprocal and non-reciprocal microwave filters is first introduced in [3], with a later extension in [44]. By using this method any filter response (i.e. with different disposition of transmission zeros, asymmetrical and symmetrical, non-reciprocal and reciprocal networks) can be synthesized. Nonetheless, the synthesized coupling matrix obtained can be non-realizable and must be reduced to obtain a feasible structure. For the experimental verification of this synthesis technique, a 4th-order Chebyshev filter is designed at 12 GHz, using mixed combline and microstrip technologies to implement the resonators and the RCCs, respectively, as shown in Figure 1.15.
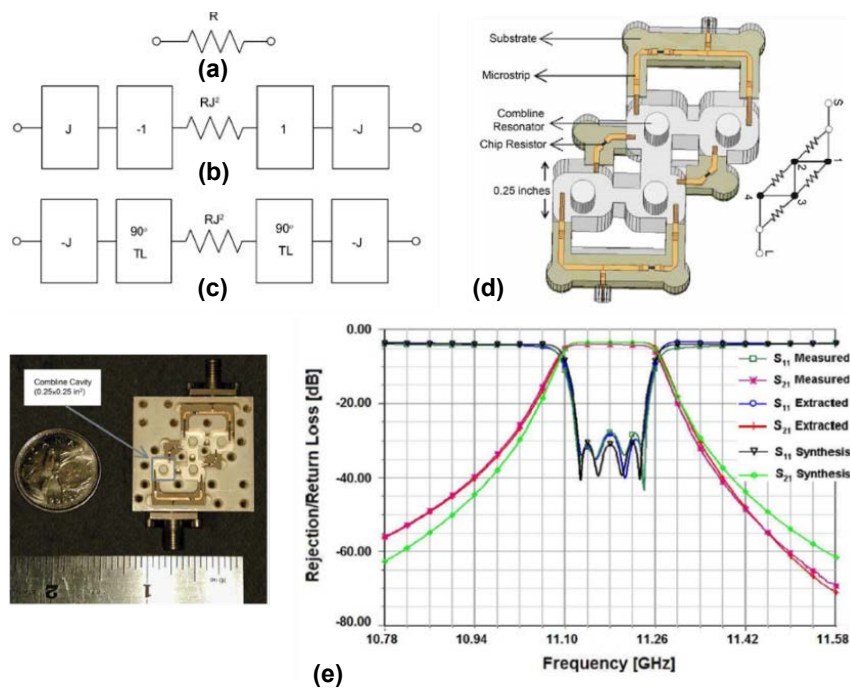
Figure 1.15: Resistive coupling realization in [3]. (a) Plain resistor. (b) Equivalent circuit with J-inverters. (c) Final equivalent model with $\lambda/4$ transmission lines and negative coupling values. (d) HFSS model of the lossy filter and its node diagram. (e) Fabricated filer and measurements versus synthesis results.

Likewise, a novel synthesis method based on an even- and odd-mode decomposition is also presented in [45]. This method is capable of synthesizing a network under very general hypotheses; therefore, it is also suitable and successfully applied to the design of lossy filters.

Finally, we do not only have all these reviewed techniques for improving the response and performance of filters, as well as shrinking their cost and size. Since filters are part of more complex components, such as diplexers and multiplexers (MUXs), their design and implementation can also be benefited. A fast review of recent advances in this area is also shown next.

As summarized in [46], the most commonly used configurations in the design and implementation of multiplexing networks are hybrid-coupled MUXs, circulator-coupled MUXs, directional filter MUXs, and manifold-coupled MUXs. A brief overview of each configuration is described. In Figure 1.16 the hybrid-coupled MUX layout is shown. Each channel consists of two identical 90° hybrids. The main advantage of this approach is its directional property, which minimizes the interaction between the channel filters. The hybrid-coupled topology allows the integration of additional channels without disrupting the existing multiplexer design, a requirement in some systems. Additionally, in this approach only half of the input power goes through each filter. Thus, the filter design can be relaxed when using this type of multiplexer in high-power applications. On the other hand, it has the disadvantage of larger size since two filters and two hybrids per channel are required. Another design consideration of such multiplexers is the phase deviation between the two filter paths that the two signals undergo before they add constructively at the channel output. The structure, therefore, must be fabricated with tight tolerances to minimize the cited phase deviation.
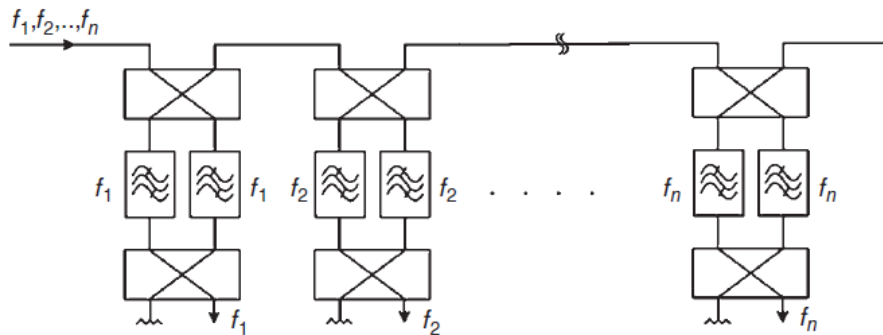
Figure 1.16: Layout of a hybrid-coupled multiplexer [46].

Concerning the circulator-coupled approach, each channel consists of a channel-dropping circulator and one filter, as shown in Figure 1.17. The unidirectional property of the circulator provides the same advantages as the hybrid-coupled approach in terms of amenability to modular integration and ease of design and assembly. The insertion loss of the first channel is the sum of the insertion loss of the channel filter and the insertion loss of the circulator. The subsequent channels exhibit a relatively higher loss due to the insertion loss incurred during each trip through the channel-dropping circulators. This is the most common realization for input multiplexers (IMUXs).
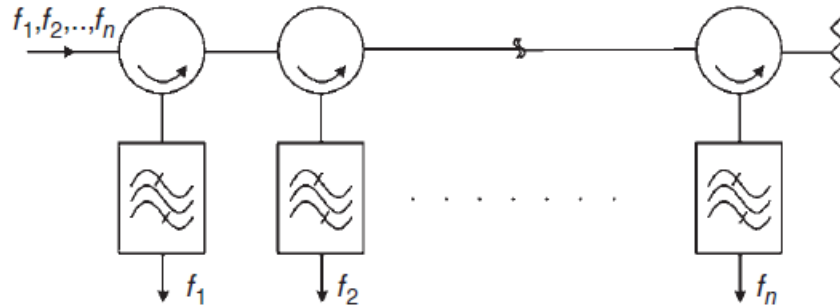
Figure 1.17: Layout of a circulator-coupled multiplexer [46].

The directional filter MUX configuration is realized by connecting directional filters in series. In Figure 1.18 a general layout is illustrated. A directional filter is a four port device in which one port is terminated in a load. The other three ports of the directional filter act as a circulator connected to a bandpass filter. However, directional filters do not require the use of ferrite circulators. Therefore, this multiplexing approach has the same advantages as the hybrid-coupled and circulator-coupled approaches, but it is limited to narrowband applications.
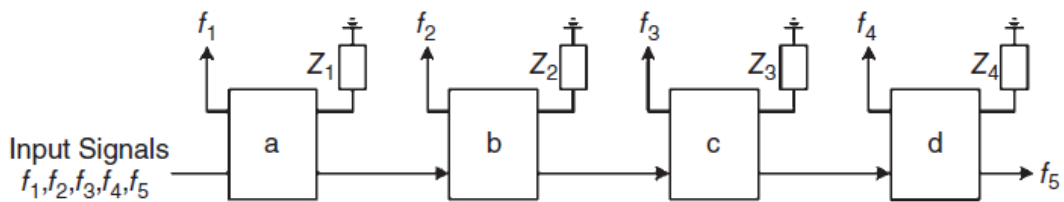
Figure 1.18: Layout of a directional filter multiplexer [46].

Finally, the manifold coupled multiplexer scheme is shown in Figure 1.19. It is the optimum choice in terms of miniaturization and absolute insertion losses. This type of multiplexer requires the presence of all the channel filters at the same time, so that the effect of channel interactions can be compensated in the design process. It implies that a manifold-coupled multiplexer is not amenable to a flexible frequency plan; any change in the allocation of channels will require a new multiplexer design. Moreover, as the number of channels increases, this approach becomes more difficult to implement. This solution is widely used for most OMUX applications.
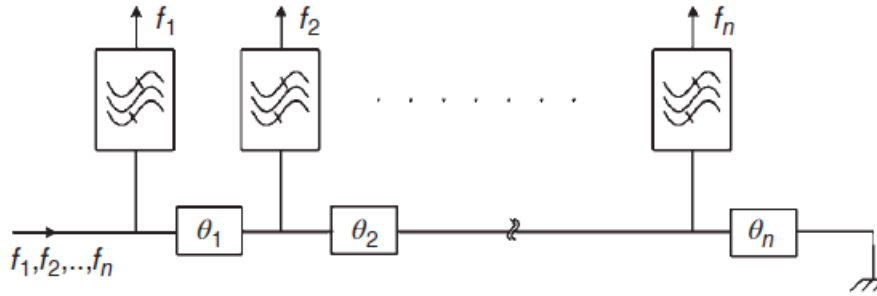
Figure 1.19: Layout of a manifold coupled multiplexer [46].

In the literature, several high-performance MUXs can be found in different configurations using waveguide technology [47]- [50], providing high quality factor, low losses, high channel isolation and high power-handling capability; but resulting heavy-weighted and high cost devices with low integration capability. On the far side, planar microstrip MUXs [51]- [58] can be also found in the literature providing favorable structures for compaction and easy integration, suitable for low cost commercial applications, but they suffer from low quality factor, high losses, worse channel isolation, especially for the contiguous-channel MUXs. A good compromise between both technologies (microstrip and waveguide), is the use of SIW structures. They have low weight, low cost, a planar form with high integration capability and a relatively high quality factor. These advantages make SIW technology to become a good candidate for developing microwave components.

In [59] a compact SIW multiplexer is proposed. This technology allows to emulate many of the properties of the classical waveguide but more compactly, hence with higher losses. A Ku-band SIW four-channel MUX prototype is designed and fabricated. To reduce the size of the MUX, the output channels are closely aligned to each other through the use of a compact SIW power combiner. In Figure 1.20 the SIW MUX structure is depicted along with the manufactured prototype and its results.

More compact implementations are presented using dual-mode resonators in SIW technology in [60] and [61]. In [60] the complementary characteristics of SIW dual-mode filters with circular and elliptic cavities are employed to design a diplexer with high isolation. The rejection at the upper side of the circular cavity and at the lower side of the elliptic cavity are very steep. Combining both topologies, a K-band diplexer with high selectivity and low insertion losses is designed, fabricated and measured. While in [61] a compact SIW diplexer using dual-mode and triangular resonators is studied. Another SIW planar diplexer with superior performance based on complementary split-ring resonators (CSRRs) is described in [62]. It is realized by a three-port device with two cascaded filters
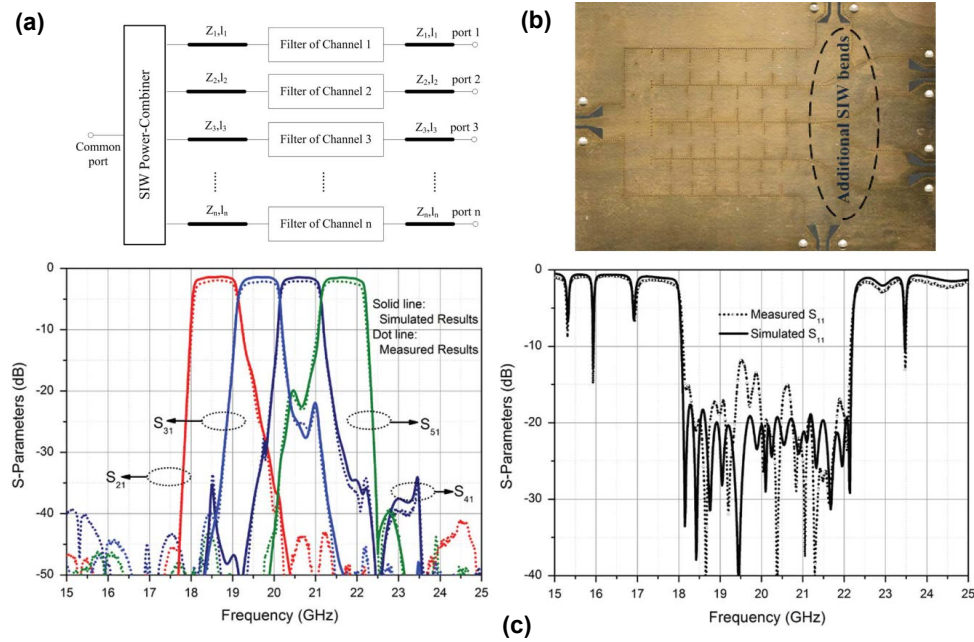
Figure 1.20: 4–Channel SIW MUX proposed in [59]: (a) Configuration; (b) fabricated proto-
type; (c) S-parameters simulations versus measurements responses.

in which TZs can be observed due to the coexistence of electric and magnetic couplings,
improving in that way, the selectivity and the out-of band rejection with the suppression
of the TE_{10} mode. Finally, in [63] a SIW diplexer with no additional elements such
as power dividers, combiners etc., composed exclusively of six SIW resonators coupled
through inductive irises, with one TZ at each channel that improves the selectivity of the
passbands around 8 GHz, is presented (Figure 1.21, left). Important advantages in terms
of size reduction, while keeping good losses as well as high rejection and isolation levels,
are achieved by using a coaxial SIW topology in [64]. The described X-band diplexer
consists on two channel filters connected to a common input port through a microstrip
T-junction, as can be seen in Figure 1.21, right.
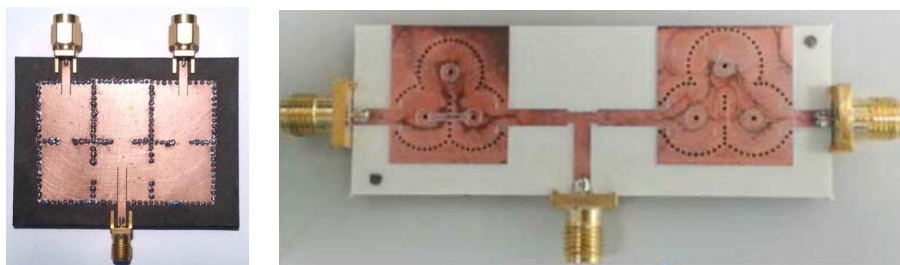
Figure 1.21: Compact X-band diplexers. Left: SIW structure with no additional elements [63].
Right: Circular triplet coaxial SIW structure [64].

1.3 Objectives

According to the theoretical framework, context and motivation exposed, the main goal of this thesis consists on the analysis, development, design, implementation, fabrication and experimental testing of microwave filtering components in planar and hybrid technologies with advanced responses and higher performances. This fundamental objective, can be structured into the next more specific objectives:

- Development of a novel technique that allows the introduction of transmission zeros in any planar filter topology, where the location of these TZs can be flexibly controllable, according to the need or application. Specifically, it is intended to study the design of filters with highly selective responses, where the zeros are very close to the passband; and in the design of filters with an ultra-wide spurious free band. In the latter case, the zeros must be placed relatively far from the filter passband.
- Study and realization of compact filter structures with high Q factor. For this purpose, it is intended to go deeper into the implementation of coaxial SIW filters by applying different Q-enhancement techniques, and subsequently evaluating their benefits and drawbacks versus the classical-conventional structure.
- Research on filters with high passband planarity for satellite communications, where stringent flatness specifications are required. The intention is to provide this feature to planar filters, and in particular to coaxial SIW topologies. Lossy methods will need to be considered.
- Validation of the proposed solutions by performing the design, simulation, optimization, implementation, fabrication and measurements of different microwave components (i.e. filters and a diplexer) with advanced responses for different applications in wireless communications. Experimental results will be compared with simulations from commercial software tools to validate each design.

1.4 Document Organization

This PhD dissertation is composed of five chapters. Thus, this document can be divided into two main parts. The first one is related with the study, analysis and development of techniques to enhance the rejection band characteristics of filters, and the second one is focused on the investigation of methods to improve the passband and attain low-cost and compact structures of higher Q and/or of increased performance.

In this first introductory chapter, a general description of the topics developed within their context and background has been presented. The state of the art has been classified in three sections. First, with the mechanisms to obtain a wide spurious-free stopband in planar filters. Second, with the overview of the techniques to introduce TZs and obtain

highly selective responses. And finally, with different methods to get filtering components with advanced responses. Concretely, solutions to enhance the Q factor, based on pre-distortion and lossy techniques, as well as to implement integrated filtering devices such as multiplexers in planar and hybrid technologies, have been discussed.

Chapter 2 The second chapter is devoted to the description and analysis of a novel design technique for the introduction of transmission zeros in any filter response. Hence, an exhaustive study of the required networks, both circuitally and mathematically, is performed to finally provide equations for the design. The described technique is applicable to any filter in planar technology, independent to the filter topology, and capable of placing the TZs in a flexible way. Several application cases of this technique are studied. Firstly, the suppression of spurious responses due to periodicity in distributed filters is addressed. This enables us to design filters with ultra-wide stopband and a high level of rejection. Secondly, the introduction of transmission zeros close to the filter passband, with the aim of improving selectivity and getting elliptical responses, is given. Finally, the enhancement of the rejection bands in topologies with adjacent channels is also described. The proposed technique is conveniently validated by means of several filter examples that are designed, manufactured and finally experimentally measured.

Chapter 3 This chapter presents the results of the study about the design of filtering structures in planar technologies with higher performances. The main challenges are analyzed, and different approaches to attain compact and low-cost components with advanced and better responses are proposed. The use of the coaxial SIW topology is considered, and various methods to improve its Q factor are studied. In addition, a general design procedure for designing multiplexers in this technology is described.

Chapter 4 The fourth chapter analyizes the coaxial SIW resonator topology and its main design parameters to control the Q factor. The Q-control capability of this technology is explored to improve the passband planarity and obtain filtering responses with very flat amplitude. A non-uniform Q lossy technique using the same technology, and without resistors, is described. The proposed solution is easy to implement and allows to achieve very compact devices with advanced responses. Moreover, various examples and application cases are designed, fabricated and measured, providing details for all considered examples.

Chapter 5 In this chapter the main conclusions of this work are summarized. Likewise, possible future lines of development, research and application associated with the contributions made in this thesis are proposed.

Chapter 2

Design of Bandpass Filters with Flexible Transmission Zeros

This chapter will present the fundamental theoretical framework to address the design of microwave filters with transmission zeros. In first place, some basic concepts about the design of microwave filters are introduced, with special emphasis on those aspects that are more interesting for the purpose of this work. The concept of transmission zero will be also described, as well as the different existing mechanisms for incorporating TZs into the filtering response. After that, we will explain the theoretical synthesis developed to introduce TZs independently of the filter structure. To do this, some of the basic network configurations for filter design will be presented. Subsequently, the fundamental concepts on matching impedance will be reviewed, being these concepts the elementary theoretical basis of the mathematical and circuital development carried out in this chapter. And finally, the synthesis methodology that must be followed for generating the TZs will be given. Last, different design examples of the proposed technique will be detailed, showing its flexible and wide application.

2.1 Basic Concepts about Microwave Filters

The design of a filter starts by obtaining a response that guarantees certain specifications. These specifications refer to some filter parameters listed next.

The fundamental parameters referred to are:

- Insertion loss, S_{21} (dB).
- Return loss, S_{11} (dB).
- Ripple (dB).
- Bandwidth (Hz).
- Attenuation or Stopband rejection (dB).
- Roll-off (dB/decade).
- Type of response: lowpass, highpass, bandpass, bandstop,...

Taking into account the requirements to be fulfilled, the transfer function is chosen [65]. This completely defines the shape of the filter and its attenuation as a funciton of the frequency. Thus, the transfer function of a passive filter is usually given by the following expression:

$$|S_{21}(j\Omega)|^2 = \frac{1}{1 + \epsilon^2 F_n^2(\Omega)} \tag{2.1}$$

where ϵ is a ripple constant, $F_n(\Omega)$ represents a filtering or characteristic function, and Ω is a frequency variable.

From it, the insertion loss (relation between the output power and the input power) can be obtained:

$$L_A(\Omega) = 10 log \frac{1}{|S_{21}(j\Omega)|^2} \ dB \tag{2.2}$$

Since $|S_{11}|^2 + |S_{21}|^2 = 1$ for a lossless, passive two-port network, the return loss response of the filter can be computed by:

$$L_R(\Omega) = 10 log[1 - |S_{21}^2|] \ dB \tag{2.3}$$

Among the most widely used transfer functions are the Butterworth, Chebyshev and Cauer (or elliptical) responses. Their lowpass responses are shown in Figure 2.1.

The Butterworth response is characterized by having a flat response in the passband. It presents an insertion loss of 3.01 dB at the cutoff frequency $\Omega = 1$, regardless of the order.

On the other hand, the Chebyshev response has a steeper roll-off than the Butterworth one, and therefore a higher selectivity and rejection. Instead, it adds a previously non-existent ripple in the passband.
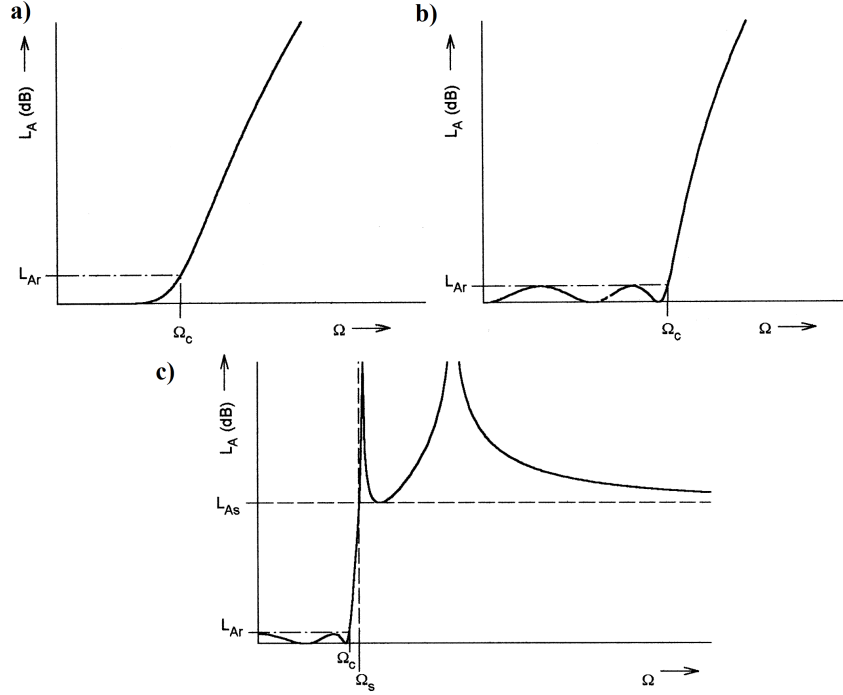
Figure 2.1: a) Butterworth lowpass response. b) Chebyshev lowpass response. c) Elliptic function lowpass response. [65].

As regards the elliptical filter, it presents the most pronounced transition band, but allows the presence of ripple in both, the passband and the stopband.

A broadly used response, which provides a compromise between planarity of the passband and higher selectivity, is the Chebyshev response. It exhibits constant ripple in the passband and completely flat shape in the stopband. The transfer function that describes this type of response is:

$$|S_{21}(j\Omega)|^2 = \frac{1}{1 + \epsilon^2 T_n^2(\Omega)} \tag{2.4}$$

where the ϵ constant is determined by the desired ripple level in the passband, L_{Ar} (in dB) as follows:

$$\epsilon = \sqrt{10^{\frac{L_{Ar}}{10}} - 1} \tag{2.5}$$

$T_n(\Omega)$ is a Chebyshev function of the first kind of order n, which is defined as:

$$T_n(\Omega) = \begin{cases} cos(ncos^{-1}\Omega) & |\Omega| \leq 1 \\ cosh(ncosh^{-1}\Omega) & |\Omega| \geq 1 \end{cases} \tag{2.6}$$

To synthesize any filter, we first obtain the lowpass prototype, which is the equivalent circuit from which it is possible to transform the response into other types of response (i.e. highpass, bandpass, and bandstop), and to conceive multiple implementations with different technologies.

The fundamental characteristics that a lowpass prototype must meet are the following ones:

- Their element values have to be normalized to make the source resistance or conductance equal to one, denoted by $g_0 = 1$.
- The cutoff frequency is $\Omega_c = 1$ rad/s.
- The number of reactive elements required is equal to the filter order n.

There are two dual structures for the implementation of lowpass prototypes in all-pole filters (e.g. Butterworth or Chebyshev) based on L-C ladder networks (see Figure 2.2).
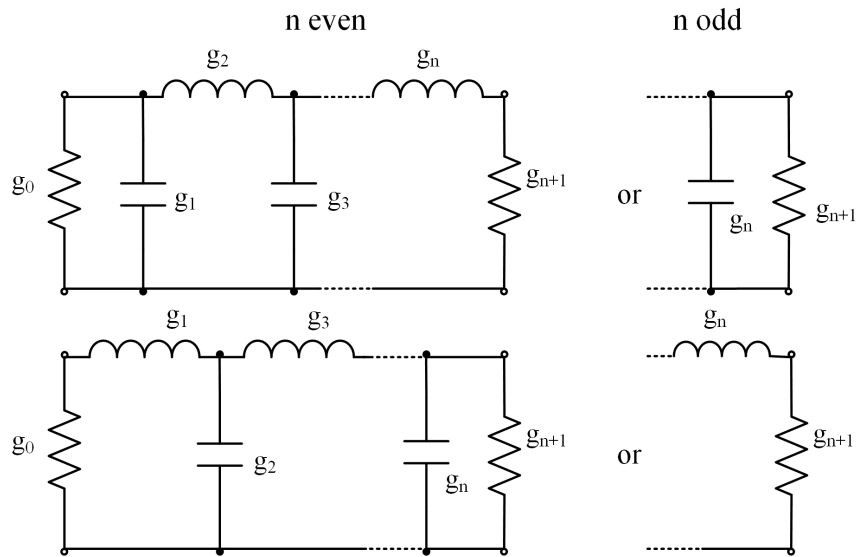
Figure 2.2: Lowpass prototypes for all-pole filters with a ladder network structure.

The values of the network elements can be obtained from the transfer function, despite the fact that it is very common the use of tables, knowing the order n of the filter and the ripple value.

Through the lowpass prototype any required response can be achieved. In particular, for a bandpass response, the elements transformation to be applied is shown in Figure 2.3.
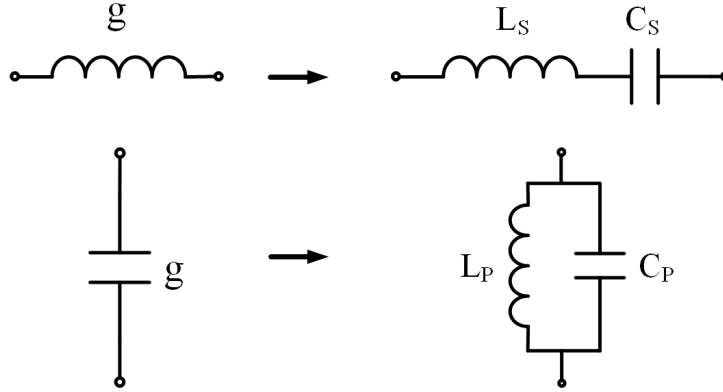
Figure 2.3: Elements transformation: from lowpass to bandpass prototype.

And the frequency transformation:

$$\Omega = \frac{\Omega_c}{FBW} \left(\frac{\omega}{\omega_0} - \frac{\omega_0}{\omega} \right) \tag{2.7}$$

with $\Omega_c = 1$, whereas FBW and ω_0 defined as follows:

$$FBW = \frac{\omega_2 - \omega_1}{\omega_0}; \quad \omega_0 = \sqrt{\omega_1 \omega_2} \tag{2.8}$$

However, starting from the bandpass equivalent circuit and making use of immittance inverters, we will obtain a more convenient structure for its implementation at microwave frequencies.

An ideal impedance inverter is a two-port network with the property that at any frequency, assuming that one port ends with an impedance Z_2, the impedance seen in the other port is:

$$Z_1 = \frac{K^2}{Z_2} \tag{2.9}$$

where K is real and defined as the impedance inverter constant. As can be seen, if Z_2 is inductive/capacitive, Z_1 will become capacitive/inductive, and hence the inverter has a phase shift of $\pm 90^o$ or an odd multiple thereof. Impedance inverters are also known as K-inverters.

Likewise, an admittance inverter is a two-port network with the property that at any frequency, if an admittance Y_2 is connected at one port, the admittance seen in the other port is:

$$Y_1 = \frac{J^2}{Y_2} \tag{2.10}$$

where J is real and named as the admittance inverter constant. Similarly, the admittance inverter has a phase shift of $\pm 90^o$ or an odd multiple thereof. Admittance inverters are also referred to as J-inverters.

From the above, it is possible to perform the following transformations:
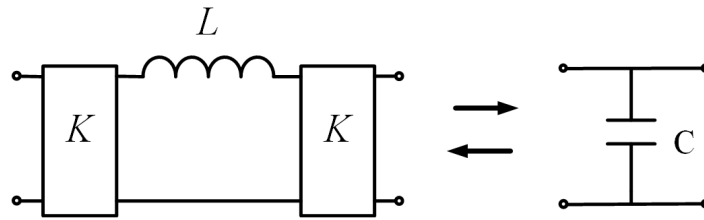
Figure 2.4: Impedance inverters used to convert a shunt capacitance into an equivalent circuit with series inductance.
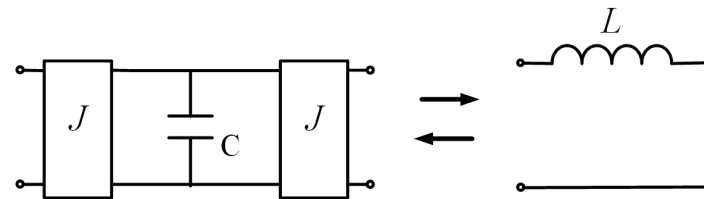
Figure 2.5: Admittance inverters used to convert a series inductance into an equivalent circuit with shunt capacitance.

In this way, it is possible to convert the response based on series and parallel LC resonators, into another identical one using inmitance inverters. Generically (for both lumped and distributed elements):

$$K_{0,1} = \sqrt{\frac{Z_0 FBW x_1}{\Omega_c g_0 g_1}} \quad , \quad K_{i,j+1} = \frac{FBW}{\Omega_c} \sqrt{\frac{x_i x_{i+1}}{g_i g_{i+1}}}\bigg|_{i=1 \text{ to } n-1} \quad , \quad K_{n,n+1} = \sqrt{\frac{FBW x_n Z_{n+1}}{\Omega_c g_n g_{n+1}}}$$

$$x_i = \frac{\omega_0}{2} \frac{dX_i(\omega)}{d\omega}\bigg|_{\omega=\omega_0}$$
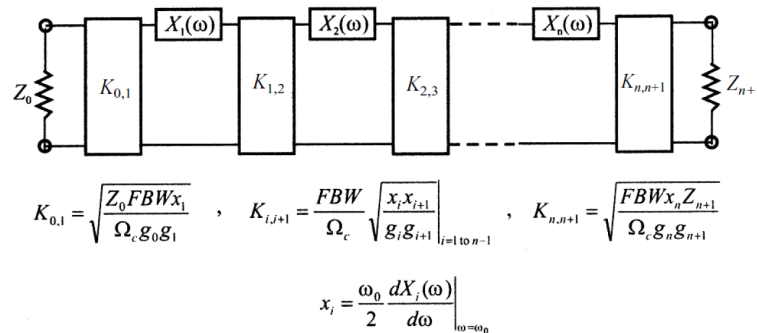
Figure 2.6: Generalized bandpass filters using impedance inverters [65].

$$J_{0,1} = \sqrt{\frac{Y_0 FBW b_1}{\Omega_c g_0 g_1}} \quad , \quad J_{i,i+1} = \frac{FBW}{\Omega_c} \sqrt{\frac{b_i b_{i+1}}{g_i g_{i+1}}}\bigg|_{i=1 \text{ to } n-1} \quad , \quad J_{n,n+1} = \sqrt{\frac{FBW b_n Y_{n+1}}{\Omega_c g_n g_{n+1}}}$$

$$b_i = \frac{\omega_0}{2} \frac{dB_i(\omega)}{d\omega}\bigg|_{\omega=\omega_0}$$
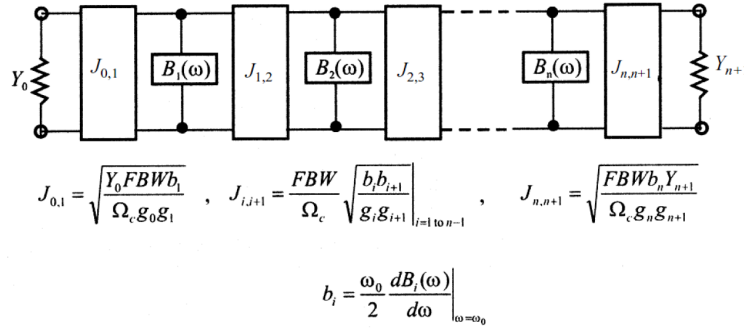
Figure 2.7: Generalized bandpass filters using admittance inverters [65].

In Figures 2.6 and 2.7, the g_i values are the original values of the lowpass prototype, FBW is the fractional bandwidth, $\Omega_c = 1$ rad/s, Z_0, Z_{n+1}, Y_0, Y_{n+1} are the characteristic impedances and admittances of the filter source and load, and the x_i and b_i are the reactance and susceptance slope parameters, respectively. These slopes parameters, as defined in the equations of the figures, for resonators have zero reactance or susceptance at center frequency ω_0.

Theoretically, the reactances $X(\omega)$ or susceptances $B(\omega)$ of distributed resonant circuits should be equal to those of lumped element resonators at all frequencies. In practice, they approximate the reactances or susceptances of the lumped element resonators only near resonance. Nevertheless, this is sufficient for narrow-band filters.

In our particular case, for bandpass filter designs we will use J-inverters and LC resonators in parallel. With that said, at microwave frequencies, the elements of this prototype are implemented by means of distributed resonant elements (transmission lines, coupled lines, other resonant structures, etc.) that must be designed to have a similar response to the synthesized model. Obviously, at higher frequencies than the operational frequency range of the filter, the response of the distributed filter will be considerably different due to high-frequency effects in the distributed topology (e.g. higher order resonances, discontinuities, excitation of higher order modes, radiation, etc.).

The technologies used to implement distributed microwave filters are diverse (coaxial, waveguide, dielectric resonators). However, one of the most widespread options is planar technology (microstrip, stripline, coplanar), due to some properties that makes it especially attractive: low cost, small size, ease of integration in circuits with active elements, such as MMIC (Monolithic Microwave Integrated Circuits). The most common distributed bandpass topologies are parallel-coupled line filters, interdigital filters, combline filters and hairpin shape filters. In this chapter, two of these classic microstrip topologies (parallel-coupled lines and combline) will be used to put into practice the theory developed in this section. It is worth mentioning that using any other topology does not involve any change in the application of the proposed method.

2.2 Transmission Zeros and Its Different Implementation Methods

The zeros of a transfer function are the roots of the numerator. In the field of filters, the TZs are the frequencies at which the filter transfer function is cancelled out. Theoretically, a TZ provides an infinite attenuation, but in practice this is not the case and the attenuation value will be higher or lower depending on the losses, method and technology used for its implementation, and other practical aspects.

The need to include TZs in a filter response is related to:

- The elimination of undesirable frequencies or spurious responses.
- Higher selectivity. By placing a TZ right after the cutoff frequency, we get a filter roll-off much more abrupt, without the need to increase the filter order.

There are different techniques for introducing TZs. Some of them are based on producing elliptical filter responses (see Figure 2.8, which shows higher slope and greater attenuation outside the passband than Chebyshev filters). However, this is achieved at the expense of greater ripple within the passband and within the stopband. For a certain order, elliptical filters have a greater number of TZs and the steepest transition region, but the presence of both ripples causes larger non-linearity in phase and worse group delay characteristics. Furthermore, this type of response is not easy to synthesize or implement using real components.
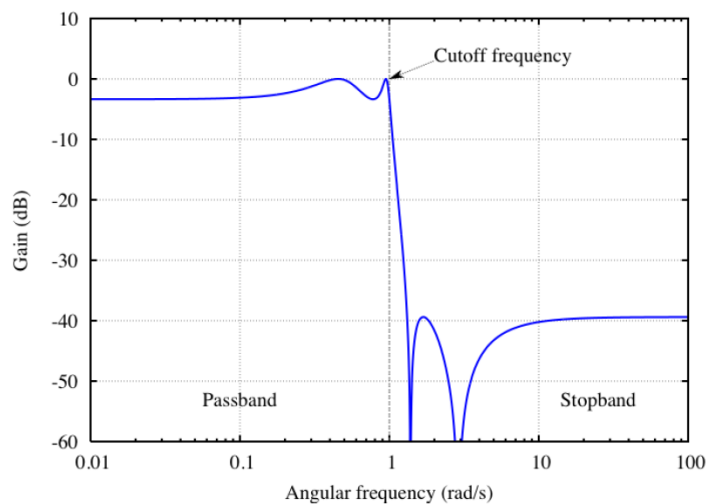
Figure 2.8: Example of an elliptical filter response.

The most generalized method for generating filtering responses with TZs consists on the introduction of cross-couplings between non-adjacent resonators [12]. In this procedure, the TZ is actually obtained thanks to the existence of more than one signal transmission path within the filter structure. In this way, when the phase difference between the signals is 180°, an energy cancellation occurs, thus the desired TZ is obtained.

In the literature we can find some examples applying this technique in filters with square open-loop resonators [1], using coaxial resonators [66], in different $\lambda/4$-resonator structures [67], and in waveguide filters [68]. In addition, slightly different versions where the cross-crouplings occur between the excitation lines (source and load) insted of between resonators are presented in [69] and [70]. In [17], parallel paths of different resonance frequencies are created between the input and output of the filter, whereas in [71] and [72] where the positions of the excitation lines are modified to provide different signal paths, instead of varying the resonator lengths. In the latter cases, the authors use hairpin resonators or open-loop ring resonators with input and output tapping excitation lines asymmetrically positioned. (see all previous solutions in Figure 2.9).
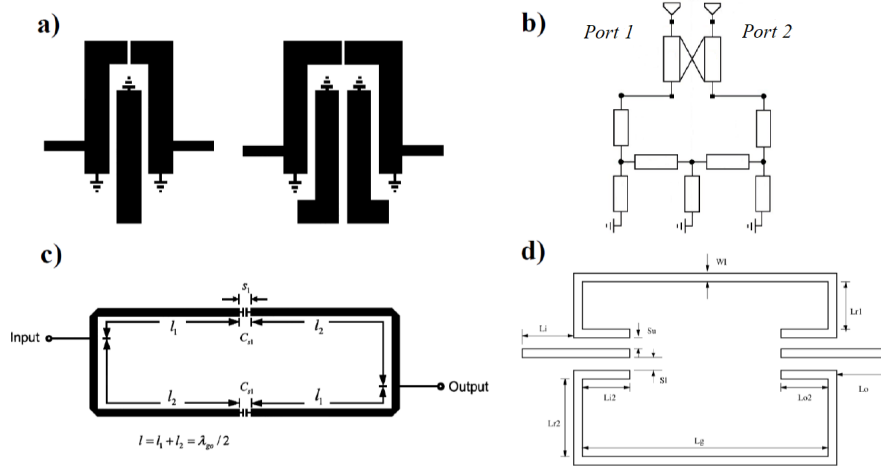
Figure 2.9: Techniques for the introduction of TZs. a) Cross-coupling between non-adjacent resonators. b) Cross-coupling between source and load. c) Assymetric tapping excitation. d) Parallel paths of different dimensions.

In filters with cross-couplings, the topology of the coupling network determines the number of TZs, while the location (proximity to the passband) is controlled by the sign and intensity of these couplings. In this way, at least four resonators are needed to achieve two TZs, being necessary to increase the order of the filter if more TZs are required. This leads into an increase in occupied area and higher insertion losses (ILs).

Another technique for including TZs is the extracted pole, originally used in waveguide filters [73], and later on with planar filtering structres [15]. In this technique each TZ is originated by means of a proper impedance (admittance) that blocks the transmission between the input and the output at a specific frequency. For this, the lowpass prototype is synthesized in the form of a complex conjugate network, where the real TZs are extracted from the structure by resonators and phase shifters (see Figure 2.10). This implies an increase in area due to the use of phase shifters. However, this method allows to have an

independent control of each TZ, being able to achieve a better adjustment to the desired response than using cross-couplings, where there is no specific control over the position of the TZs, as there is no direct correspondence between each TZ and a particular coupling or network element.
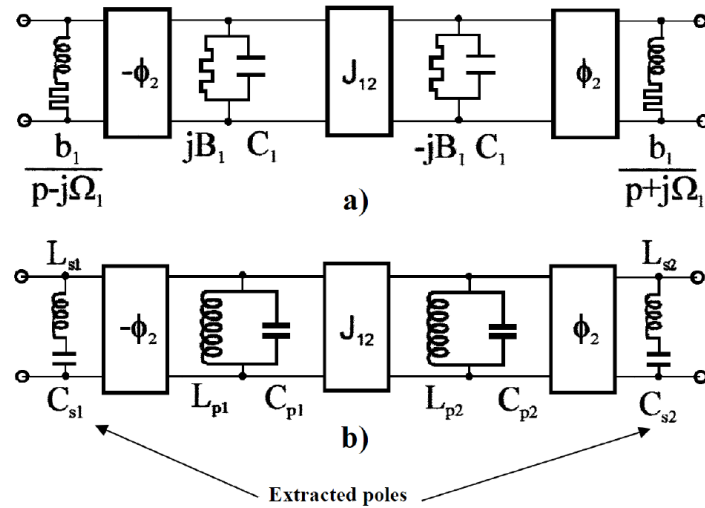
Figure 2.10: Synthesis of a 4-pole filter applying the pole extraction. a) Lowpass prototype. b) Bandpass transformation of lumped elements with two attenuation poles extracted.

As it has been seen, the described techniques are linked to the design of the filter, and normally their application leads to more complex topologies of higher order, higher losses and larger size in order to achieve TZs in the final response. As a consequence, its applicability is limited in many practical cases.

In this thesis, a simple method for the introduction of TZs at the filter response is proposed. The inclusion of the TZs is made independently of the filter design. The proposed method is inspired by the old image parameter method for synthesizing filters. This method achieves simple filters by cascading elementary building blocks that, superposing their responses, meet certain specifications. In this method, each block or section is matched with its adjacent one, and they usually consist on a lowpass or highpass response, impedance matching section, etc. In addition, there are some networks already studied and typically used such as the basic L section, T and π prototypes, M-derived and terminating sections. However, the procedure that will be presented next, does not follow exactly the image parameter method, although it has taken advantage of some of its theoretical principles in an original structure, proposed to satisfy the increasingly sophisticated requirements of wireless communication systems.

2.3 Synthesis of Transmission Zeros. Bisected π Sections.

In this part of the memory, the theoretical synthesis for the introduction of TZs into any planar filter structure will be addressed. First, basic network configurations for filter design will be presented. Next, fundamental concepts about impedance matching (elemental part of the circuit and mathematical theoretical analysis) will be reviewed. Finally, the synthesis methodology for the design of independent and adjustable TZs will be described.

2.3.1 Network Topologies for Filter Design

A filter is a reactive network that freely passes the desired bands of frequencies while almost totally suppressing all other bands. Theoretically, this network is composed of purely reactive elements, since otherwise the attenuation would never reach zero in the passband. In practice, this zero attenuation is not achieved, since the elements are never purely reactive and have small losses.

Filters are composed of symmetric 'T' or 'π' sections. These 'T' and 'π' sections, at the same time, can be considered as combinations of L-sections, formed by two elements: one in series and the other one in parallel, as can be seen in Figure 2.11.
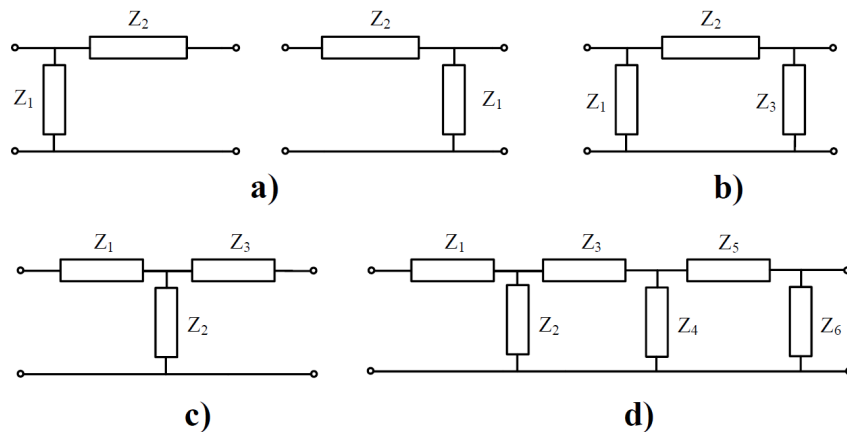
Figure 2.11: Network topologies. a) L sections. b) π network. c) T network. d) Ladder network.

Then, depending on the configuration of the elements, in any structure it is possible to obtain a lowpass characteristic (inductances in series), highpass (capacitors in series), bandpass (series resonator in series or parallel resonator in parallel) or bandstop (parallel resonator in series or series resonator in parallel).

Finally and as shown before (Figure 2.2), the ladder network structure, the most typical and used topology for filter design, is composed or can be seen as a cascade connection of several 'L', 'T' or 'π' sections.

2.3.2 Impedance Matching

Impedance matching consists of making that two different terminations (Z_{SOURCE}, source, and Z_{LOAD}, load) can be coupled efficiently within a certain frequency range. This is necessary since RF communication systems are integrated of different networks or electronic circuits that are interconnected with each other. On the other hand, the power level in this area is normally small, this means that it is necessary to obtain a condition of maximum power transfer when the connection is produced. Maximum power transfer is achieved when the resistive component of the source is identical to the load, and the reactances are canceled ($Z_{SOURCE} = Z_{LOAD}^*$). Therefore, the task will be to develop a network that can transform the source impedance into the load impedance cancelling its reactive parts simultaneously.

There are different matching networks that can be used. The main factors to be considered for selecting one or the other are its frequency response, operational bandwidth, complexity and ease of implementation. In this section, we will exclusively describe the impedance matching by means of LC networks of two elements, which is the method used and selected (according to the aforementioned factors) for the design of the proposed structures in this work.

In general, for the impedance transformation we will consider impedances formed by a real part R (resistance) and an imaginary part X (reactance). This implies, configurations resistive - capacitive (RC) in series or in parallel, or circuits resistive - inductive (RL) in series or in parallel, which need to be transformed appropriately. Table 2.1 shows the most common impedance transformations, together with their corresponding equations. Only general expressions and those for series-to-parallel conversion are provided, since to apply the inverse conversion (parallel-to-series) it would only be necessary to isolate the elements with subscript 'S' from the given expressions and consider Q_P instead of Q_S.
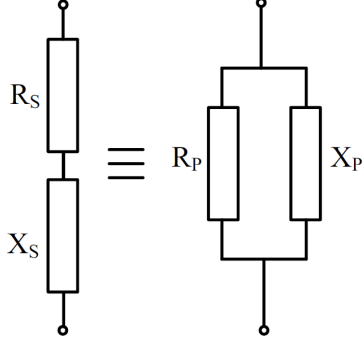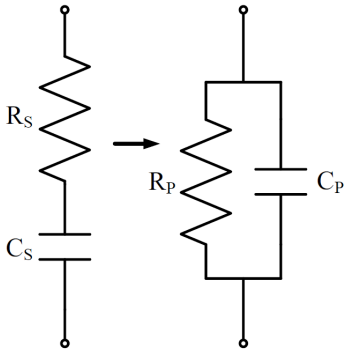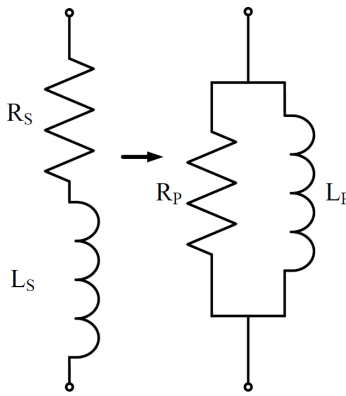
GENERAL CASE	$Q = Q_S = \frac{X_S}{R_S} \quad (2.11a)$ $Q = Q_P = \frac{R_P}{X_P} \quad (2.11b)$ $\frac{R_P}{R_S} = Q^2 + 1 \quad (2.12)$ $\frac{X_P}{X_S} = \frac{Q^2+1}{Q^2} \quad (2.13)$
RC - SERIES TO PARALLEL	$Q = Q_S = \frac{X_S}{R_S} = \frac{1}{\omega R_S C_S}$ $R_P = R_S(1 + Q^2) \quad (2.14)$ $C_P = \frac{C_S}{1+\frac{1}{Q^2}} \quad (2.15)$
RL - SERIES TO PARALLEL	$Q = Q_S = \frac{X_S}{R_S} = \frac{\omega L_S}{R_S}$ $R_P = R_S(1 + Q^2)$ $L_P = L_S\left(1 + \frac{1}{Q^2}\right) \quad (2.16)$

Table 2.1: Impedance transformations. RC and RL series-to-parallel impedance conversions.

The simplest impedance transformation network is the 'L' network, which requires only two reactive elements. As in filters case, such a network can have a highpass or lowpass characteristic. Table 2.2 shows the two possible 'L' configurations, together with their design equations for purely resistive sources and loads.

Basic L-networks topologies and their design equations.
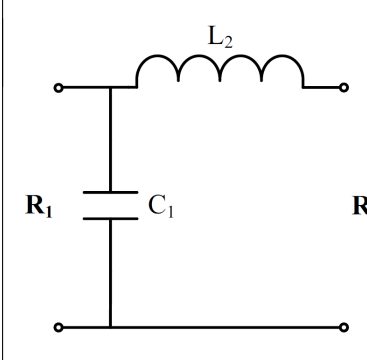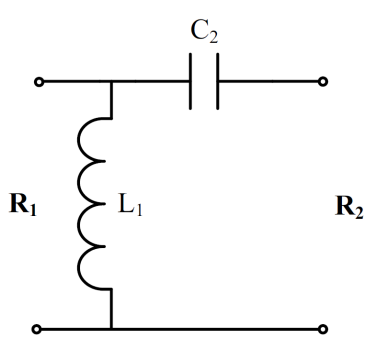
$$\omega C_1 = \frac{Q}{R_1} \qquad\qquad \omega L_1 = \frac{R_1}{Q}$$

$$\omega L_2 = Q \cdot R_2 \qquad\qquad \omega C_2 = \frac{1}{Q \cdot R_2}$$

$$Q = \sqrt{\frac{R_1}{R_2} - 1} \quad (2.17)$$

$$R_1 > R_2$$

Table 2.2: Basic L-networks topologies and their design equations.

It has to be noticed that the Q of the network is determined by the ratio of impedances to be matched and not by the designer. Therefore, for small impedance transformations, the networks in 'L' are of low Q; and for large transformations of impedance, the L-networks are of high Q. Also, equation (2.17) requires that the reactance in parallel of the 'L' structure to be placed on the side of the highest impedance.

Finally, it should be mentioned that there are other impedance matching networks of three reactive LC elements called 'T' and 'π' networks, which provide greater flexibility in the choice of design parameters (e.g. Q). However, they present a frequency response that is of narrower bandwidth than the one of a simple L-network, which is of narrow band too (impedance matching is perfectly achieved only at the design frequency and in a range of frequencies around it, which normally does not exceed of 40% [74]).

2.3.3   Synthesis of Transmission Zeros. Bisected π Terminations.

With the elementary theory outlined, we can now address the synthesis of the transmission zeros (TZs) of our designs. Thus, the topology of the sections proposed to include TZs in a filter response is shown in Figure 2.12. These are bisected π-sections (BPS) that are cascaded at the filter input/output.They can also be understood as 'L' networks where the impedance of the shunt branch is formed by an LC resonator.
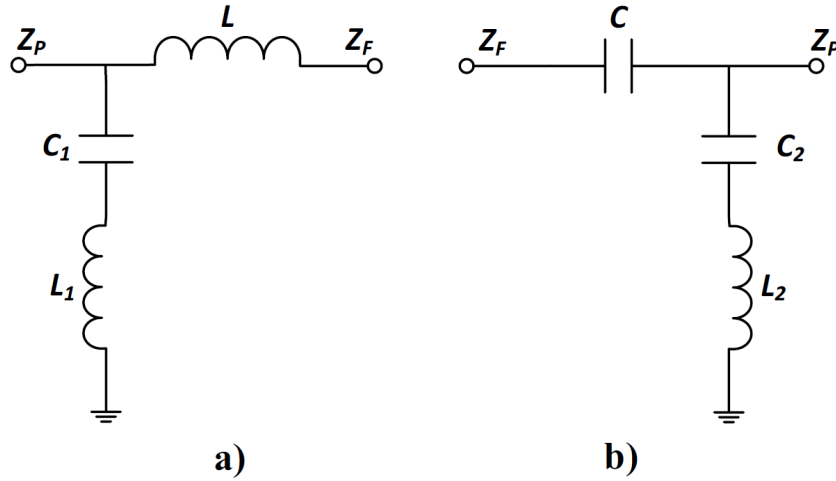
Figure 2.12: Ideal circuit schematics of the proposed terminating sections to introduce TZs. a) Lowpass section. b) Highpass section.

As can be deduced, the section that introduces a TZ located at upper frequencies than the filter passband, will present a lowpass response (inductance L in series); whereas the section that introduces a TZ at lower frequencies than the passband will have a highpass response (capacitance C in series). This allows the introduction of the TZ at desired frequencies without disturbing the in-band filter response.

The study of each network is performed as follows:

- Terminating Lowpass Section (TZ at the upper stopband, Figure 2.12a):

Analyzing the proposed scheme, we see that the frequency of the TZ, ω_{TZ}, will be determined by the series resonator $L_1 - C_1$, through the next expression:

$$\omega_{TZ}^2 = \frac{1}{L_1 C_1} \tag{2.18}$$

On the other hand, the connection of this cell with the filter terminations has to be done under certain matching conditions in order to keep the level of in-band return loss, while enabling at the same time to locate the TZ at the prescribed frequency.

In this way, applying the series-to-parallel conversion (equations (2.11a), (2.14) and (2.16)) and forcing a matching condition between the port impedance, Z_P, and the load seen by the lowpass section (i.e. the filter impedance, Z_F) at the filter center frequency, ω_0, we obtain the following expressions for the network elements:

$$L = \frac{Z_F \sqrt{\frac{Z_P}{Z_F} - 1}}{\omega_0} \tag{2.19}$$

$$C_1 = \frac{\omega_{TZ}^2 - \omega_0^2}{\omega_{TZ}^2 \omega_0} \cdot \frac{\sqrt{\frac{Z_P}{Z_F} - 1}}{Z_P} \tag{2.20}$$

$$L_1 = \frac{1}{\omega_{TZ}^2 C_1} \tag{2.21}$$

As the series matching element must be placed next to the termination with smallest resistance, we shall assume that $Z_P > Z_F$ without loss of generality.

- Terminating Highpass Section (TZ at the lower stopband, Figure 2.12b):

Proceeding similarly in obtaining the design equations for the dual network, the resonance and the impedance matching conditions are imposed. The resonator $C_2 - L_2$ will provide the desired TZ and, in this case, the series-to-parallel conversions that need to be applied correspond to the expressions (2.11a), (2.14) and (2.15). Thus:

$$C = \frac{1}{\omega_0 Z_F \sqrt{\frac{Z_P}{Z_F} - 1}} \tag{2.22}$$

$$C_2 = \frac{\omega_0^2 - \omega_{TZ}^2}{\omega_{TZ}^2 \omega_0} \cdot \frac{Z_P - Z_F}{Z_F Z_P \sqrt{\frac{Z_P}{Z_F} - 1}} \tag{2.23}$$

$$L_2 = \frac{1}{\omega_{TZ}^2 C_2} \tag{2.24}$$

This set of equations establishes the circuit values for both bisected π-networks in terms of ω_{TZ}, ω_0, Z_F and Z_P. For instance, the theoretical response of the proposed networks with $f_0 = 4$ GHz, $Z_F = 35 \ \Omega$, $Z_P = 50 \ \Omega$ and $f_{TZ} = 4.5$ GHz for the lowpass terminating section, and with $f_{TZ} = 3.5$ GHz for the highpass terminating section, can be observed in Figure 2.13.
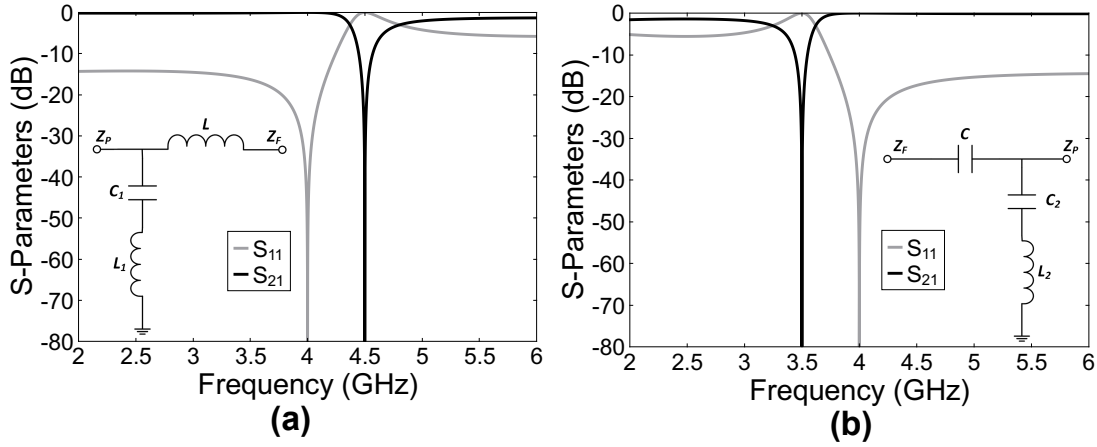
Figure 2.13: Ideal S-parameters rsponses of the proposed bisected π - networks. (a) Lowpass Section for f_{TZ} = 4.5 GHz, f_0 = 4 GHz, Z_F = 35 Ω and Z_P = 50 Ω. (L = 0.9 nH, C_1 = 0.1 pF and L_1 = 11 nH). (b) Highpass Section for f_{TZ} = 3.5 GHz, f_0 = 4 GHz, Z_F = 35 Ω and Z_P = 50 Ω. (C = 1.7 pF, C_2 = 0.16 pF and L_2 = 13 nH).

In the graphs, we can verify both, the presence of the TZs at the frequencies established for each case, and the matching frequency set to f_0 = 4 GHz. Moreover, as it has been proved, this technique uses an external structure which is matched and cascaded at the filter input/output, allowing the introduction of TZs without affecting the filter response. Furthermore, the described procedure is simple and general, thus an independent flexible and controllable location of TZs (above or below the passband), providing also equations for the synthesis of each network element required.

2.4 Application Case I: Microwave Filters with Ultra-Wide Spurious Free Stopband

As seen in chapter 1, the addition of TZs in filter responses is used to improve selectivity and/or eliminate nearby interferences, as well as to cancel spurious frequencies and achieve rejection bands with better characteristics (e.g. wider, with higher attenuation level, etc.). A wide spurious-free stopband is a typical requirement in bandpass filter designs employed, for example, in frequency conversion applications with image frequency rejection as shown in Figure 2.14.

The filters in the shown diagram are basically in charge of properly selecting the output spectrum of the amplifiers. For this reason, in these filters (operating at intermediate frequencies, IFs, between 1 - 4 GHz) high rejection levels are generally required up to 3-7 times f_0. For this purpose, the design of a wide stopband microstrip filter providing high rejection levels is going to be described. The presented terminating bisected π-sections
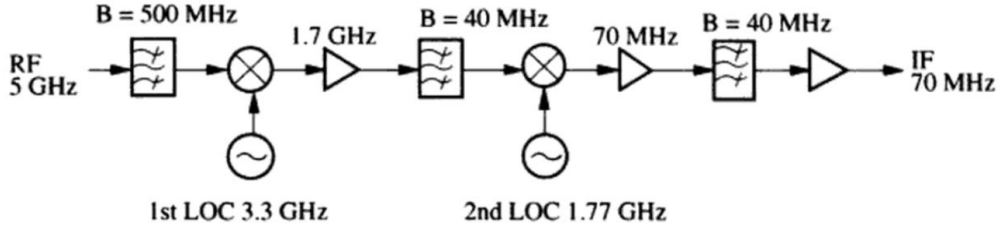
Figure 2.14: Example of a frequency converter in the receiving stage using the double-conversion system [75].

for introducing TZs will be used. In this case, to attenuate and improve the out of band of the filter we will employ exclusively the lowpass cell, since its spurious responses are located at frequencies higher than its passband.

2.4.1 Lumped Lowpass Bisected π Section with Parasitics

Considering the application goal and the described networks, lumped and/or quasi-lumped elements can be good candidates for implementing the proposed cell. Regarding lumped components, they allow further miniaturization, do not show periodicity within the operating frequency range, and as it will be demonstrated they enable us to introduce additional TZs due to the series self-resonance of the inductor L.

Studying the ideal S-parameters response and the synthesis values for the proposed terminating lowpass network, in the case of placing the TZs farther from the matching frequency, f_0, some slight differences can be appreciated (see Figure 2.15).

The frequency response has similar features to those shown in the synthesis of the TZs, however, the values of the elements obtained are of different order of magnitude. This is logical and is reflected in the synthesis equations (2.19)-(2.21). In them, it can be observed that the proximity of the TZ with respect to the matching frequency, f_0, notably affects the obtained values for the elements of the networks. In additon, it should be noticed that another design parameter, which also involves different results in the equations, has been modified. This parameter is the impedance ratio. In this case, a port impedance of 60 Ω and a typical load (filter) impedance of 50 Ω have been considered.

Now, considering the real equivalent model where parasitics are included, as illustrated in Figure 2.16 (a), interesting effects are produced. Analyzing the influence of the self-resonance frequency (SRF) of each lumped component, it is obvious that the series inductance L and the shunt capacitor C_1 are the elements that can introduce additional TZs in the response due to each component self-resonance. Thus, the series inductor L would generate an additional TZ at a finite frequency depending on its parasitic capacitance value C_P. On the contrary, no additional TZ would be produced by the shunt
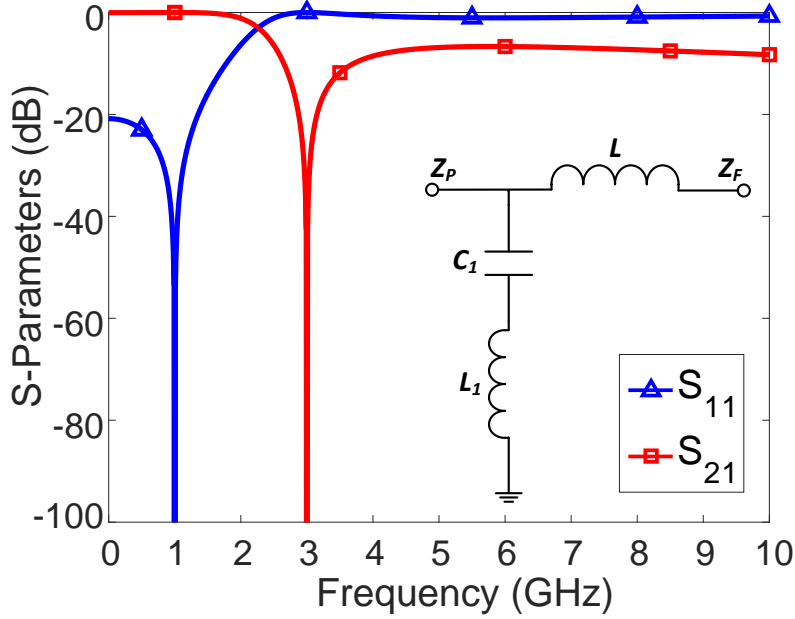
Figure 2.15: S-parameters response of the lowpass terminating section with ideal lumped elements for $f_{TZ} = 3$ GHz, $f_0 = 1$ GHz, $Z_F = 50\ \Omega$ and $Z_P = 60\ \Omega$. ($L = 3.6$ nH, $C_1 = 1$ pF and $L_1 = 2.7$ nH).

capacitor, due to the absorption of the parasitic inductance L_{LS1} (lower value) into the shunt inductor L_1 (higher value).

Therefore, although the self-resonance phenomenon of lumped elements is generally a drawback in most RF and microwave circuits, in these cells it can be used profitably to improve the filter stopband response. To do this, it is necessary to control the position of this TZ, so an additional capacitor C_{add} is added in parallel with the inductance L, as shown in Figure 2.16 (b). Hence, the SRF originated by L can be shifted to lower frequencies by increasing the value of C_{add}. A first value of the required capacitance can be obtained from the desired TZ frequency location, by taking into account the parasitic contribution C_P of the real inductor and the stray capacitance from the SMD assembly pads.

Finally, due to the low values required in the L_1 parameter when the TZ is located far from f_0, the shunt inductor L_1 can be easily implemented using a quasi-lumped short-circuited stub with l « $\lambda/8$.

To demonstrate all the described effects, the ideal network of Figure 2.15 has been simulated using commercial SMD components (*Coilcraft - 0402HP*: $L = 3.6\ nH$ and $L_1 = 2.7\ nH$, and *AVX-Accu-P 0402*: $C_1 = 1\ pF$), and the results are presented in Figure 2.17 (a). The response is similar to the theoretical one, since the matching and the TZ are maintained at 1 GHz and 3 GHz, respectively, but a second TZ appears at
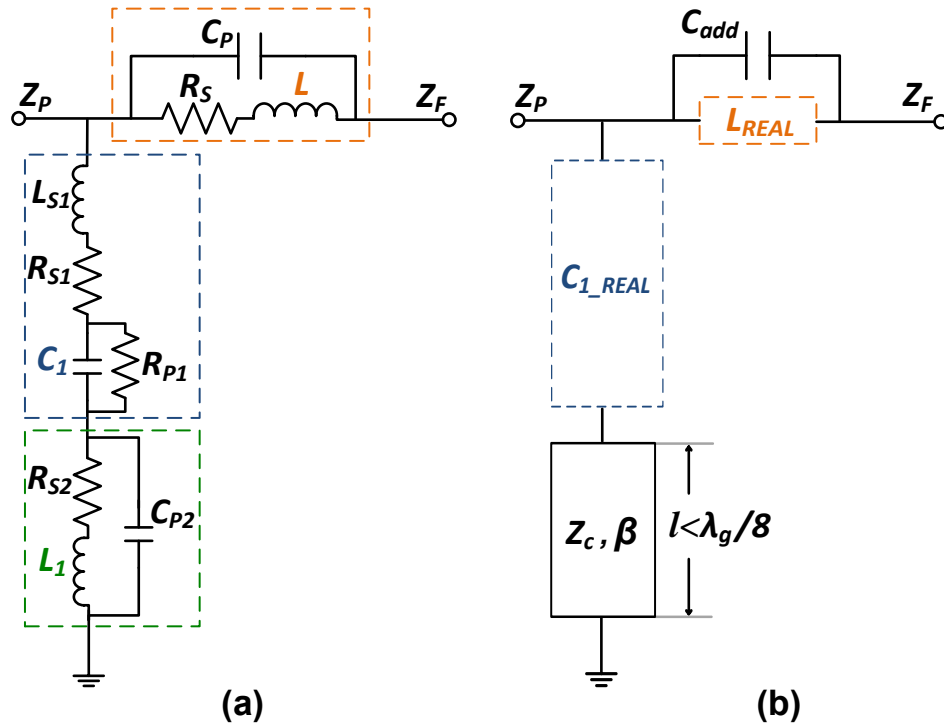
Figure 2.16: Lumped bisected π-section. (a) Equivalent circuit of the network with real lumped elements. (b) Modified lumped bisected π-section.
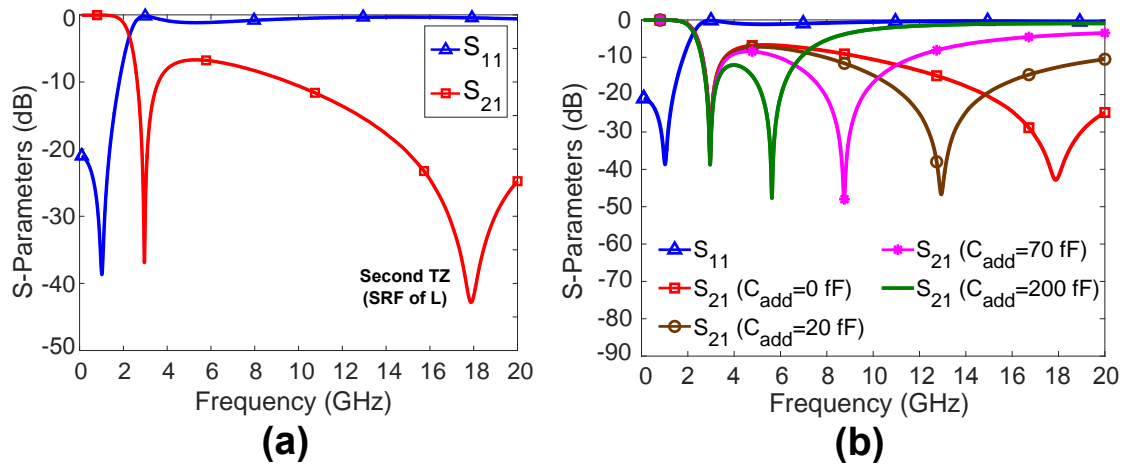
Figure 2.17: Transmission and reflection characteristics of the lumped bisected π - sections with parasitics. (a) Real lumped elements cell. (b) Tunability of the second TZ vs different values of C_{add}.

18 GHz originated from the SRF of the real inductance L. In this context, the tuning of this second TZ with different values of C_{add} can also be observed in Figure 2.17 (b), where small values of C_{add} are needed to shift this TZ in a wide frequency range.

2.4.2   Filter Design

● **Strongly-Loaded Microstrip Combline Filter**

In line with the explained concepts and to validate them, the design of a bandpass filter with an ultra-wide spurious free stopband of the following characteristics is proposed:

– 3-pole Chebyshev bandpass filter with 0.1 dB of passband ripple.
– Fractional Bandwidth, FBW = 10%.
– Center frequency, $f_0 = 1$ GHz.
– Frequency of the first spurious response, $f_1 > 2 \cdot f_0$ (In order to obtain, from the design of the filter itself, a moderately wide rejection band).

It is well-known that in combline filters the frequency of the first spurious band can be controlled by a proper resonator design. Thereby, this combline topology will be the one selected for the filter design.

According to the specifications and following the combline filter design process detailed in [65], the lowpass prototype coefficients for a 3-pole 0.1 dB ripple Chebyshev response are:

$$g_0 = g_4 = 1, \quad g_1 = g_3 = 1.0136, \quad g_2 = 1.1474$$

Resonator and input/output port impedances are chosen as $Z_a = 65 \ \Omega$ and $Z_A = 50 \ \Omega$ respectively. Then, the resonator length is set slightly below $\lambda_{g_0}/8$ by strongly loading the microstrip line using discrete capacitors, thus moving the first spurious band up to $4 \cdot f_0$ (meeting comfortably with the f_1 requirement). Consequently, the use of strongly loaded resonators not only allows to achieve wider rejectin bands, but also implies more compact filter structures. The required parameters of the filter (i.e., slope parameter b, lumped capacitance C_d and admittance inverter values $J_{i,i+1}$) can be obtained from the corresponding expressions shown in Table 2.3.

Figure 2.18 shows the full-wave EM simulation results of the designed filter. The designed combline filter block can be seen in Figure 2.19, within a box of dashed blue line. As expected, the passband requirements are met, obtaining better RL than 14 dB over the entire bandwidth and 0.67 dB of IL at the center frequency. In the same way, the out-of-band requirements also satisfy what was expected, with two spurious bands appearing in the frequency range up to 12 GHz, the first one being located at 4 GHz, and the second at 7 GHz, achieving a rejection greater than 25 dB up to $3.5 \cdot f_0$.

Parameter	Result	Layout Value
Z_A	50 Ω	2.153 mm
Z_a	65 Ω	3.5 mm
$\theta_0 = \beta l; \ l = \frac{\lambda_{g_0}}{8}$	40°	$l_1 = l_3 = 21.728$ mm; $l_2 = 20.728$ mm
$b = \frac{cot\theta_0 + \theta_0 csc^2\theta_0}{2Z_a}$	0.022	–
$C_d = \frac{cot\theta_0}{Z_a\omega_0}$	2.9 pF	2.2 pF 0402 AVX-Accu-P
$J_{01} = J_{34} = \sqrt{\frac{bFBW}{g_0 g_1 Z_A}}$	0.007	180 μm
$J_{12} = J_{23} = bFBW\sqrt{\frac{1}{g_1 g_2}}$	0.002	2.53 mm

Table 2.3: Filter synthesis and layout values.
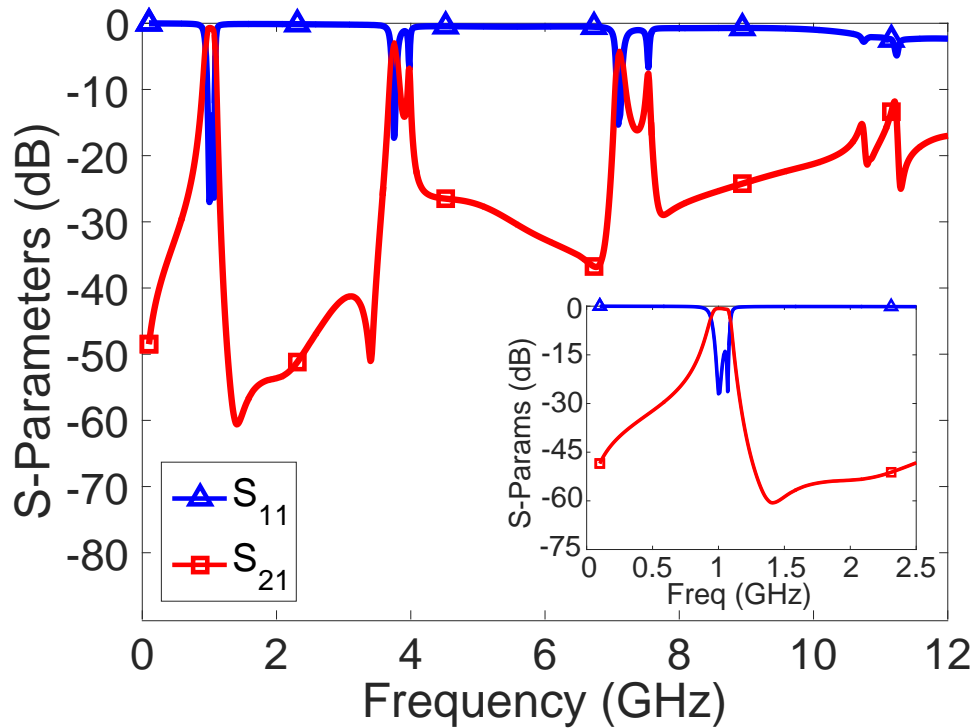
Figure 2.18: EM simulation results of the strongly-loaded microstrip combline bandpass filter.

- **Filter with Four Transmission Zeros**

In order to truly achieve an ultra-wide rejection band in the filter, it is convenient to attenuate these two spurious bands that appear around 4 and 7 GHz. Let us set as a goal, to achieve an attenuation greater than 30 dB up to $10 \cdot f_0$. To do this, two lumped BPS networks are added to the designed filter structure, one at the input and the other at the ouput. In this manner, it is possible the introduction of four TZs at different frequencies to suppress the two additional undesirable spurious bands. The frequency distribution of TZs has to be done adequately. Therefore, an optimization procedure combining the 3D EM simulation of the filter with the circuital models of the terminating cells has been performed. The proper location of the TZs and the corresponding element values are shown in Table 2.4.
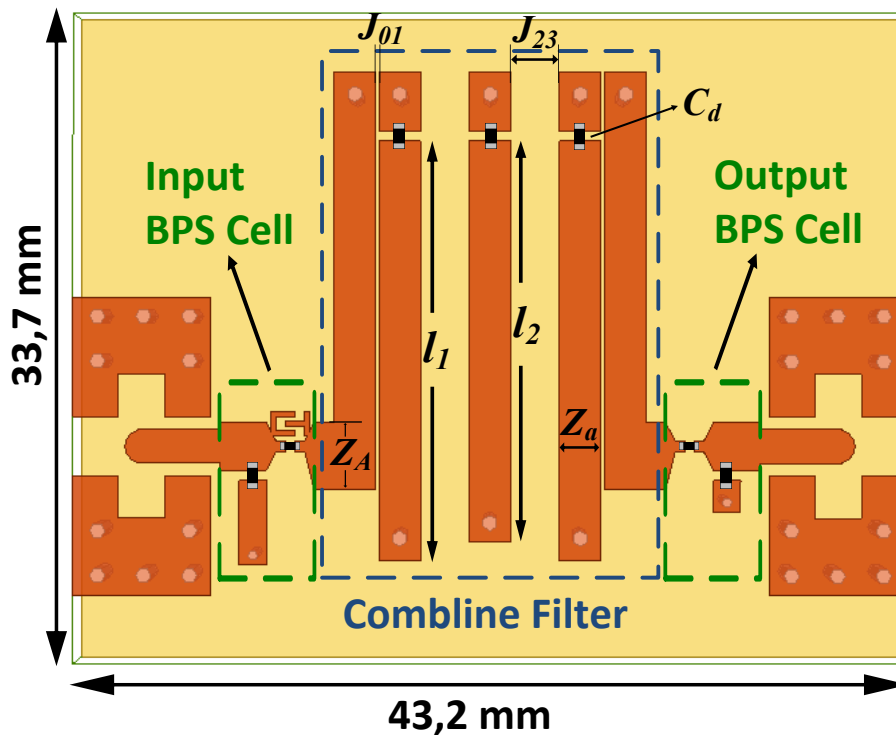
Figure 2.19: Layout of the microstrip combline filter with two lumped bisected π-network.

As the filter impedance $Z_F = Z_A$ is 50 Ω, the input/output port impedance Z_P is chosen as 60 Ω. The ratio $\frac{Z_P}{Z_F}$ must be a trade-off between matching bandwidth and practical implementation of filter and port impedances, as well as of values obtained for lumped elements.

Frequency	Method	Parameters Values
$f_{TZ1} = 3$ GHz	Input section L-L_1-C_1	$L = 3.6$ nH $C_1 = 1.1$ pF $L_1 = 2.7$ nH
$f_{TZ2} = 3.85$ GHz	Output section L-L_1-C_1	$L = 3.6$ nH $C_1 = 1$ pF $L_1 = 1.5$ nH
$f_{TZ3} = 7$ GHz	SRF of L of Input section	$C_{add} = 150$ fF
$f_{TZ4} = 9.5$ GHz	SRF of L of Output section	$C_{add} = 80$ fF

Table 2.4: Frequency distribution of TZs and results of the cell parameters.

The implementation of the cell parameters, shown in Table 2.4, have been made using lumped elements, with the exception of the L_1 inductors that have been implemented through short-circuited stubs of $Z_0 = 80.5\ \Omega$ and via diameter of 0.5 mm. The stub lengths are 4.4 mm and 1.65 mm for the input and output BPS cells, respectively.

The TZs originated by the SRF of L are also influenced by the SMD package stray capacitance that has been estimated in 70 - 80 fF using 3D EM simulations. Thus, no additional capacitance is needed at the output cell, while a $C_{add} = 70$ fF is required at the input section. An interdigital capacitor structure, consisting on 3 fingers of 1.5 mm of length and 0.25 mm of width and gap, are used to reach this capacitance value.

The layout of the complete filter is depicted in Figure 2.19. The occupied area is only 43x33 mm^2 for a 1 GHz filter. It should be remarked the negligible size increment ought to the insertion of both terminating BPS cells. The simulation results of the full structure are shown in Figure 2.20. The introduction of 4 TZs allows to achieve the proposed requirements, and to attenuate the two spurious bands that were intended to be mitigated. As can be seen in the results, the IL and RL remain almost the same as for combline filter without the BPS sections.
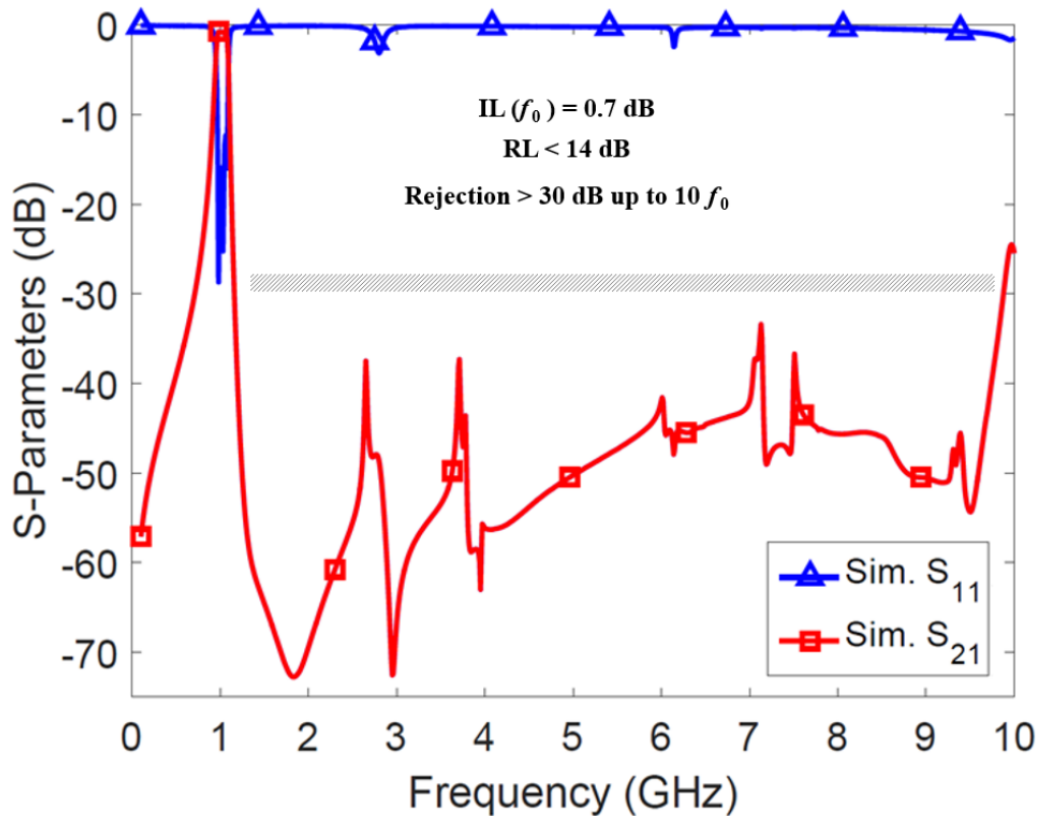
Figure 2.20: EM simulation results of the strongly-loaded microstrip combline bandpass filter with 2 lumped BPS cells.

- **Experimental Results**

After achieving good EM simulation results, the next step is to manufacture the designed filter and verify with measurements its agreement with simulations results. Thus, the filter has been fabricated in a 1.524 mm-thick Rogers RO4003C substrate ($\epsilon_r = 3.55$, $tan\delta = 2.7 \cdot 10^{-3}$). A photograph of the manufactured device is shown in Figure 2.21. Measured S-parameters results can be seen in Figure 2.22, and are in very good agreement with the simulated values. The mid-band IL are 1.2 dB, with RL better than 13 dB within a 3-dB bandwidth of 12%. A rejection higher than 22 dB is obtained up to 10 GHz, providing an ultra-wide stopband even if a slight frequency shift of some TZs can be observed, due to the fabrication tolerances regarding the interdigital capacitor.
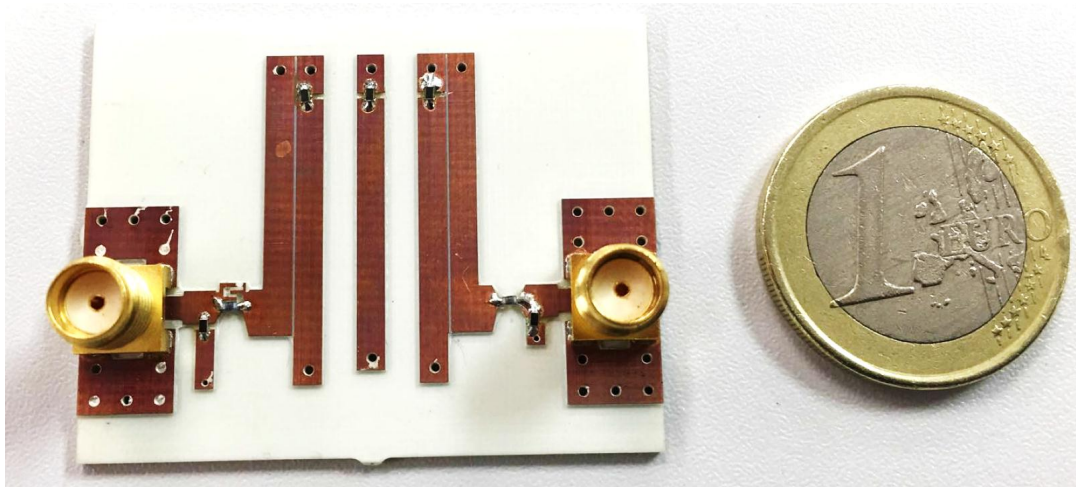
Figure 2.21: Photograph of the fabricated filer.
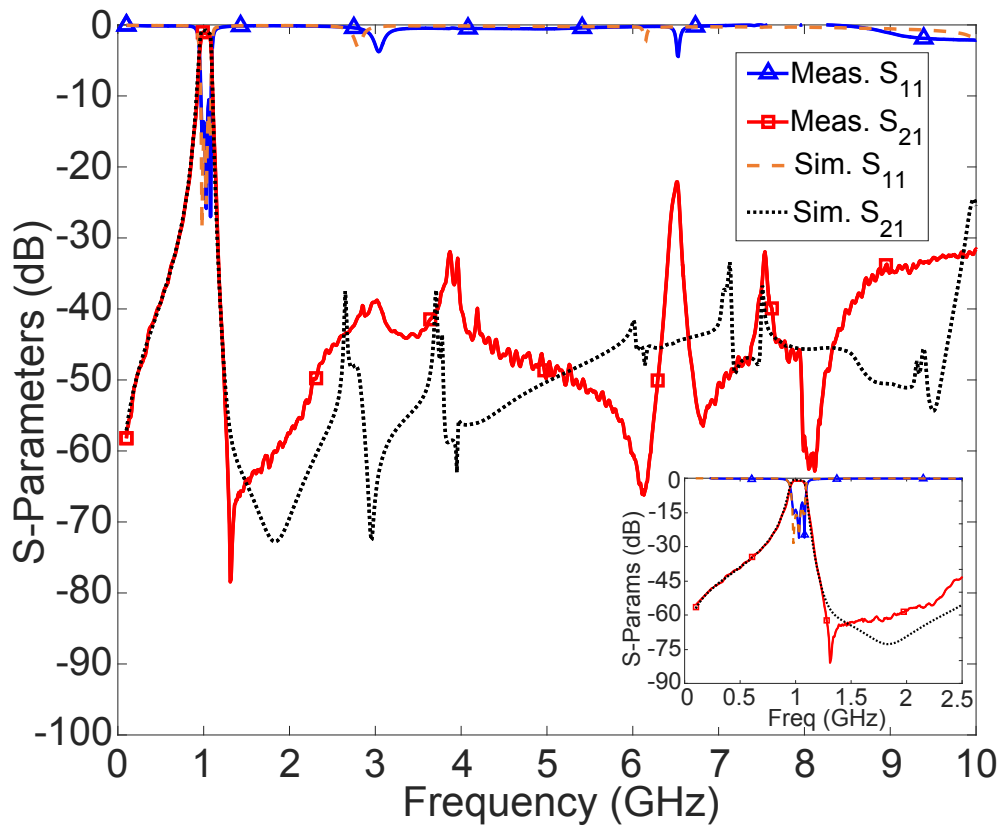
Figure 2.22: Measurements of the fabricated filter compared with its EM simulations.

2.5 Application Case II: Microwave Filters with Improved and Highly Selective Responses.

In this section, the design of four bandpass filters with selective responses, thanks to the developed technique of introduction of TZs, will be addressed. We will focus on the mechanism used to introduce zeros in the response, trying to reflect the potential, flexibility and the different possibilities offered by making use of the proposed technique. In this way, the design of a classic filtering structure (bandpass filter of parallel coupled lines) will be initially presented. It will be employed with different configurations and distributions of TZs by adding the studied BPS terminations. Finally, we will use a different filter topology (combline), demostrating its general applicability, to design a quasi-elliptical filter, placing the TZs even closer to the passband.

2.5.1 Filter Design

A 3-pole Chebyshev bandpass filter centered at $f_0 = 4$ GHz, with 5% FBW and in-band RL higher than 20 dB, implemented in microstrip techonology is proposed.

- **Synthesis**

  Based on the above, the corresponding lowpass prototype coefficients are:

$$g_0 = g_4 = 1, \qquad g_1 = g_3 = 0.8516, \qquad g_2 = 1.1032$$

Its schematic is shown in Figure 2.23 a), while the bandpass prototype after the proper transformations appears in Figure 2.23 b).
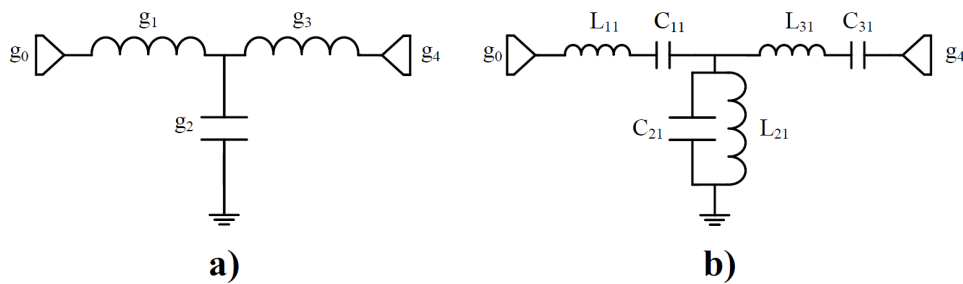
Figure 2.23: Synthesis of filter prototypes. a) Lowpass prototype. b) Bandpass prototype.

Starting from the bandpass prototype, and using the admittance inverters, it is obtained the next structure for implementing the filter (see Figure 2.24).

Analyzing the prototype circuit model, and from the exposed theory, the element values can be calculated using the following expressions:
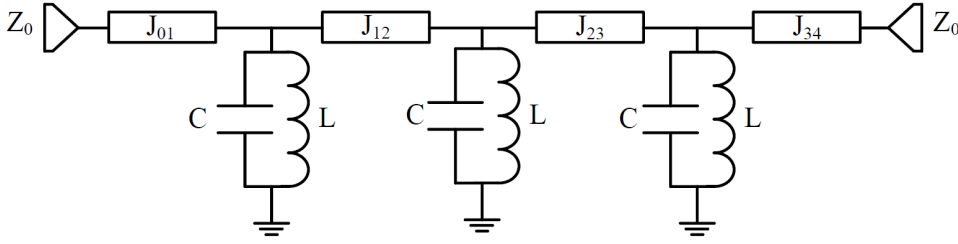
Figure 2.24: Prototype of the bandpass filter using admittance inverters and LC resonators in parallel.

$$J_{01} = J_{34} = \sqrt{\frac{Y_0 FBW b_1}{\Omega_c g_0 g_1}}; \quad J_{12} = J_{23} = \frac{FBW}{\Omega_c}\sqrt{\frac{b_1 b_2}{g_1 g_2}} \tag{2.25}$$

where Y_0 is the input/output characteristic admittance of the filter, derived from the characteristic impedance ($Y_0 = \frac{1}{Z_0}$) that is a typical design parameter. In this case, the input/output port impedance for the filter is set as $Z_0 = 35\ \Omega$. This level will be scaled up to an end port impedance of $Z_P = 50\ \Omega$ once the terminating sections are added.

As previously explained in this chapter, the design equations of these terminating networks are based on matching conditions. The matching is performed through L networks of two elements. In this kind of matching networks, the Q is set by the network itself, not being a design parameter (equation (2.17)). In this way, the proper ratio Z_P/Z_F is chosen as a trade-off between matching bandwidth and practical implementation of the filter and port impedances, as well as feasibility of the element values of the BPS terminating sections.

The slope parameter, b_i, is another design parameter that we will set and will be the same for all resonators, being calculated through:

$$b = \frac{\omega_0}{2}\frac{dB(\omega)}{d\omega}\Big|_{\omega=\omega_0} \tag{2.26}$$

The susceptance, $B(\omega)$, is the imaginary part of the admittance of the resonators, and for those of the prototype in Figure 2.24 it is:

$$Y = \frac{1}{j\omega L} + j\omega C = j\left(\omega C - \frac{1}{\omega L}\right) \Rightarrow B(\omega) = \left(\omega C - \frac{1}{\omega L}\right) \tag{2.27}$$

Applying now the equation 2.26 we can obtain that:

$$b = \frac{\omega_0}{2}2C = \omega_0 C \qquad (2.28)$$

With this expression and setting b=1, we can obtain the values for all the elements of the filter prototype (Table 2.5)

ELEMENT	EXPRESSION	VALUES
Z_0	-	35 Ω
C	$\frac{b}{\omega_0}$	39.8 pF
L	$\frac{1}{\omega_0^2 C}$	39.8 pH
$J_{01} = J_{34}$	$\sqrt{\frac{Y_0 FBW b_1}{\Omega_c g_0 g_1}}$	0.041
$J_{12} = J_{23}$	$\frac{FBW}{\Omega_c}\sqrt{\frac{b_1 b_2}{g_1 g_2}}$	0.051

Table 2.5: Summary of the equations and element values of the 4 GHz filter prototype (Figure 2.24).

In next Figure 2.25, we can check that the theoretical design meets the specifications of this example.
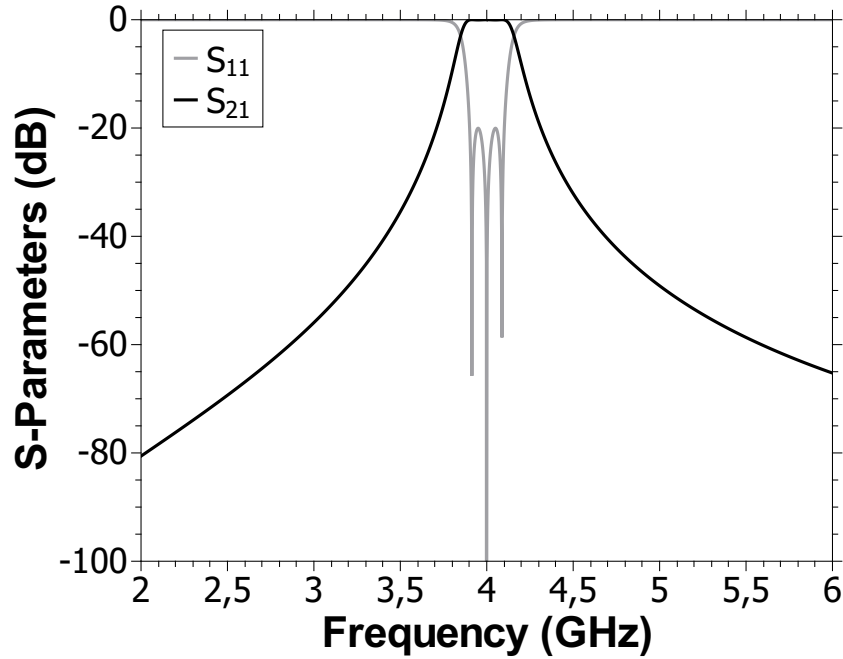
Figure 2.25: S-parameters response of the bandpass filter using admittance inverters and LC resonators in parallel.

- **Design**

The filter will be implemented in microstrip technology using a 508 μm-thick Rogers RO4003C substrate ($\epsilon_r = 3.55$, $tan\delta = 2.7{\cdot}10^{-3}$) with a metallization of 35 μm of copper and 5 μm of nickel-gold finishing. Specifically, it will be used a known topology of parallel coupled $\lambda/2$ resonators, characterized by the absence of any via to the ground plane or lumped elements, which makes the design simpler.

For the design process, the group delay method (presented in [76] by Ness) will be applied. This method is based on the measurements of the group delay of the reflection coefficient, S_{11}. The frequencies of each coupled resonator and the couplings coefficients can be deduced from these group delay results. The advantage of this method is that provides a systematic and sequential approach for adjusting the filter response.

The equations used for the calculations of the group delay in the proposed 3-pole filter are given next:

$$\Gamma_{d1} = \frac{4Q_{ext}}{\omega_0}; \quad Q_{ext} = \frac{g_0 g_1}{FBW} \tag{2.29}$$

$$\Gamma_{d2} = \frac{4}{\omega_0 Q_{ext} k_{12}^2}; \quad k_{12} = \frac{FBW}{\sqrt{g_1 g_2}} \tag{2.30}$$

where Q_{ext} is the external Q factor, and k_{12} is the coupling coefficient between resonators 1 and 2. In our filter case, these parameters are $Q_{ext} = 17$ and $k_{12} = 0.051$, and by substituting in the previous formulas we obtain:

$$\Gamma_{d1} = 2.71 \text{ ns} \quad \Gamma_{d2} = 3.51 \text{ ns}$$

These group delay values should be reached at the filter center frequency, and with aproximated shapes shown next in Figure 2.26.

Figure 2.26: Group delay frequency response for one resonator (left), and for two couple resonators (right).

A good starting point for the application of the Ness method is obtained with the following considerations:

The total length of the resonator is iniatially calculated as $\lambda/2$ at f_0:

$$l = \frac{\lambda}{2} = \frac{\lambda_0}{2\sqrt{\epsilon_r}} = \frac{c}{2f_0\sqrt{\epsilon_r}} = 19 \ mm \tag{2.31}$$

Moreover, each resonator is parallel-coupled with its adjacent along half of its length ($\approx \lambda/4$), where an step-impedance is then produced. Therefore, as starting values, these coupled section lengths will be of $\lambda/4$. Then, the even- and odd-mode characteristic impedances of the coupled microstrip line resonators are determined by:

$$(Z_{0e})_{j,j+1} = \frac{1}{Y_0}\left(1 + \frac{J_{j,j+1}}{Y_0} + \left(\frac{J_{j,j+1}}{Y_0}\right)^2\right) \qquad j = 0 \ to \ n \tag{2.32}$$

$$(Z_{0o})_{j,j+1} = \frac{1}{Y_0}\left(1 - \frac{J_{j,j+1}}{Y_0} + \left(\frac{J_{j,j+1}}{Y_0}\right)^2\right) \qquad j = 0 \ to \ n \tag{2.33}$$

Finally, the width of the excitation line, related to Y_0, corresponds to the selected value for Z_0 of 35 Ω.

With these data, we begin with the proper adjustment of the response until reaching the final structure of the parallel coupled-line bandpass filter (see Figure 2.27), which presents an EM simulation results as shown in Figure 2.28. The layout values of the designed filter are collected in Table 2.6.

From the simulation results, it is confirmed that the design meets the specifications, presenting RL better than 20 dB in the filter bandwidth and IL at center frequency of 2.7 dB. This high value of IL is due to the inclusion of nickel metallization in the EM simulation model.
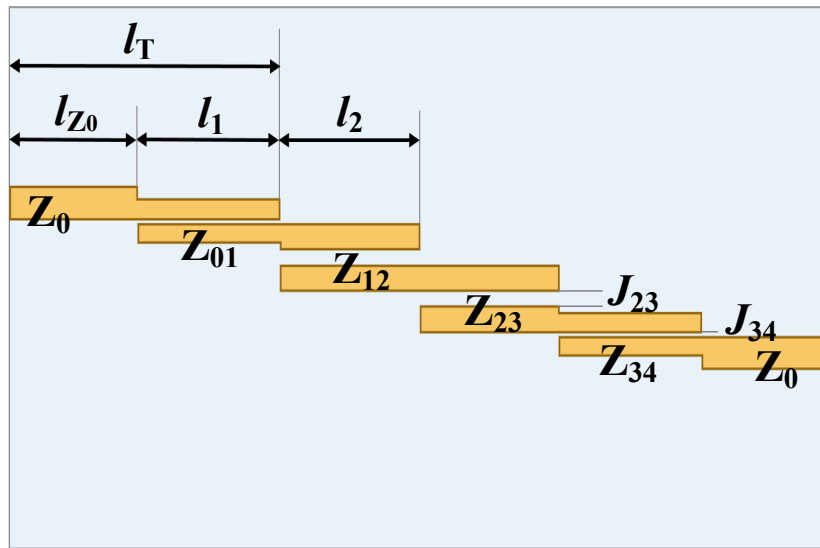
Figure 2.27: Layout of the conventional microstrip parallel coupled-line bandpass filter designed.
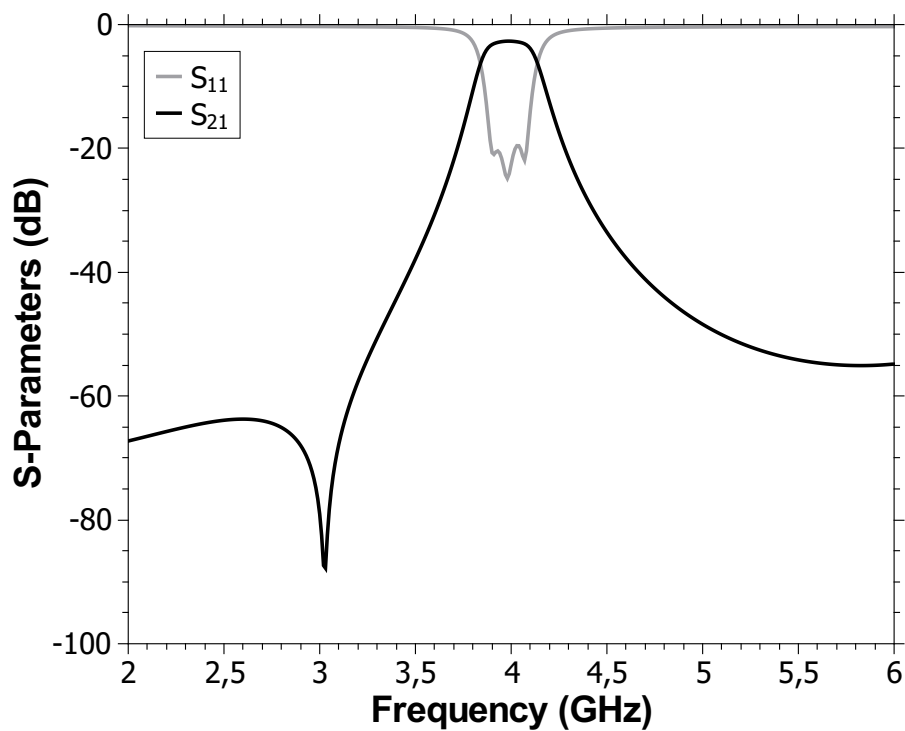
Figure 2.28: EM simulation results of the conventional microstrip parallel coupled-line bandpass filter designed.

Parameter		Result	Layout value [mm]
Z_0		35 Ω	1.85
$J_{01} = J_{34}$		0.0087	0.2
$J_{12} = J_{23}$		0.0023	0.8
$Z_{01} = Z_{34}$	Even Mode	48.9 Ω	1.1
	Odd Mode	30 Ω	
$Z_{12} = Z_{23}$	Even Mode	38 Ω	1.5
	Odd Mode	32.4 Ω	
$l_{Z_0} \approx \lambda/4$			10
$l_1 = l_4$		9.95 mm	11.12
$l_2 = l_3$			10.9
$l_T \approx \lambda/2$		19.9 mm	21.12

Table 2.6: Filter synthesis and layout values.

2.5.2 Filter with 1 Transmission Zero at Lower Stopband

In a first example, the introduction of a single TZ at the lower stopband of the designed filter response has been considered. Therefore, a terminating section with highpass response has been chosen to implement the TZ. The scheme of the proposed solution is depicted in Figure 2.29.
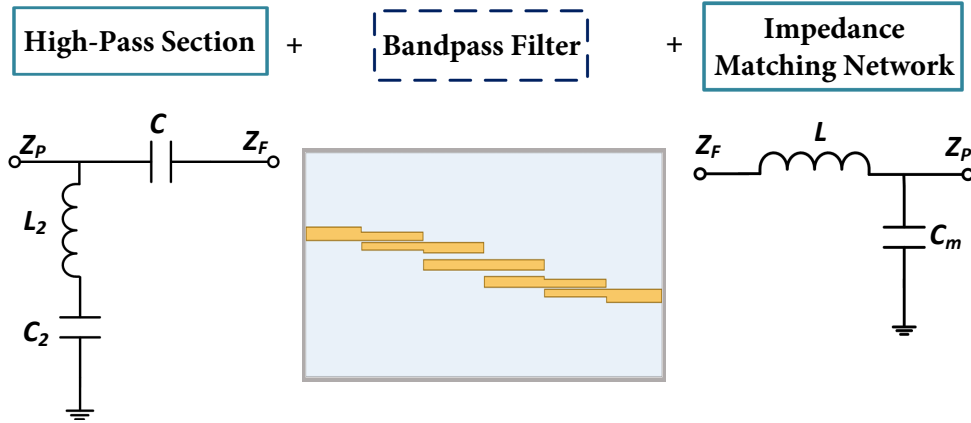
Figure 2.29: Configuration of the filter with 1 TZ at lower stopband.

As can be seen, no changes are required on the bandpass filter that remains the same, except for the introduction of two terminations at the filter source and load. Thus, on one side the section that generates a TZ in the response (i.e. Highpass Section) has been introduced, while at the other side an L-matching network has been included for scaling the filter impedance up to $Z_P = 50$ Ω.

A location of the TZ at 3.5 GHz, that is close to the filter passband, has been proposed. Therefore, applying the equations (2.22) to (2.24) for $Z_P = 50 \; \Omega$, $Z_F = 35 \; \Omega$, $f_0 = 4$ GHz and $f_{TZ} = 3.5$ GHz, the synthesis values of Table 2.7 can be obtained (where the values for the L-matching network are also included).

Parameter	Synthesis Value	Implementation
C	1.7 pF	1.2 pF 0402 AVX–Accu-P
C_2	0.16 pF	Open-circuited stub $l << \lambda/8$ [W=1mm ($Z_0 = 50 \; \Omega$), l=2mm]
L_2	13 nH	6.2 nH Coilcraft–0402HP
L	0.9 nH	1.3 nH Murata LQP15MN1N3W02
C_m	0.5 pF	Open-circuited stub $l << \lambda/8$ [W=1mm ($Z_0 = 50 \; \Omega$), l=4.6mm]

Table 2.7: Element results of the "Highpass Section" and the "Impedance-Matching Network".

The added sections are implemented by lumped and quasi-lumped elements. At these frequencies, for a proper use of lumped components, the real equivalent model or the measured S-parameters has to be considered, taking into account the effective reactance of the devices. Thus, the reference of the commercial SMD components used in the design can be found in Table 2.7. Note that capacitances C_2 and C_m can be easily implemented using open-circuited stubs of length $<< \lambda/8$.

The final layout of the 4 GHz bandpass filter with a TZ at 3.5 GHz is presented in Figure 2.30.
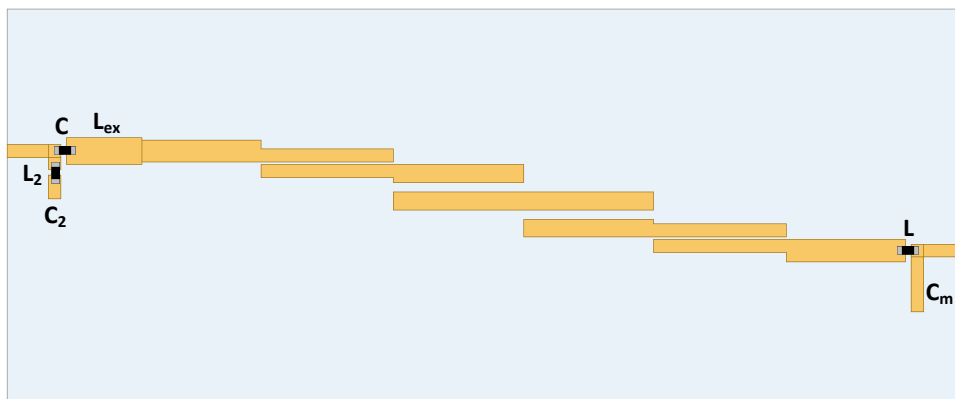
Figure 2.30: Layout of the filter with 1 TZ at lower stopband.

In the filter layout of Figure 2.30, the additional line section L_{ex} is included in order to compensate the multiple reflections (S_{11}) produced after connecting two lossy filter networks. This effect would not occur if both networks were lossless.

The simulation results of the filter with a TZ at 3.5 GHz are compared with the original filter response in Figure 2.31. As can be easily seen, the attenuation achieved at 3.5 GHz after including the TZ is 67.5 dB, instead of 37.9 dB on the conventional implementation. Moreover, the in-band filter response is fully preserved with mid-band IL about 3 dB and RL better than 20 dB within the passband. It can be also perceived a slight drop of the S_{11} around 2.7 GHz as a consequence of the aforementioned reflections, despite the inclusion of the L_{ex}.
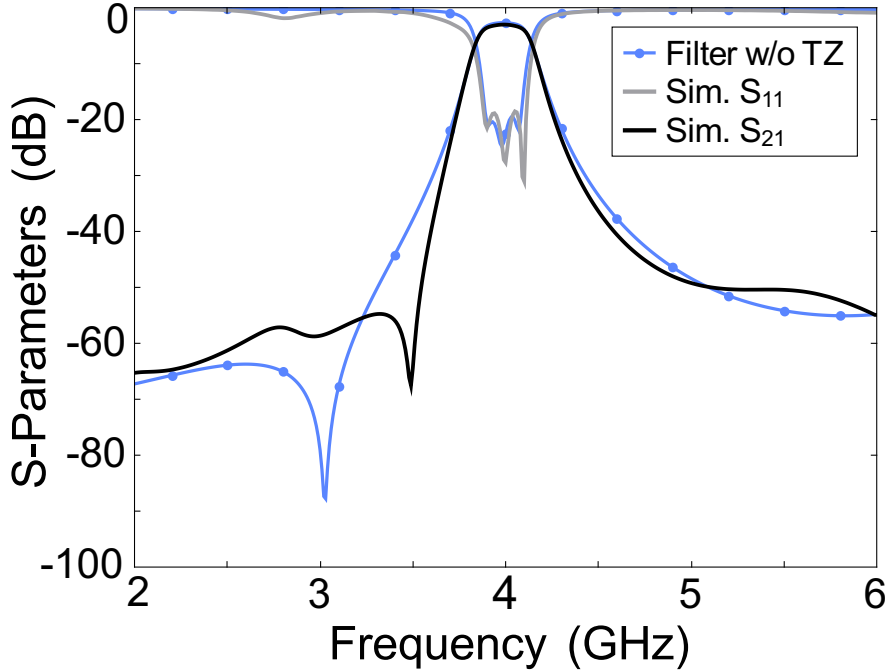
Figure 2.31: Comparison of the simulation results of the filter with 1 TZ at lower stopband with the conventional microstrip parallel coupled-lines bandpass filter without TZs.

After these satisfactory design results, the filter is fabricated in RO4003C substrate. Figure 2.32 shows a photograph of the fabricated filter with 1 TZ at the lower stopband. The filter dimensions are 10 x 3 cm^2 of size, and the area required by the input and output networks is almost negligible. The measurements compared with simulations are presented in Figure 2.33. As can be seen, both are in excellent agreement, validating in this way the developed approach. The measured IL at $f_0 = 4$ GHz are 3.28 dB, while the RL remain better than 20 dB within the passband. The TZ in the manufactured device is located at 3.46 GHz, very close to the desired frequency, and the maximum rejection level is 73.3 dB.
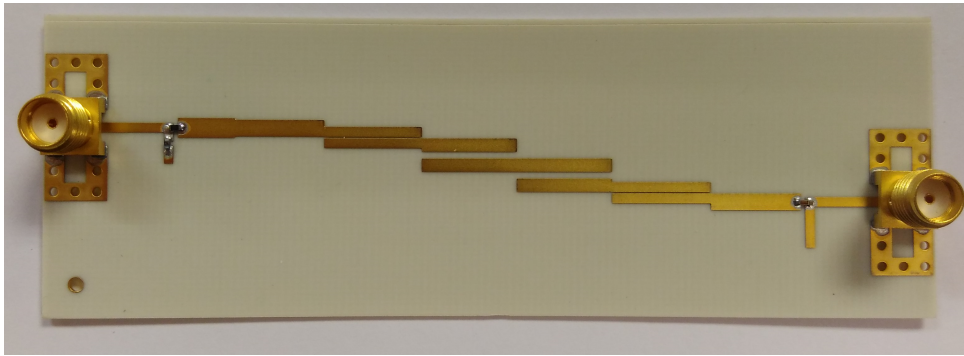
Figure 2.32: Photograph of the fabricated filter with 1 TZ at lower stopband.
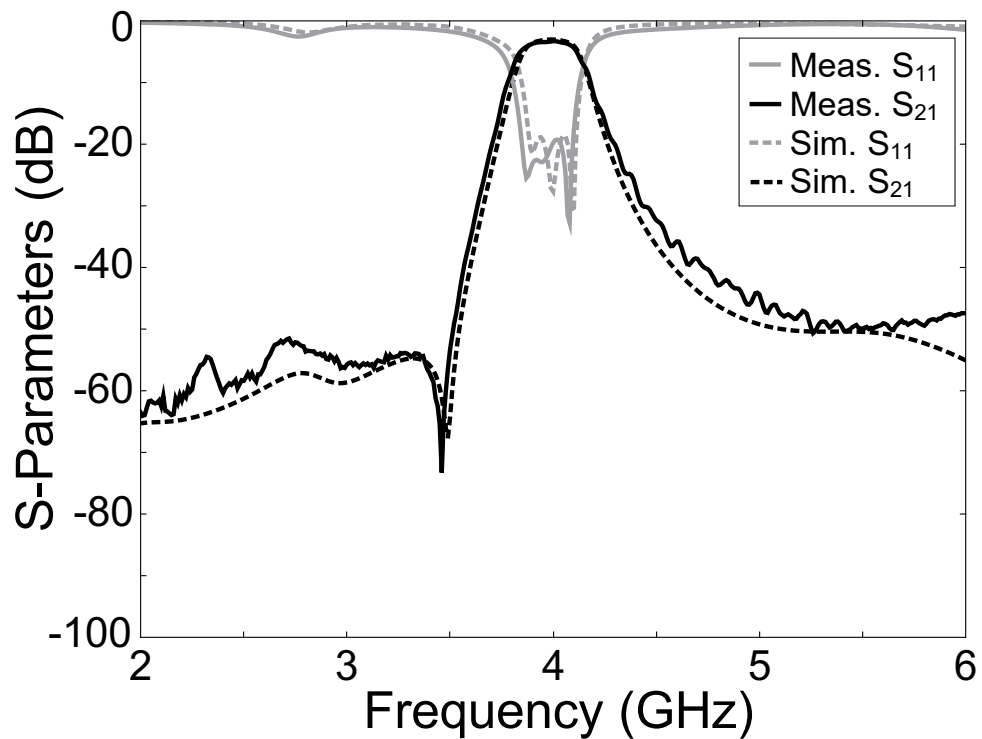
Figure 2.33: Measurements versus simulations of the fabricated filter with 1 TZ at lower stopband.

2.5.3 Filter with 2 Transmission Zeros at Upper Stopband

A second example is proposed by inserting two TZs in the filter response, both located at the upper side of the passband. Hence, the two sections to be added to the filter are lowpass in this case. An scheme of the proposed topology can be seen in Figure 2.34.
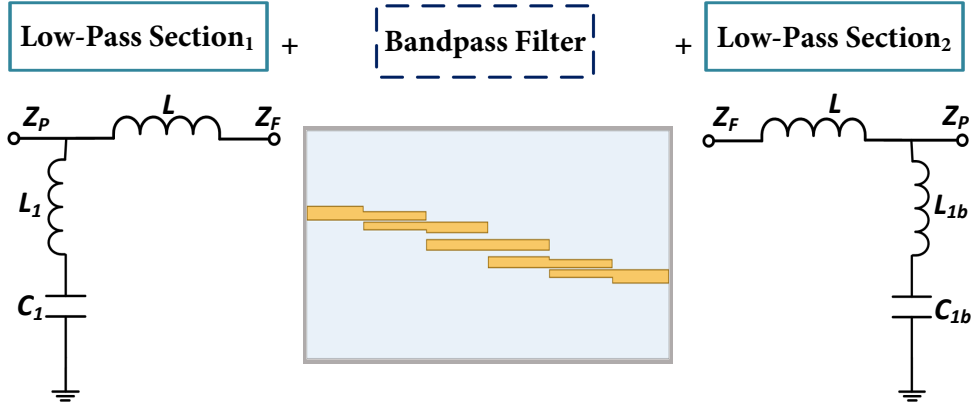
Figure 2.34: Configuration of the filter with 2 TZs at upper stopband.

As in the first example, the parallel coupled-line filter is no modified, and only two terminating sections are inserted on each side for providing two independently adjustable TZs (Lowpass Section$_1$ and Lowpass Section$_2$). The frequencies of the zeros are set to 4.5 and 5 GHz in this example. The equations (2.19) to (2.21) are solved for $Z_P = 50\ \Omega$, $Z_F = 35\ \Omega$, $f_0 = 4$ GHz, $f_{TZ1} = 4.5$ GHz and $f_{TZ1b} = 5$ GHz; and the values of Table 2.8 are obtained, being implemented again using lumped and quasi-lumped elements.

Parameter	Synthesis Value	Implementation
L	0.9 nH	1.3 nH Murata LQP15MN1N3W02
C_1	0.1 pF	Open-circuited stub $l << \lambda/8$ [W=1mm ($Z_0 = 50\ \Omega$), l=1mm]
L_1	11 nH	6.1 nH Murata LQW15AN6N1D10
C_{1b}	0.2 pF	Open-circuited stub $l << \lambda/8$ [W=1mm ($Z_0 = 50\ \Omega$), l=1.35mm]
L_{1b}	4.3 nH	4.3 nH Murata LQW15AN4N3B00

Table 2.8: Element results of the "Lowpass Section$_1$" and "Lowpass Section$_2$".

The filter structure with the 2 TZs is shown in Figure 2.35. The full-wave EM simulated filter performance is presented in Figure 2.36.

As can be seen, the introduction of the two TZs does not impact the original in-band filter response in terms of insertion and return losses. The first zero introduced at 4.5 GHz represents an improvement in rejection with respect to the response without TZs greater than 20 dB, but the effect of the second one has less impact. This is due to the
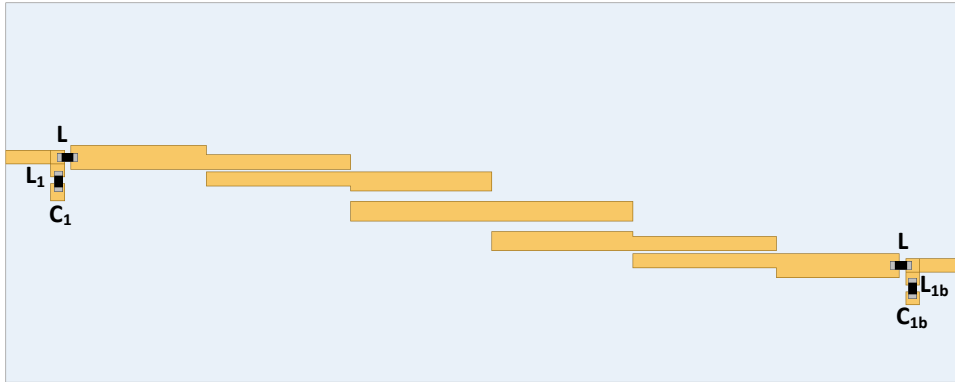
Figure 2.35: Layout of the filter with 2 TZs at upper stopband.
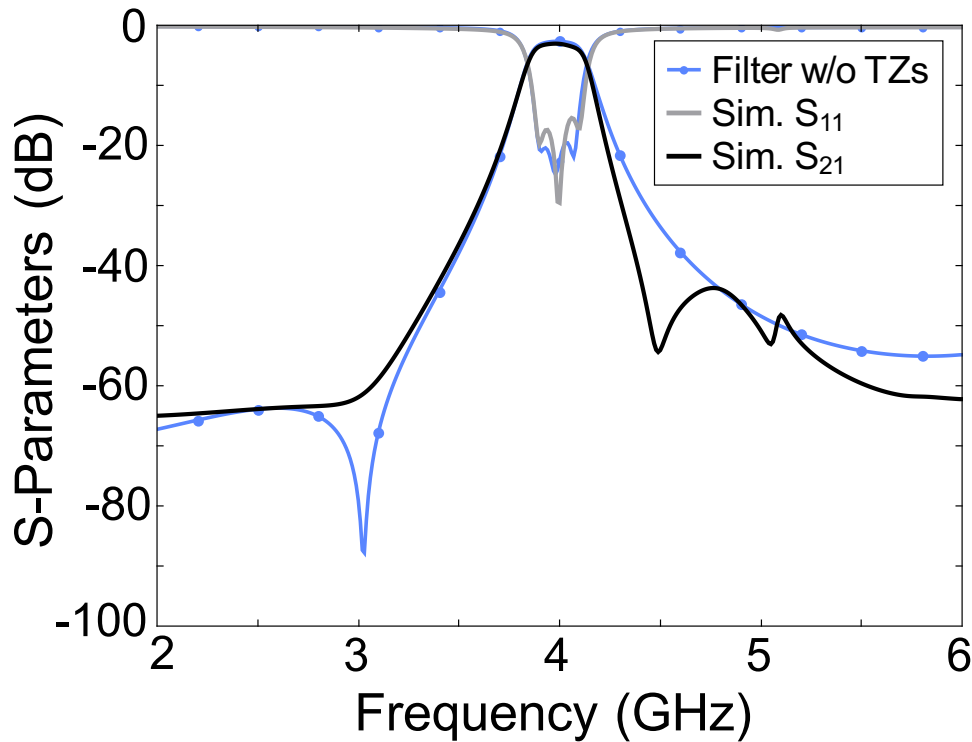
Figure 2.36: Comparison of the EM simulation results of the filter with 2 TZs at upper stopband with the conventional microstrip parallel-coupled bandpass filter without TZs.

high intrinsic attenuation of the filter at that frequency, coupled to the limited quality factor of the TZ_{1b}. On the other hand, the in-band characteristics, IL at f_0 and minimum RL in the bandwidth, take a value of 3 dB and 15.4 dB, respectively.

Likewise, this filter is manufactured and a photograph of the prototype is depicted in Figure 2.37. The total occupied area is 9.4 x 3 cm^2 with a negligible contribution from the terminating sections. The simulations compared with measurements are shown in

Figure 2.38 and are also in very good agreement, even if the frequencies of the TZs have been slightly shifted towards higher frequencies in this case, appearing at 4.55 and 5 GHz. The reason is the greater influence of C_1 and C_{1b} in the tuning of the TZs ought to their small values. Measured IL at f_0 are 3.23 dB, while RL are better than 17 dB within the passband. Finally, the attenuation achieved with the TZs is 54.28 dB at 4.55 GHz and 56.21 dB at 5.24 GHz.
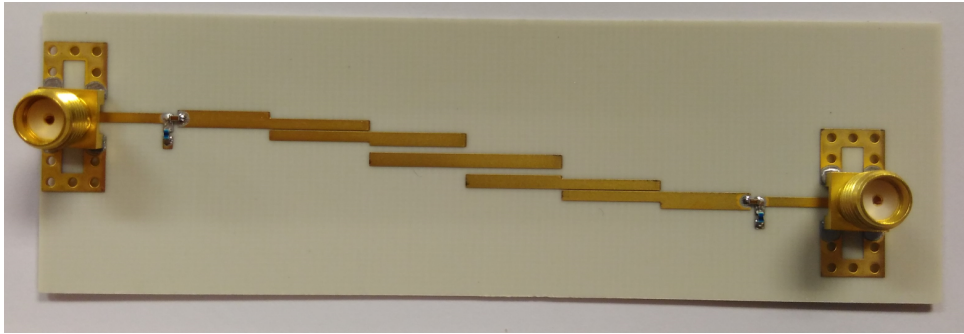
Figure 2.37: Photograph of the fabricated filter with 2 TZs at upper stopband.
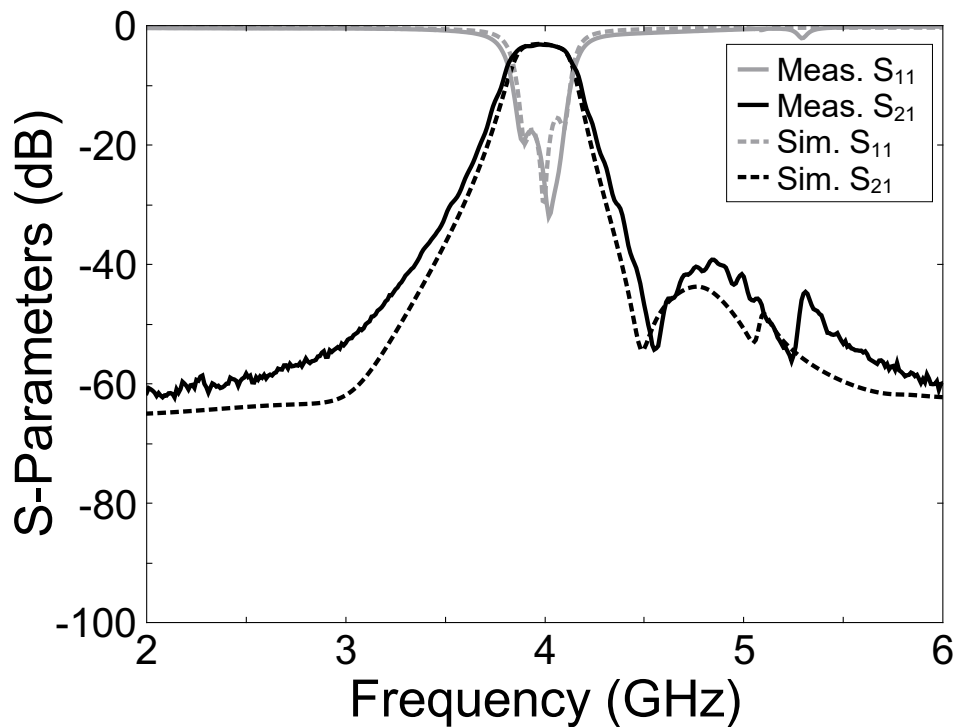
Figure 2.38: Measurements versus simulations of the fabricated filter with 2 TZs at upper stopband.

2.5.4   Filter with 2 Transmission Zeros: 1 at the Lower Stopband and 1 at the Upper Stopband

Another disposition of 2 TZs is going to be developed in this section. Now the TZs are added symmetrically and closer to the passband, one on each side. Hence, both terminating sections (i.e. highpass and lowpass) are needed. The configuration adopted is shown in Figure 2.39.
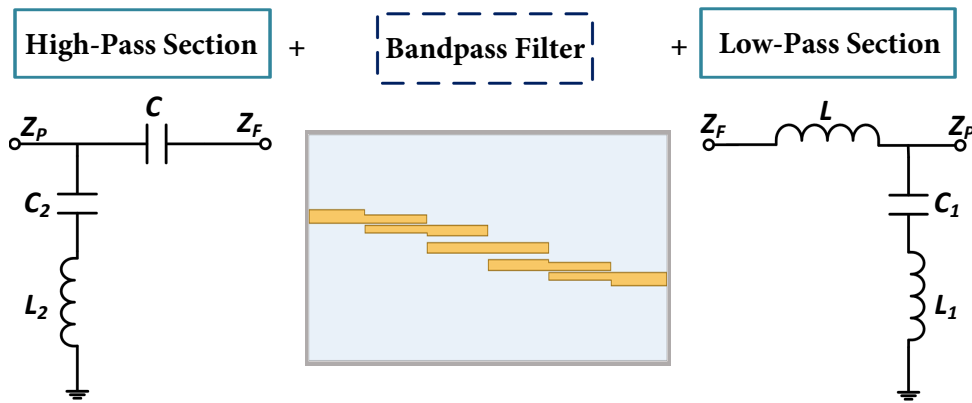
Figure 2.39: Configuration of the filter with 2 TZs, one on each side of the passband.

The filter structure keeps unmodified, and the cascaded connection with the two terminating sections is simply made. The frequencies of the TZs are set symmetrically at 430 MHz away from f_0. Applying the equations (2.19) to (2.24) for $Z_P = 50\ \Omega$, $Z_F = 35\ \Omega$, $f_0 = 4$ GHz, $f_{TZ1} = 3.57$ GHz and $f_{TZ2} = 4.43$ GHz, the synthesis values of Table 2.9 are calculated.

As can be easily recognized from the synthesis expressions of the terminating networks, the nearness between f_0 and f_{TZ} has a great impact on the shunt-resonator element values. This effect is graphically represented in Figure 2.40 by obtaining the resonator element values for $f_0 = 4$ GHz, $Z_F = 35\ \Omega$, and $Z_P = 50\ \Omega$ at different TZ locations.

For very selective filters, where the ratio $f_{TZ}/f_0 \rightarrow 1$, the inductive part of the resonator (L_1 and L_2) becomes higher and the capacitive part (C_1 and C_2) becomes lower. In this case, the very high inductance values for L_1 and L_2 will prevent from using lumped inductors, which would require a high Q-factor value and a self-resonant frequency far enough from the filter passband. A distributed implementation in microstrip technology could also be considered by means of quasi-lumped elements or distributed resonators (e.g. open-ended $\lambda/4$ transmission line), nevertheless the required characteristic impedance would be totally unrealizable.

Parameter	Synthesis Value	Implementation
C	1.7 pF	1.2 pF 0402 AVX–Accu-P
C_2	0.13 pF	$\lambda/4$ short-circuited line $[W = 1.1$ mm $(Z_0 = 50\ \Omega)$, $l = 10.25$ mm $(f_{TZ1} = 3.57$ GHz$)]$
L_2	15 nH	$J_{TZ1} = 0.007 \rightarrow C_{TZ1} = 0.25$ pF
L	0.9 nH	1.3 nH Murata LQP15MN1N3W02
C_1	96.2 fF	$\lambda/4$ short-circuited line $[W = 1.1$ mm $(Z_0 = 50\ \Omega)$, $l = 8.74$ mm $(f_{TZ2} = 4.43$ GHz$)]$
L_1	13 nH	$J_{TZ2} = 0.006 \rightarrow C_{TZ2} = 0.2$ pF

Table 2.9: Element results of the "Highpass Section" and "Lowpass Section".
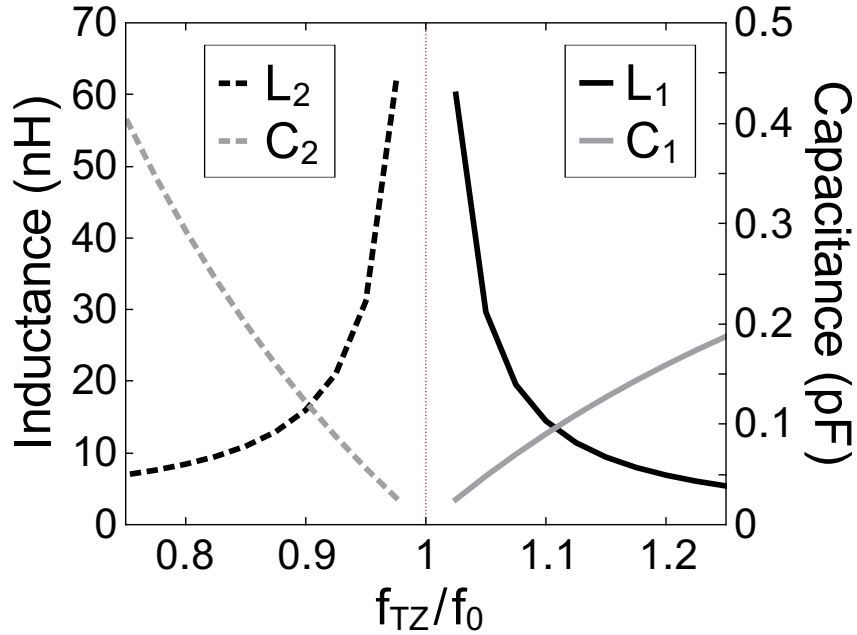
Figure 2.40: Variation of C_1, L_1, C_2 and L_2 versus f_{TZ}/f_0 ratio for $f_0 = 4$ GHz, $Z_F = 35\ \Omega$, and $Z_P = 50\ \Omega$.

Thus, the equivalent scheme shown in Figure 2.41 is proposed for implementing the series resonator, by using an admittance inverter coupled to a parallel resonant circuit.
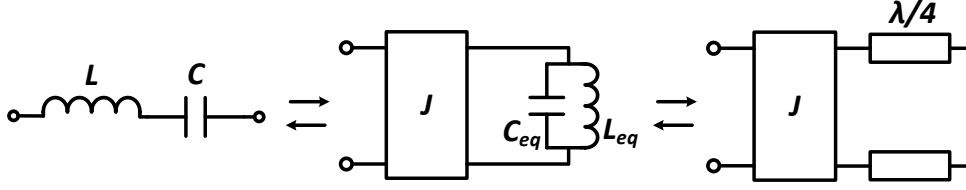
Figure 2.41: Schematic synthesis and proposed equivalent circuit of the resonator of the terminating sections for their practical implementation when $f_{TZ}/f_0 \to 1$.

By equating the input impedance of both circuits, the next relationship can be obtained

$$J^2 = \frac{C_{eq}}{L} = \frac{C}{L_{eq}} \qquad (2.34)$$

As can be seen, a new degree of freedom is introduced by the admittance inverter. Given any resonator centered at f_{TZ}, a proper $J-$inverter can be found.

A parallel resonator can be implemented using a short-circuited transmission line of length $\lambda/4$ and characteristic impedance Z_0, where its equivalent capacitance and inductance are

$$C_{eq} = \frac{\pi}{4\omega_0 Z_0}; \quad L_{eq} = \frac{4Z_0}{\pi\omega_0} \qquad (2.35)$$

So, in this case, the admittance inverter constant can be computed as

$$J = \sqrt{\frac{\pi}{4Z_0\omega_0 L}} = \sqrt{\frac{\pi\omega_0 C}{4Z_0}} \qquad (2.36)$$

Therefore, the use of an admittance inverter enables us to reach feasible element values for the equivalent resonator modelled by a parallel LC circuit. Thereby, the cells can be easily implemented at microwave frequencies using both lumped and distributed elements.

In this manner, the technological realization is based on a hybrid solution of lumped and distributed elements. Thus, the series elements of the TZs networks (L and C) are implemented by lumped elements, whereas the elements of the parallel branch (i.e resonator L_1, C_1, L_2 and C_2) are implemented using the proposed equivalent network based on inverters and distributed resonators of length $\lambda/4$. The needed parameters for its implementation appear in Table 2.9. As the required coupling values, J_{TZ1} and J_{TZ2}, are reasonably high, lumped elements (C_{TZ1} and C_{TZ2}) have been also used to achieve them.

The simulation results of the pseudo-elliptic filter are compared with the response of the bandpass filter without TZs in Fig. 2.43. These results allow us to verify that the introduction of TZs using the method described in this paper significantly improves the out-of-band performance in terms of rejection and selectivity, without disturbing the in-band response of the original filter without TZs. Thus, IL at mid-band frequency are about 3 dB, while the matching worsens slightly within the passband with a minimum value of 17.5 dB. Lastly, the TZs are correctly located achieving a rejection of 54.1 dB at 3.57 GHz, and 52.3 dB at 4.43 GHz. This implies an improvement of more than 20 dB compared to the attenuation values of the filter without TZs.

As in previous examples, this filter has been manufactured using the same substrate (0.508 mm -thick RO4003C). A photograph of the prototype is shown in Figure 2.42. Its final dimensions are 9.74 x 3 cm^2. The measurements together with the simulations are plotted in Fig. 2.43. The experimental characterization fits almost perfectly with the simulations results. The IL at f_0 reach 3.3 dB, and the RL are better than 18.4 dB over the entire bandwidth. The TZs present a minimal frequency shift, being located at 3.61 GHz and 4.48 GHz, while achieving an attenuation of 45.2 dB and 52.2 dB respectively.
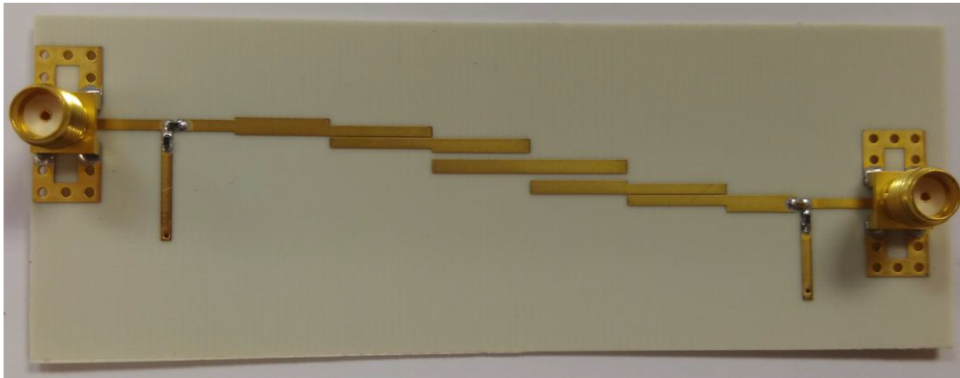
Figure 2.42: Photograph of the fabricated prototype filter with 2 TZs, one on each side of the passband (pseudo-elliptic response).
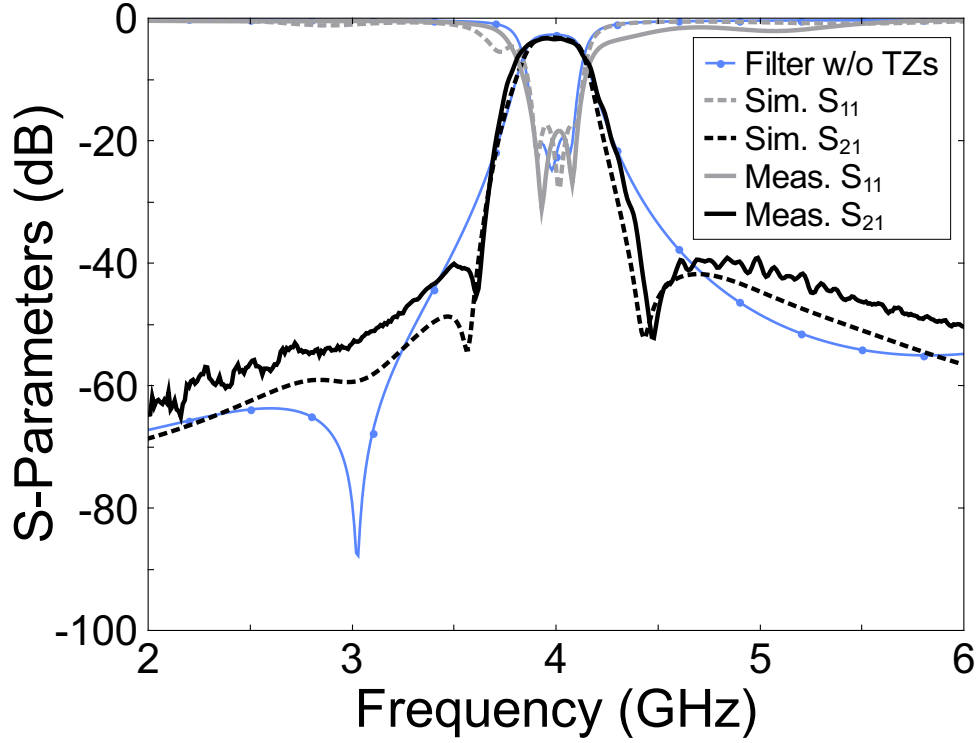
Figure 2.43: Measured and simulated results of the fabricated filter with 2 TZs, one on each side of the passband, in comparison with the bandpass filter without TZs.

2.5.5 Highly Selective Combline Microstrip Bandpass Filter

Another example with the TZs even closer to the passband and using a different filter topology is addressed. Thus, the design of a two-pole Chebyshev band-pass filter with 0.1 dB pass-band ripple and 5% FBW at a design frequency $f_0 = 4$ GHz employing a microstrip combline structure is now contemplated. The input/output filter impedance is set as $Z_F = 45$ Ω just to end with a typical port impedance of $Z_P = 50$ Ω, once the terminations are cascaded. The combline resonators are of 85 Ω impedance and $\lambda/4$ long for no capacitive loading, and the TZs are located at 250 MHz away from the f_0. Therefore, the element values of the sections are $L = 0.6$ nH, $C_1 = 30$ fF and $L_1 = 46$ nH for the lowpass section, and $C = 2.7$ pF, $C_2 = 36$ fF and $L_2 = 49$ nH for the highpass section.

As in the previous example, the technological realization is based on a hybrid solution of lumped and distributed elements. The only difference is the implementation of the TZs coupling values (i.e. J_{TZ1}, J_{TZ2}), which are made through interdigital capacitors instead of SMD components.

The simulation results of the combline pseudo-elliptic filter are compared in Figure. 2.45 with the response of the combline filter without TZs. The presence of the TZs on the band-pass filter response can be seen at 3.75 GHz with a rejection of 16.76 dB, and at 4.25 GHz with 29.45 dB of attenuation, while keeping the in-band response.

This highly selective combline filter has been fabricated using the same Rogers RO4003C substrate but with different thickness. In this case the substrate thickness is 1.524 mm. The manufactured prototype is displayed on Figure 2.44. The photograph shows the different parts of the filter, presenting at the source and load the lowpass (LP) and highpass (HP) terminating sections cascaded with the combline filter. Its final dimensions are 3.7 x 3.7 cm^2. The introduced terminating networks require some additional space compared to the filter without TZs, although some modifications on the half-section layout (e.g. folding the series-shunt resonator) could be carried out in order to reduce this extra size.

The measurements together with the simulations are plotted in Figure 2.45. The experimental characterization are in very good agreement with the simulations. The measured IL at f_0 are 2.2 dB and the RL are better than 16 dB on the passband. The TZs accomplish a very selective response in comparison with the response without them, appearing at 3.76 GHz and 4.29 GHz obtaining 12.5 dB and 25.4 dB of rejection, respectively.
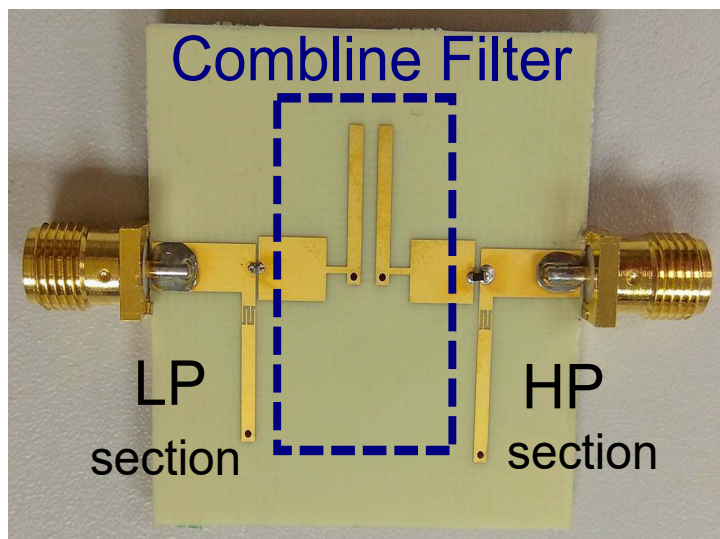
Figure 2.44: Photograph of the manufactured combline filter with pseudo-elliptic response (TZs very close to the passband).
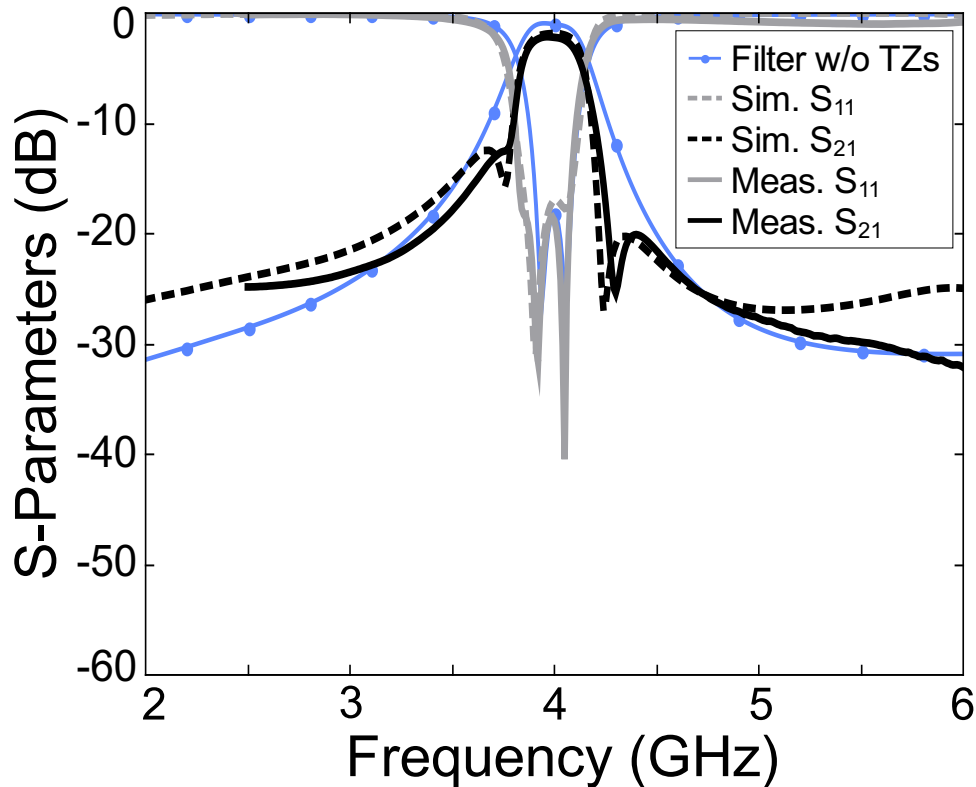
Figure 2.45: Measured and simulated results of the fabricated highly selective combline band-pass filter, in comparison with the combline bandpass filter without TZs.

2.6 Application Case III: Microwave Dual-Band Planar Filter with Improved Rejection.

Lastly, in this context of introducing TZs in different filter responses for several microwave front-ends, a dual-band filter for Software Defined Radio (SDR) and fifth generation (5G) applications, with improved rejection by using the proposed terminating sections of this thesis, is going to be described next.

Lately, multi-band communication systems have been developed at microwave frequencies, that operate over multiple communication standards simultaneously. New wireless applications like LTE and 5G use, instantaneously, several bands of radio frequency instantaneously to assign the bandwidth resource necessary to increase data transmission rates. With this increasing demand for multi-service wireless systems, multi-band microwave components, such as bandpass filters (BPF), have raised great interest.

According to the above needs, the aim in this section is the design of a dual-band BPF with a compact size, low losses, high selectivity and practical operation bands. The specifications are summarized as follows:

- Passband 1: 900 to 1000 MHz (Channel BW = 100 MHz);
  Center frequency, $f_0 = 950$ MHz.
- Passband 2: 1427 to 1518 MHz (Channel BW = 91 MHz);
  Center frequency, $f_0 = 1472.5$ MHz.
- IL at f_0: To be minimized.
- IL at $f_0 \pm 50\% BW$: To be minimized.
- Low-side rejection: From 500 to 850 MHz To be maximized.
- Inter-band rejection: From 1050 to 1350 MHz To be maximized.
- High-side rejection: From 1600 to 2000 MHz To be maximized.
- Footprint: To be minimized.

2.6.1 Dual-Band Combline Bandpass Filter with Terminating Bisected π Sections.

Figure 2.46 shows the scheme of the proposed filter. The structure is based on the topology presented in [77] for a dual band combline BPF loaded by lumped series resonators, where terminating sections have been added at the input and at the output to introduce additional TZs and improve the selectivity of the passbands.
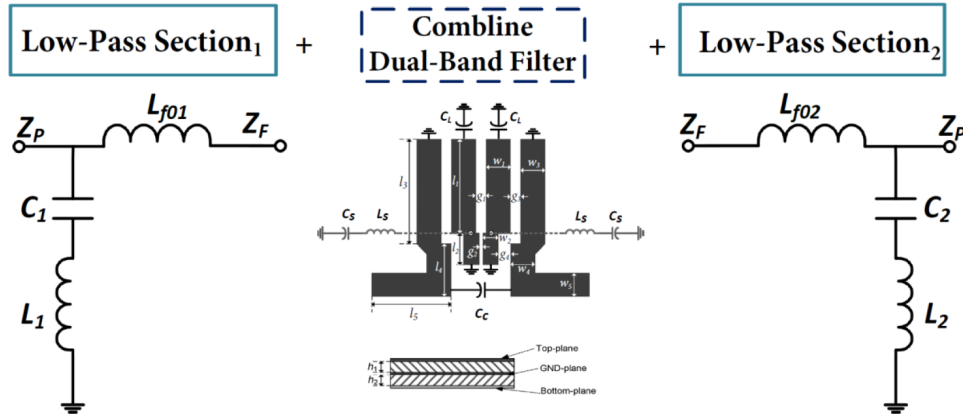
Figure 2.46: Configuration of the proposed dual-band bandpass filter with terminating lowpass sections.

On the one hand, the combline dual-band BPF consists in a quarter-wavelength resonator, l_1, with an additional shorted transmission line, l_2, loaded by a capacitor, C_L, to reduce size and improve the spurious response. This quarter-wavelength resonator is also loaded by a lumped series resonator, C_S and L_S, on the bottom plane. The resonant frequency of the $C_S - L_S$ should be the same as the center frequency of the upper passband, f_{upper} (where l_1 is a quarter-wavelength). The lower band, f_{lower}, is achieved from the original quarter-wavelength transmission line, $l_1 + l_2$, and taking into account the loading

effect of the lumped series resonator. On the other hand, lumped lowpass terminating sections are included at the input and output of the filter to introduce one TZ at the upper stopband of each passband. The lumped element implementation for the TZs cells results a good option at these operational frequencies and supposes a minimun increment of area, allowing a more compact design as is required. Finally, the lumped capacitor C_C is placed between both ports to create a source-load cross-coupling, enhancing the rejection out of the two bands.

The design procedure starts by setting the resonance frequency of $C_S - L_S$ to the center frequency of the upper band, $f_{upper} = 1472.5$ MHz. A smaller value of L_S and a larger value of C_S increases the bandwidth of the upper band. Since the lumped series resonator becomes a short circuit at the upper resonant frequency, the bandwidth and the center frequency of the upper band can be easily adjusted through the gaps and the lengths of the combline resonators. Next, by connecting additional lines (l_2) to the combline BPF a lower passband is obtained, and can be controlled independently from the parameters of the upper band (l_2 changes the center frequency, and the gap g_2 controls the bandwidth of the lower passband). Finally, the TZs using the terminating half sections ($L_{f_{01}} - C_1 - L_1, L_{f_{02}} - C_2 - L_2$), and cross-coupling ($C_C$) are included in the response.

Considering the explained design procedure, the proposed dual-band filter is designed using a 0.813 mm thick Rogers RO4003C ($\epsilon_r = 3.55, \tan \delta = 2.7 \cdot 10^{-3}$) substrate in each layer. The filter structure employs three layers (Top-plane, GND-plane, and Bottom-plane, see Figure 2.46), where the lumped-element series resonators are located at the bottom plane and coupled to the comblines through via holes, achieving in this way higher compactness for the device. The main dimensions of the filter, to obtain a simulated response as shown in Figure 2.48, are listed in Table 2.10. In order to improve the rejection of each band, terminating sections are cascaded to the filter. The parameters and the necessary SMD components of each Lowpass section are also in Table 2.10. Additional capacitors, $C_{Q_{ext}}$, are included in the structure between the excitation lines and the resonators, in order to achieve the proper external coupling needed in the combline structure to reach specifications, avoiding in this form infeasible gaps for manufacturing and providing an extra post-tuning element to adjust the response, in case of deviations.

The simulation results provide a satisfactory response given the required goals for the dual-band bandpass filter. The insertion losses at the center frequency of the passband 1, IL($f_0 = 950$ MHz) are 1.9 dB, while in the passband 2, IL($f_0 = 1472.5$ MHz) are 2 dB. The RL in both passbands are better than 13.5 dB, and the rejections in the low-side is higher than 10 dB, between both bands greater than 13 dB, and in the high-side better than 16 dB.

Param.	Value	Param.	Value	Param.	Value
l_1	10 mm	w_1	1.5 mm	g_1	0.5 mm
l_2	7.1 mm	w_2	1 mm	g_2	0.9 mm
l_3	10.15 mm	w_3	1.5 mm	g_3	0.13 mm
l_4	7 mm	w_4	1.5 mm	g_4	0.13 mm
l_5	0.5 mm	w_5	2 mm	w_{port}	1.45 mm
l_{port}	7 mm	h_1	0.813 mm	h_2	0.813 mm
C_S	2.5 pF	L_S	3 nH	C_L	2.2 pF
C_C	0.5 pF	$C_{Q_{EXT}}$	0.8 pF	-	-
Lowpass Section$_1$ ($Z_P = 50\ \Omega, Z_F = 40\ \Omega$, $f_{01} = 0.9$ GHz, $f_{TZ1} = 1.1$ GHz)			$L_{f_{01}} = 0.4$ nH; $L_1 = 52$ nH; $C_1 = 0.3$ pF		
Lowpass Section$_2$ ($Z_P = 50\ \Omega, Z_F = 40\ \Omega$, $f_{02} = 1.5$ GHz, $f_{TZ2} = 1.93$ GHz)			$L_{f_{02}} = 4.2$ nH; $L_1 = 5.6$ nH; $C_1 = 0.9$ pF		

Table 2.10: Layout dimensions and SMD component values of the dual-band combline BPF with terminating bisected π-sections.

Simulations and measurements of the fabricated prototype are depicted in Figure 2.48, and a photograph of the dual-band filter is shown in Figure 2.47. The filter area (excluding connectors) is 9.9 x 24 mm^2. The measured results show good agreement with the simulated ones. However, due to the loading effect of the series resonator added to assembly problems, measured bandwidths are narrower than simulations, affecting also the exact location of the introduced TZs frequencies in the upper band. In this way, the insertion losses for both pasbands at their center frequencies are IL($f_0 = 950$ MHz) 2.31 dB and IL($f_0 = 1472.5$ MHz) 2.33 dB. The measured RL whitin the bandwidth is better than 13 dB, and the rejections in the low-side and between bands are the same ones as in simulation, and in the high-side is higher than 14 dB.
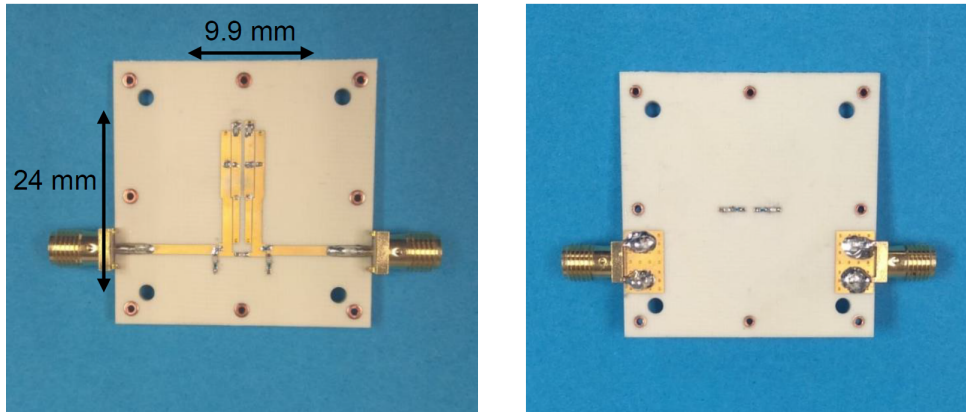
Figure 2.47: Photographs of the fabricated dual-band BPF prototype with TZs. Top view (left). Bottom view (right).
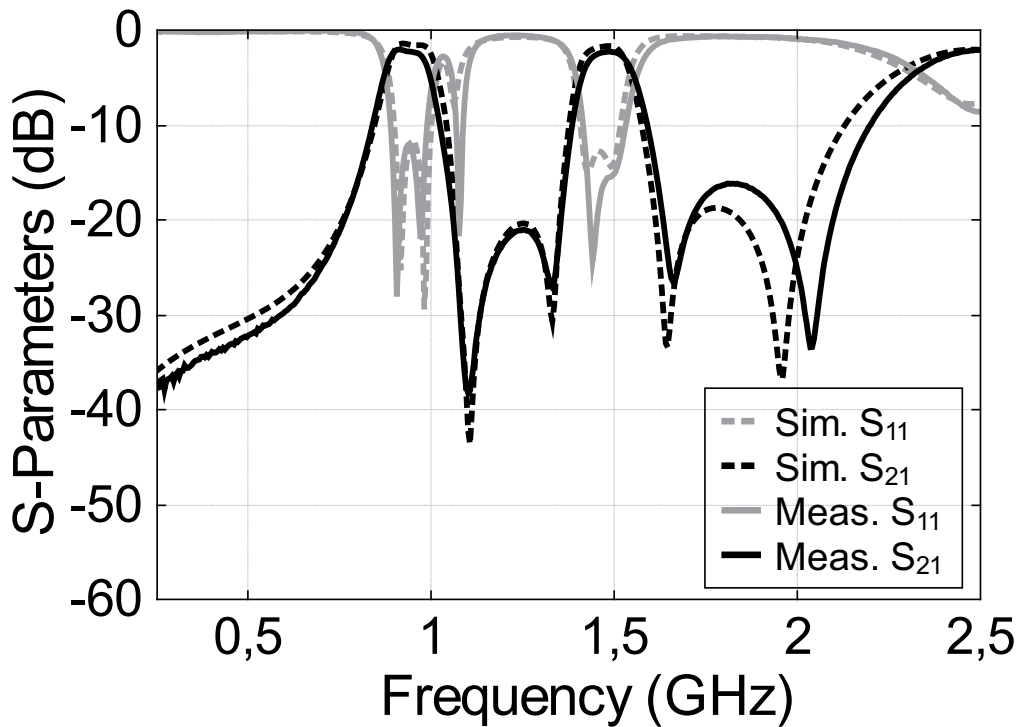
Figure 2.48: Simulated and measured S-parameter responses of the dual-band BPF with terminating lowpass sections.

A simple, modular and compact in size solution with improved selectivity for a dual-band BPF has been presented. Thus, a filter prototype showing good agreement between measurements and simulations is designed and manufactured, thus the effectiveness of the presented approach.

Filter Design with Advanced Responses

This chapter describes the results obtained during the research work of this doctoral thesis in the area of high-performance and compact filter design. As will be exposed, both characteristics are difficult to meet at the same time. For this reason, several techniques and solutions will be studied and proposed to achieve enhanced and advanced microwave filters. Firstly, the pros and cons of different technologies for achieving compact filters will be reviewed. Then, a compromise solution between performance and miniaturization, as it is SIW and coaxial SIW structures, will be considered, and different methods for improving the response of filters in these technologies will be presented. Finally, a general procedure to design diplexers and multiplexers in planar technologies will be described.

3.1 Limitations of Planar Technology

Small size, high selectivity and low insertion losses of RF/microwave bandpass filters are required for many applications in wireless communication systems. For instance, the satellite communications industry demands for low-mass, low-loss, and narrow-band filters with severe specifications on amplitude selectivity and phase linearity. Cellular communications base-stations, for its part, demand low-loss high power-handling selective filters with small physical size, capable of being manufactured in tens of thousands at a reasonable cost.

However, obtaining components with high performance characteristics and responses, such as those mentioned above, leads to the use of more expensive, heavy and bulky technologies, such as waveguides. In contrast, the characteristics of low cost, easy integration,

and compaction are achieved in planar technology, but the power-handling capability and Q factors are usually very low (they can usually have Q values lower than 100).
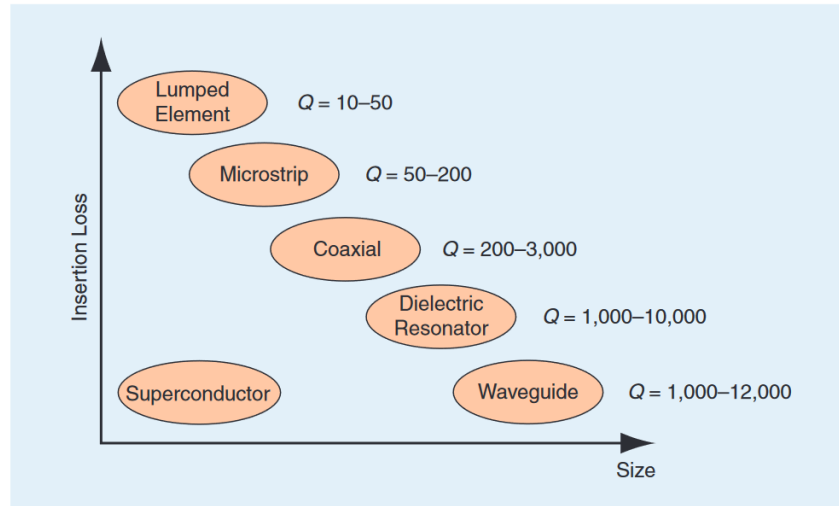
Figure 3.1: Relative insertion losses and size for various RF resonators from [46].

Figure 3.1 shows the relative insertion losses and size of typical microwave resonators. The estimated range of unloaded Q values for each resonator technology at 5 GHz is also shown in the same figure [46].

For a frequency range from RF to microwave, various kinds of resonators including the coaxial, dielectric, waveguide and microstrip/stripline technologies have been used, as it is illustrated in the cited Figure 3.1. In one hand, coaxial resonators have electromagnetic shielding structure, low-loss characteristic; dielectric resonators also present low-size characteristics, acceptable temperature stability; and waveguide resonators, which have long been used in the microwave frequency range, present low-loss features and practical application feasibility up to 100 GHz. However, the greatest drawbacks of these non-planar technologies are size, mass and cost, which are significantly larger than for other resonators available in the microwave region such as planar structures. Nevertheless, the use of the planar resonators (i.e. microstrip/stripline) leads to a drastic increase in insertion losses compared to other type of RF resonators, making it difficult to apply to narrow-band filters.

Still, current trends in the development of RF, microwave, and millimeter-wave systems are being oriented towards the low-cost and high-density integration of front-end circuits and components. These requirements lead to advances in generation of methods for cost-reduction, integration of components such as multiplexers and miniaturization techniques employing dielectric resonators in the case of waveguide components. On the contrary, solutions for improving the Q and obtain higher performances in the design of

planar devices are also being provided. This is now mainly driven by the invention and development of the concept of Substrate Integrated Circuits (SICs). In particular, recent studied technologies as Substrate Integrated Waveguide (SIW) and coaxial SIW suppose an intermediate solution capable of filling the technological gap between microstrip or stripline (planar type) and dielectric resonator or metallic waveguide (non-planar type), since they combine the best parts of both classical technologies (planar and waveguide ones), and offer high-quality factors that are close to those of non-planar structures with the size- and cost-related advantages of printed planar circuits.

3.2 SIW and Coaxial SIW Resonators

SIW technology is a hybrid solution between planar transmission lines designs and 3D waveguide implementations. In fact, a SIW structure consists on a classical waveguide that is integrated with a planar dielectric substrate, such as Printed Circuit Board (PCB). A SIW resonator is designed with a dielectric material, two parallel metal plates, and a series of metallized vias, which connect the lower and upper metal plates and delimitate the dimensions of the integrated dielectric cavity. This technology is a suitable choice for designing and developing microwave components because of their great potential offering a good trade-off between size and performance. When compared to the classical rectangular waveguide, SIW topologies present smaller Q-factors and greater insertion losses, but they are lighter-weight and smaller, of lower cost, and easier to manufacture, integrate and package with other planar circuits. SIW technology also offers superior performance than the classical planar counterpart. Optimized SIW filters can reach a Q factor of 200-800 using low-loss substrates and standard fabrication procedures [23]. Despite the advantages in height and weight, typical SIW filters still occupy a rather large area, in comparison with most of their planar counterparts, and consequently they are not usually well-suited for low-frequency microwave applications.

The size of a SIW cavity can be reduced by using different approaches. For instance, more compact implementations can be obtained by using folded SIW cavities [23], or by loading a SIW cavity with dielectric rods [78], both at the expense of less-standard manufacturing processes. Other approaches achieve further miniaturization but at a cost of important degradation of the Q-factor. For example, quarter-mode SIW structures can lead to 40-60% degradation of the unloaded Q-factor compared to a classic SIW cavity resonator [79].

As can be deduced, there is a trade-off between resonator size and Q-factor value. The smaller the resonator size compared to the guided wavelength (λ_g), the lower the unloaded Q-factor. With this in mind, it is convenient to find a balance between compactness and Q-factor degradation. In [80] it was proved that loading a cavity with a

capacitive post reduces the resonant frequency while still maintaining a relatively high unloaded Q-factor. The proposed structure can be seen in Figure 3.2. A properly designed capacitive post, consisting of a short-circuited via hole capacitively loaded at the top by an isolated metal patch, enables the realization of single-layer coaxial SIW resonator; which is capable of the SIW size reduction without a significant Q-factor degradation.

(a) (b)
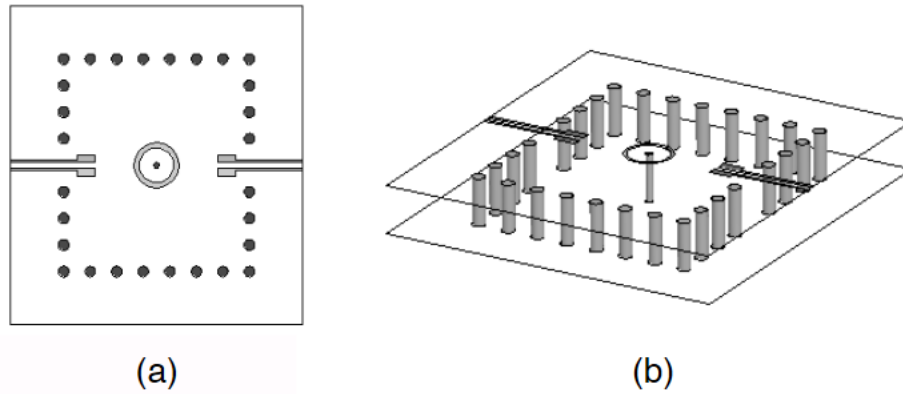
Figure 3.2: Top view (a) and 3D plot (b) of the capacitively loaded SIW resonator (Coaxial SIW resonator) [80].

The main potential advantages of coaxial SIW structures are listed next [81].

- By increasing the length of the post or the loading capacitance, a huge size reduction can be achieved compared to conventional SIW cavity resonators.
- Both inductive and capacitive couplings can be achieved on the top layer to obtain filter responses allocating finite transmission zeros (TZs). Moreover, other advanced topologies, such as multimode resonators, singlets, and doublets, can also be implemented by translating their well-known metallic waveguide counterparts.
- The easy access to loading capacitance enables the direct integration of lumped capacitors as well as tuning elements, such as varactors, p-i-n diodes, or RF MEMS

In the following sections, the coaxial SIW structure will be employed for designing compact and miniaturized devices providing advanced and high-performance filtering responses; increasing and exploiting the potential and flexibility of this technology.

3.3 Q-Factor Enhancement Techniques in Coaxial SIW Resonators

The insertion losses, IL, within the bandpass filter depends on three principal factors: the unloaded quality factor of resonators Q_u, the fractional bandwidth $\Delta f/f_0$, and the filter order N. Depending on these factors, we can evaluate the minimum IL within the passband at frequency f_0 as follows [4]:

$$IL(f_0) \approx 4.343 \frac{N}{Q_u \frac{\Delta f}{f_0}} \tag{3.1}$$

It is well-known that, in order to increase the selectivity of the filter response, we need to increase the number of resonators involved, i.e. N. However, according to equation (3.1), this leads to a rise in the IL value at the same time, which leads us to increase the unloaded quality factors to compensate for it.

Once the material and type of resonator are chosen, the Q_u value is unfortunately constrained. In order to increase the Q_u value, one often must increase the size of the resonator, resulting in a larger and heavier filter. The finite Q value will also translate into energy dissipation. The filter will also exhibit finite band-edge sharpness related to the particular Q value. This phenomenon, as can be deduced from (3.1) is more pronounced for filters with narrow relative bandwidth.

As has been reviewed in the state of the art section (in chapter 1), many Q-factor improvement techniques involve the introduction of air and, consequently, an associated size increase. Following this idea, a novel coaxial SIW resonator is going to be considered. Its topology, including its main design parameters, is displayed in Figure 3.3.
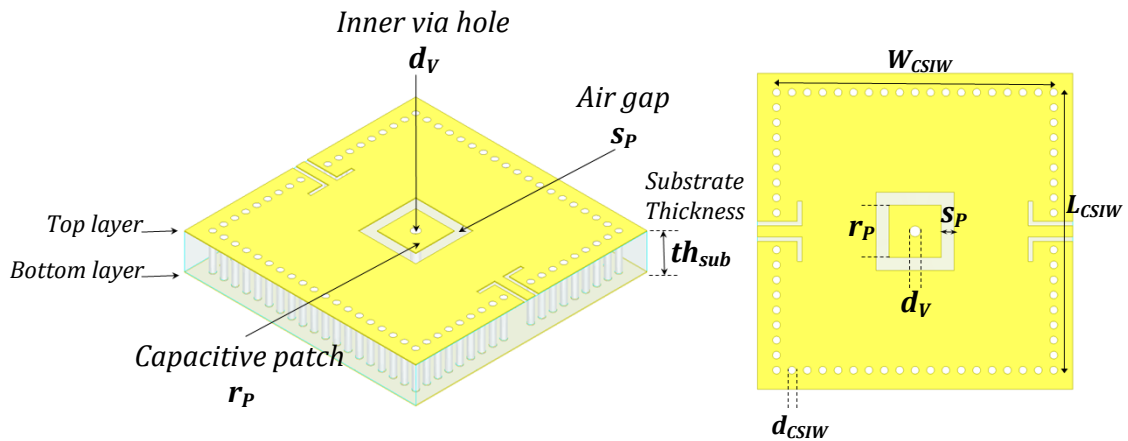
Figure 3.3: 3D and top view of the coaxial SIW resonator.

A coaxial SIW resonator consists on a SIW cavity where a plated via hole has been inserted at the center. The inductive section of the combline resonator has been obtained by the plated via hole, which is connected to ground at one of its ends.

At the other side, a metallic patch having a size much bigger than the post diameter d_v is connected. Between this patch and the top metal plane a small air gap s_p is inserted, so generating a high capacitance towards ground (termed loading capacitance C_l), which represents the capacitive section of the coaxial resonator. In particular, the fringing fields across the air gap generate the integrated loading capacitance, which can be clearly seen by observing the electric field distribution around the air gap as it is shown Figure 3.4. In this part of the resonator is where the field pattern is maximum, so in this position is where the air is going to be introduced with the intention of improving its Q_u. Considering the current limitations in the technology from a manufacturing point of view, two layout versions for introducing air in the resonator structure are proposed. The first one is shown in Figure 3.5, by introducing non-plated via holes. The other option can be seen in Figure 3.6, and consists in creating slots in the capacitive gap.
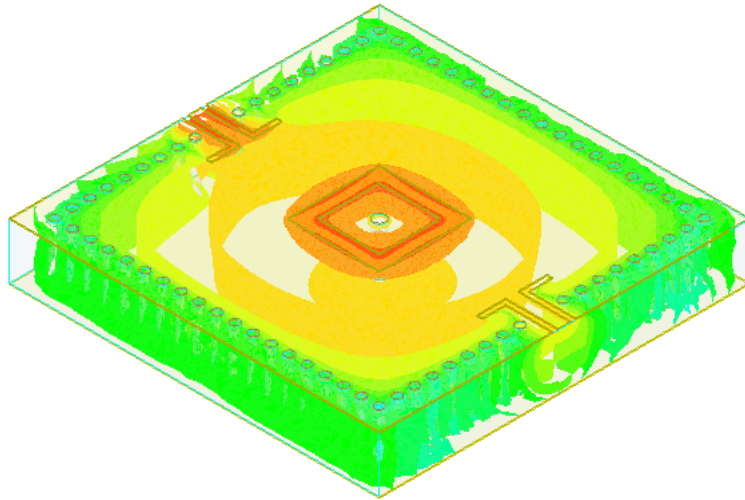
Figure 3.4: 3D electric field distribution for a coaxial SIW cavity.

To evaluate the effect on the Q-factor, we are going to compare the best Q value that can be achieved in the conventional coaxial SIW, for a given material and at certain frequency, with the Q value that can be achieved by adding these modifications for including air. In this way, we proceed to design on a 1.524 mm thick-Rogers RO4003C substrate ($\epsilon_r = 3.55$, $\tan \delta = 0.0027$), with a metallization of 35 μm of copper and 5 μm of nickel-gold finishing, a coaxial SIW resonator centered around 10 GHz.
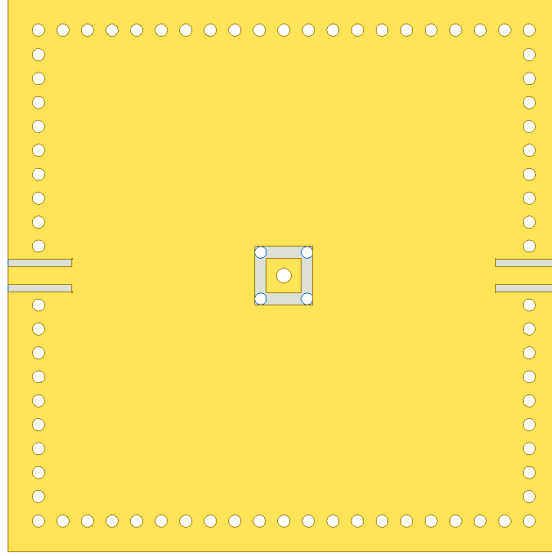
Figure 3.5: Coaxial SIW resonator with non-plated via holes to improve its Q_u.
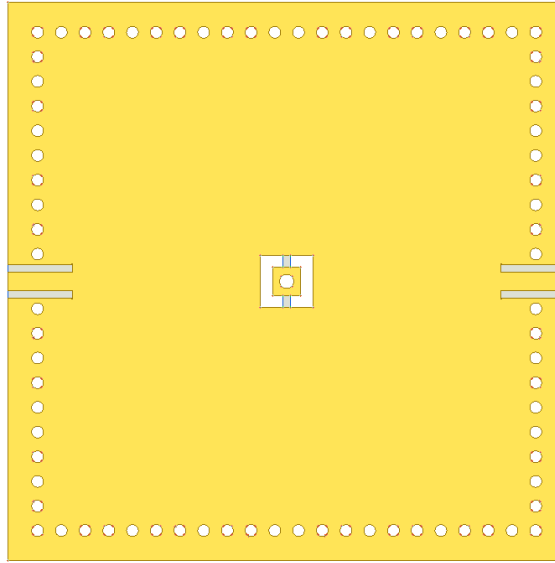
Figure 3.6: Coaxial SIW resonator with slots to improve its Q_u.

In order to achieve the maximum Q_u value in this structure, the patch must be small (less capacitive load), resulting in a larger cavity. Thus, a coaxial SIW resonator of $W_{CSIW} = L_{CSIW} = 10$ mm, $d_v = 0.3$ mm, $r_p = 0.6$ mm and $s_p = 0.23$ mm (see Figure 3.3)is simulated obtaining an estimated Q-factor of 280. Then, without modifying these parameters, 4 non-plated via holes of 200 μm diameter are introduced in s_p, and the estimated Q-factor reached is around 300. Finally, including the slots in the gap, leaving two little metal strips for patch subjection, the estimated Q-factor is simulated to be 330. The obtained simulations for the Q_u value estimation are shown in Figure 3.7.
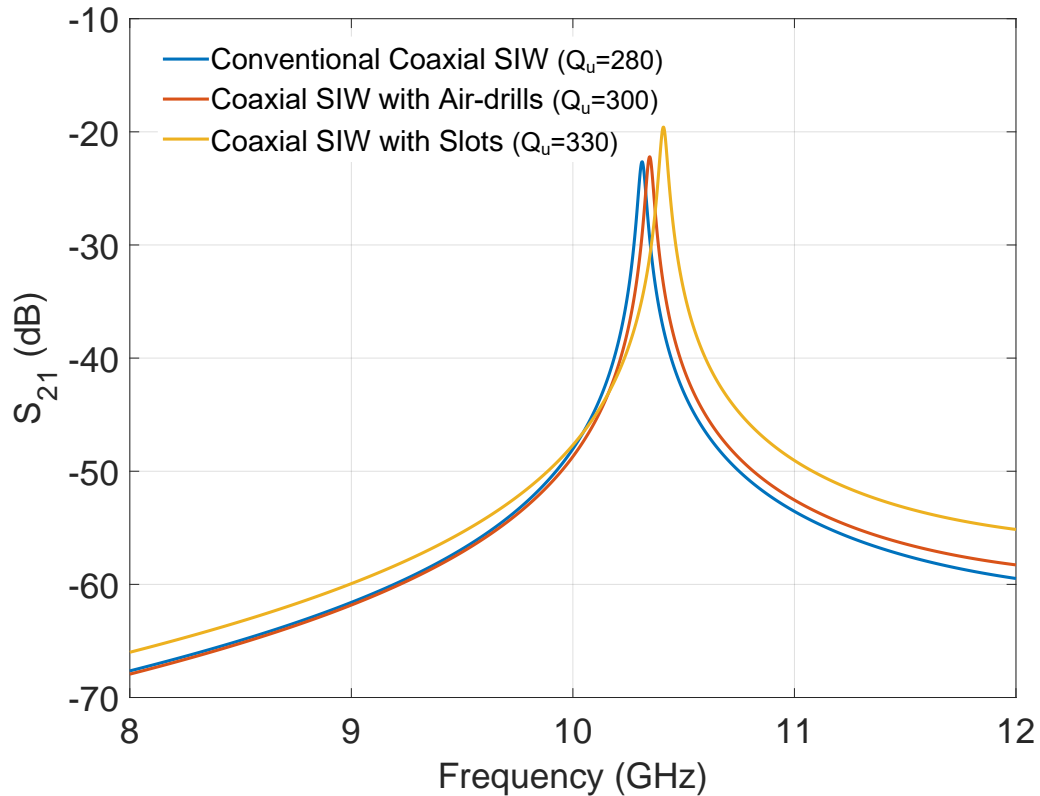
Figure 3.7: S_{21} parameter of each resonator to estimate its Q_u value.

As observed in the results for estimating the Q values (Figure 3.7), a slight Q-factor increase is achieved introducing air with respect to the original structure. The more air is introduced, the greater the Q-factor is increased. Thus, the best Q-factor is reached by performing slots.

As has been proven, the presented techniques allow a moderate improvement in the Q-factor of the coaxial SIW resonator. This slight Q-factor improvement can be key in meeting or not certain specifications. In addition, both proposed techniques are easy to implement and involve a negligible increment in terms of resonator size.

3.4   Manifold Multiplexer Design in SIW and Coaxial SIW Topologies

More advanced and complex devices, such as diplexers and multiplexers, are key components to meet the integration, compactness and high performance features searched for the new trends in microwave communications. For instance, in satellite communications, multiplexers are commonly used to split the signal that reaches the satellite, so each channel can be amplified separately, for then, being combined again and retransmitted back to the Earth.

There are different possible configurations for implementing microwave multiplexers, as it was shown in section 1.2.3 of chapter 1. Some of them make use of couplers or circulators, which provide a high isolation between channels resulting in a modular configuration, and are relatively more easy to design. Nevertheless, these configurations also have some drawback, such as the added losses introduced by these combining elements, which are quite bulky too. Manifold-coupled multiplexers, on the other hand, are preferable in terms of both size and performance, since they use a simple common length to connect all the filters. Unfortunately, the design can be extremely difficult, due to the strong interaction between different channels. This leads to a design process of the whole structure, which usually involves a huge number of parameters to be considered at the same time. In this context, an effective and general procedure to design multiplexers, in the manifold configuration, using SIW and coaxial SIW technologies will be described.

The model used as starting point for synthesizing a manifold multiplexer (MUX) is explained in [50] for waveguide technology. In this sense, further transformations will need to be considered for the implementation in the aforementioned SIW technologies.
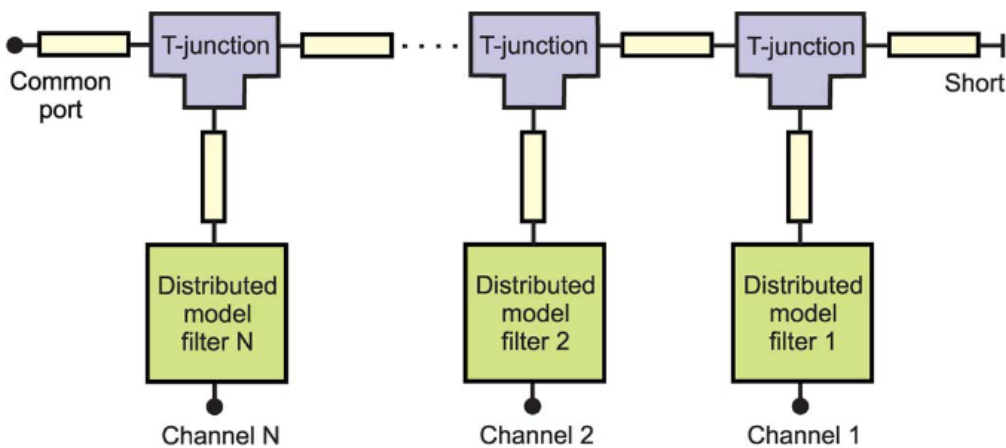
Figure 3.8: Structure of the generalized distributed model of a manifold multiplexer [50].

Figure 3.8 shows the diagram of the distributed model of a general manifold multiplexer. The T-junctions are usually simulated with a full-wave EM solver. They must be simulated only once, since their dimensions will not change during the design process. The waveguide sections along the manifold, and the ones connecting the manifold with the filters, can also be simulated with an EM solver, or alternatively modeled with an equivalent circuit.

Following the design steps detailed in [50], the procedure starts with:

1. The synthesis of each channel filter. At this point, the filters are considered isolated, and each of them is designed to comply with the frequency specifications of the corresponding channel.

2. Connect the model of the channel filters to the manifold. The initial spacings between the T-junctions must be normally set at $\lambda_g/2$. The spacing between the last T-junction and the short circuit is $\lambda_g/4$ for the H-plane configuration, and $\lambda_g/2$ for the E-plane case. The stub lengths between the filters and the T-junctions are also initialized at $\lambda_g/2$.

3. Run an optimization process to reach the desired specifications following the optimization steps explained in [50].

After these steps, it is achieved a satisfactory response with respect to the requirements. The second phase is the design of the multiplexer 3D structure for running EM simulations. Since the SIW components use a large amount of metallic vias, which require high-density meshing associated with a large number of unknowns, very long computation time with a high-performance workstation has to be used for the full-wave simulations. It is then impossible to design complicated coaxial SIW structures, such as diplexers and multiplexers (MUXs), by using a brute-force direct optimization method. Hence, a novel high-efficiency and high-accuracy design technique needs to be developed for the computer-aided design of these SIW and coaxial SIW MUXs.

The design procedure consists of characterizing and designing, using a full-wave EM model, part by part of the multiplexer, contrasting at all time and modifying, if necessary, the reference synthesis model, to ensure that the specifications achieved in the theoretical model are still met. This update of the reference model is necessary since in a manifold topology, as seen in chapter 1 (Introduccion), the interaction effect produced between each of its parts must be compensated in the design.

The recommended order to proceed in this part by part design process, using EM characterization, is:

1. EM-based design of the manifold lengths corresponding to the spaces between the T-junctions, and between the last junction and the short circuit, including the common port connectorization (if required).

2. Inclusion of the EM results of the designed part in the multiplexer model, and re-optimization (if needed) of the remaining design parameters.

3. EM-based design of the channel filters including the lengths between the filters and the T-junctions, as well as the connectorization (if required).

4. EM-based simulation and optimization of the full MUX.

For better illustrating all this design procedure, an example of a manifold diplexer implementation in SIW and coaxial SIW technologies is proposed, and described in detail, in the next section.

3.5 Application Case IV: Improved-Q Ka-Band Coaxial SIW Diplexer

The complete design procedure of a SIW manifold MUX, based on coaxial SIW filters with one of the previously proposed Q-enhancement techniques, is going to be described and applied to the case of a Ka-band diplexer with stringent requirements for space applications. Higher Q-factor, further miniaturization and self-packaging are pursued on the device, reasons why coaxial SIW resonators are employed. A set of realistic specifications have been considered. Then, analyzing the specifications, a solution based on the model shown in Figure 3.8 is synthesized. Finally, the followed design method for this kind of complex filtering structures will be reported.

3.5.1 Diplexer Specifications

Here below, we summarize the specifications of the diplexer for space applications:

- Topology: Manifold diplexer in SIW and coaxial SIW technologies.
- Center frequencies, f_0: 18.45 GHz (Channel 1, CH1) and 19 GHz (Channel 2, CH2).
- Channel Bandwidth (BW) = 500 MHz.
- Insertion Losses at $f_0 < 5$ dB.
- Insertion Losses Flatness:
  $f_0 \pm 30\%$ BW < 0.5 dBpp
  $f_0 \pm 45\%$ BW < 0.6 dBpp
  $f_0 \pm 50\%$ BW < 1 dBpp
- Narrow-band Isolation:
  $f_0 \pm 65\%$ BW > 20 dB
  $f_0 \pm 100\%$ BW > 30 dB
- Group Delay Variation:
  $f_0 \pm 30\%$ BW < 2 nspp
  $f_0 \pm 45\%$ BW < 3 nspp
  $f_0 \pm 50\%$ BW < 6 nspp
- Input and Output Return Losses: $f_0 \pm 50\%$ BW > 18 dB
- Footprint: To be minimized.
- Mass: To be minimized.
- Interface: SMA coaxial connector.

Examining the proposed requirements, it is interesting to note that the IL flatness specifications, together with the levels of rejection required near to the channel passbands, are very demanding for the SIW technology, since both specifications require either high Q-factor resonators, or applying pre-distortion or lossy techniques (see chapter 1) to flatten the passband response.

3.5.2   Diplexer Model Synthesis

As it is described in previous section, the synthesis of the diplexer model begins with the synthesis of each channel filter. Considering the specifications to be met, since both channels have the same bandwidth, we can select indistincly any channel for studying the synthesis aspects. In this case, the CH1 is chosen. Firstly, to determine the filter order, the narrow-band isolation is evaluated for a 6th, 7th and 8th-order filter, as depicted in Figure 3.9.
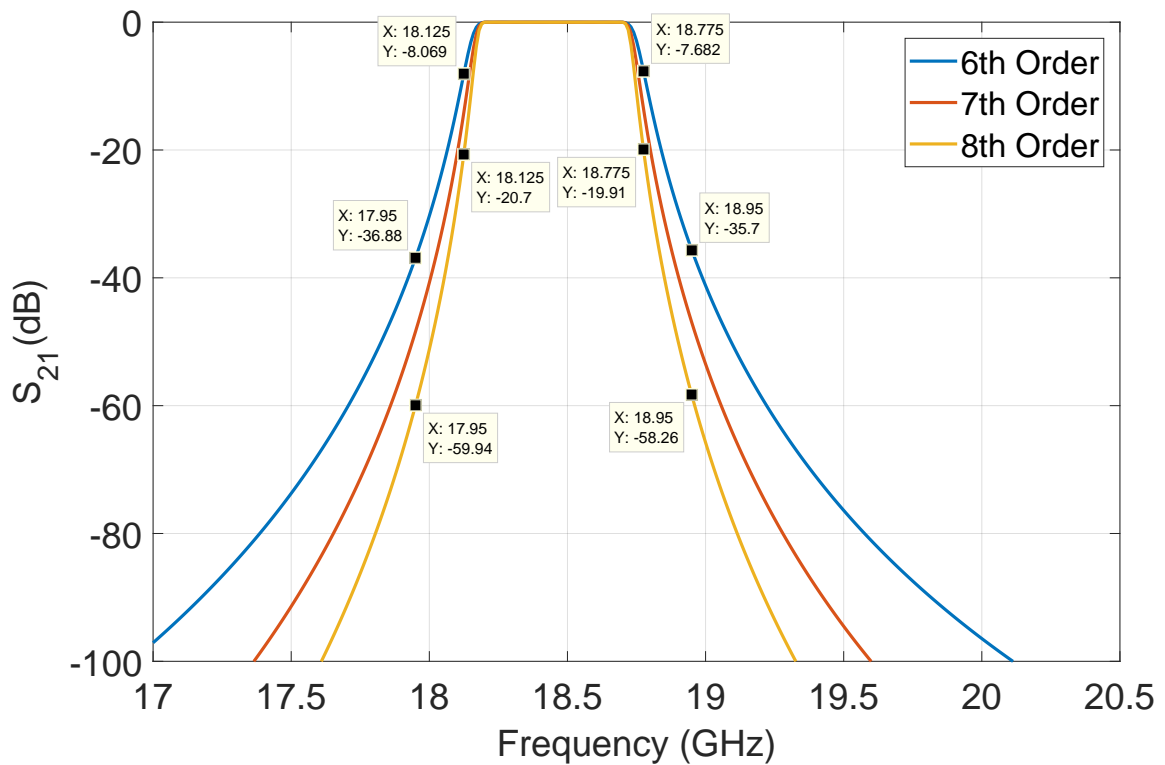
Figure 3.9: S_{21} theoretical response of channel 1 for a 6th, 7th and 8th-order filter.

Observing the attenuation reached in each case, for the 8th-order filter the required rejection level will be almost met, but the IL and complexity of the structure would be increased. ThIS is why, to reach the attenuation goals, it is decided to design a 6th-order filter with 2 transmission zeros in the response.

Now, attending to the IL and IL flatness requirements, the Q-factor needed is studied. In Figure 3.10, we can see the coupling scheme to synthesize the bandpass filter response of the channel 1 of the diplexer. Two cross-couplings between the resonators 2-5 and 1-6 have been introduced to achieve the desired out of band rejection levels.
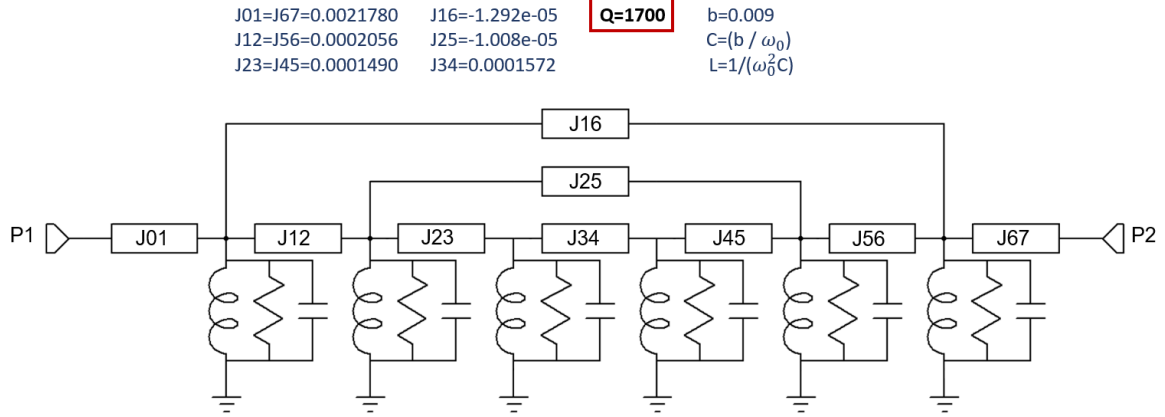
Figure 3.10: Theoretical coupling scheme to synthesize the filter response of the channel 1 of the Ka-band diplexer.

The minimum value of the Q-factor required for meeting all specifications is 1700. This value of Q-factor provides the frequency response depicted in Figure 3.11.

As can be seen, the response would meet all the narrow-band isolation requirements, as well as the requested IL and RL within the bandwidth. To see the variation of the IL within the passband and verify if the flatness requirements are also met, we will represent a normalization of the S_{21} parameter with the curve shown in Figure 3.12. This curve is the result, for each frequency, of the subtraction of the S_{21} value and the maximum value of the S_{21} ($S_{21} - S_{21}\text{max}$). In this way, if the variation between the passband IL value is greater than the values required (shown in the mask of Figure 3.12), the curve value would fall below the drawn mask. Therefore, observing the graph we see that the planarity conditions are achieved.

Finally, the group delay response is shown in Figure 3.13, and from the markers in the graph we can check that the specifications related to this parameter are also fulfilled.
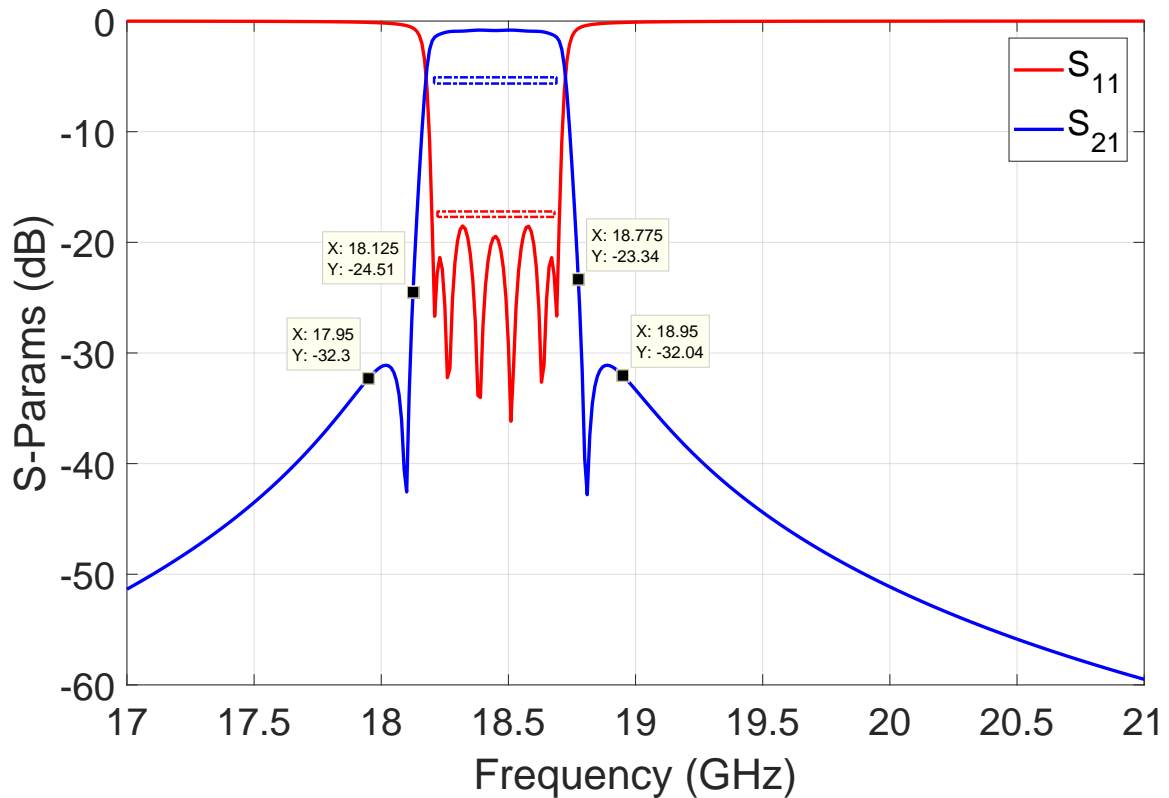
Figure 3.11: Theoretical S-parameters response of the synthesized filter for channel 1 with a Q-factor of 1700.

The minimum value of Q-factor required to meet specifications is, therefore, about 1700. This value is very high and difficult to achieve for coaxial SIW technology. For this reason, a study to estimate the possible values of the Q-factor that could be achieved in different materials is carried out. In table 3.1, the estimated Q_u for the conventional coaxial SIW resonator in the studied materials are listed .

From the previous Table 3.1, we can conclude that the required Q value can not be reached by coaxial SIW technology, not even with low-loss materials such as quartz. At this point, it is decided to evaluate the best performance of the considered topology, even if some specifications cannot be achieved. The material chosen, as a trade-off between good performances and low cost, is Rogers RT Duroid 5880 substrate of 1.575 mm thickness.

With the aim of improving the performance of the coaxial SIW resonator, one of the proposed techniques in the previous section for enhancing the Q-factor is going to be employed. Specifically, the introduction of 4 non-plated via holes placed in the capacitive gap is applied. Then, the Q_u of the coaxial SIW resonator with 4 non-plated via holes in the structure is estimated at the center frequnecy of the diplexer. Using Rogers RT
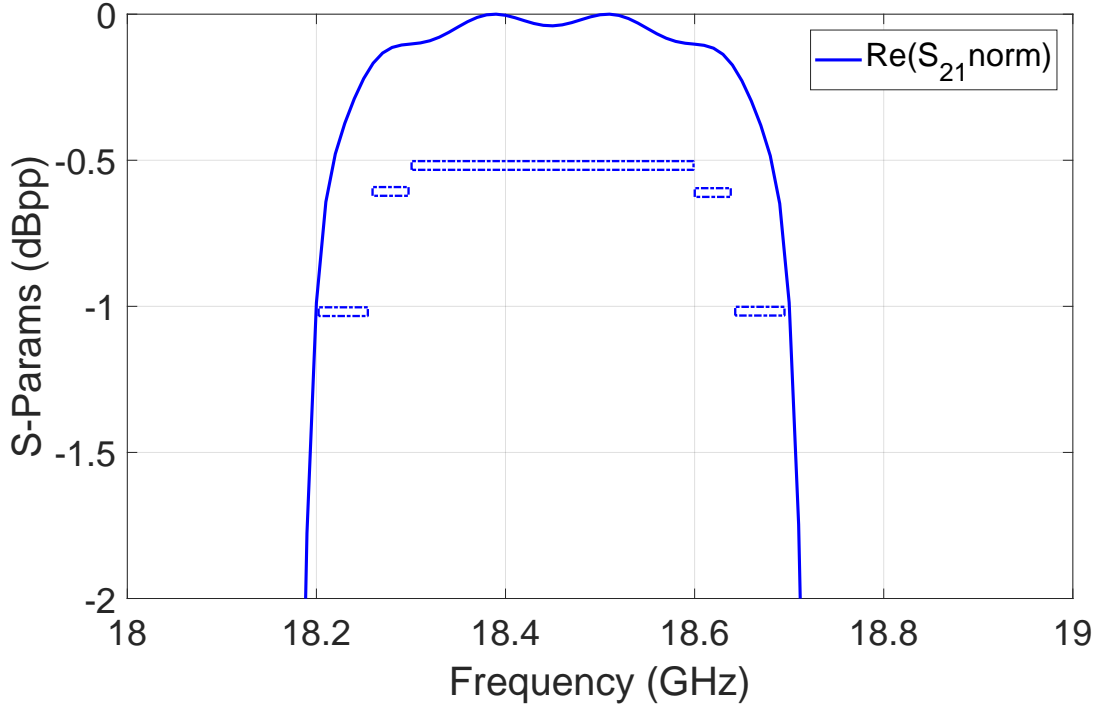
Figure 3.12: Curve of the difference: $S_{21} - S_{21}\text{max}$ to check flatness conditions for channel 1 with a Q-factor of 1700.

Substrate	Characteristics	Q_u
LTCC DuPont 9K7	ϵ_r=7.1; tanδ=0.0015; 4 layers of 224μm (896μm); conductive paste	$\approx$300
Quartz	ϵ_r=3.8; tanδ=0.0001; thsub=1 mm; copper 35μm	$\approx$910
Alumina 99.6%	ϵ_r=9.7; tanδ=0.0002; thsub=0.8 mm; copper 35μm	$\approx$720
Rogers RT Duroid 5880	ϵ_r=2.2; tanδ=0.0009; thsub=1.575 mm; copper 35μm	$\approx$600
GaAs	ϵ_r=12.9; tanδ=0.0004; thsub=635μm; copper 35μm	$\approx$560

Table 3.1: Study of Q_u values for the coaxial SIW resonator in different materials (thsub is the substrate thickness).

Duroid 5880 substrate (ϵ_r=2.2; tanδ=0.0009) of 1.575 mm of thickness, and considering 35 μm of copper metalization and gold finishing, a maximum value for the Q-factor of 620 is obtained. The designed resonator layout, and its simulation for estimating the Q_u value, are illustrated in Figures 3.14 and 3.15.
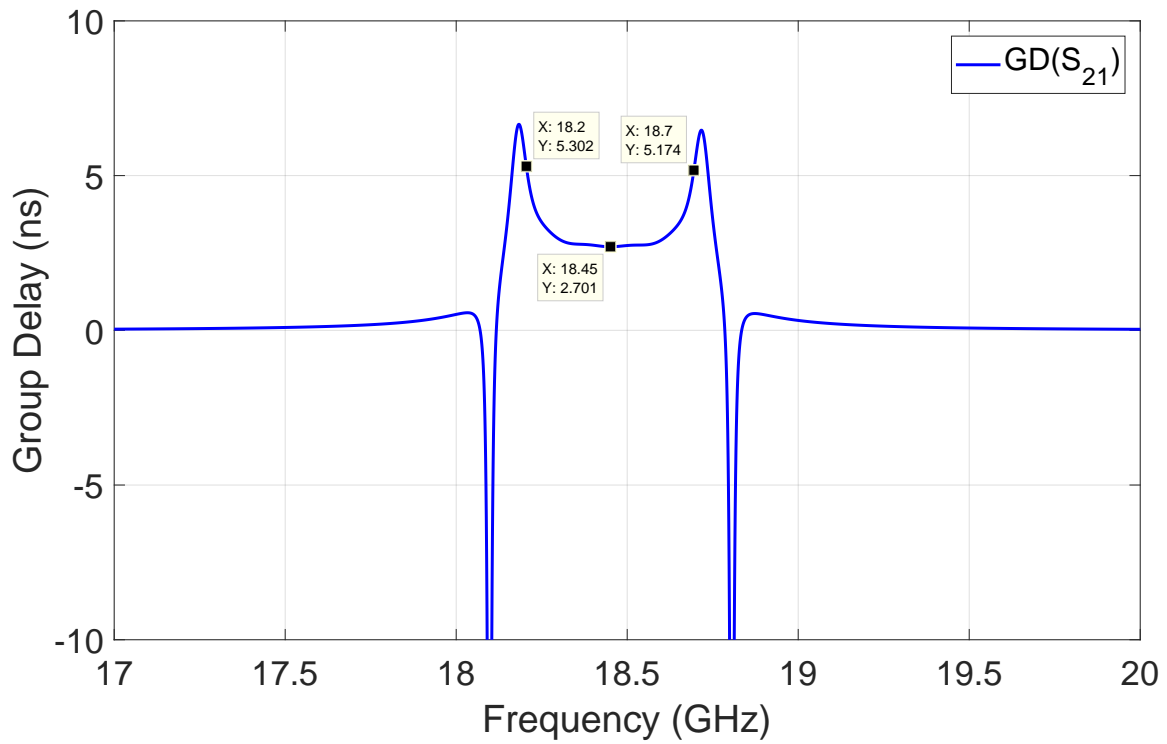
Figure 3.13: Group delay response of the channel 1 with a Q-factor of 1700.
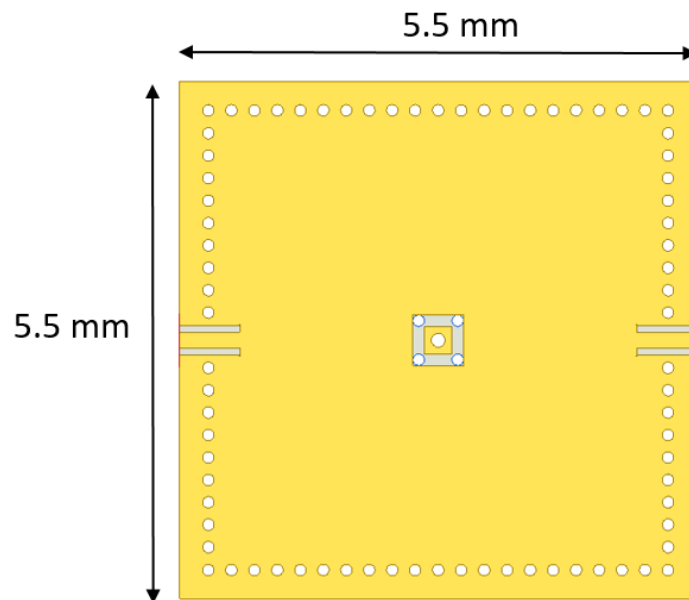
Figure 3.14: Layout and cavity dimensions of the Ka-band coaxial SIW resonator with 4 non-plated via holes to estimate the Q_u value.
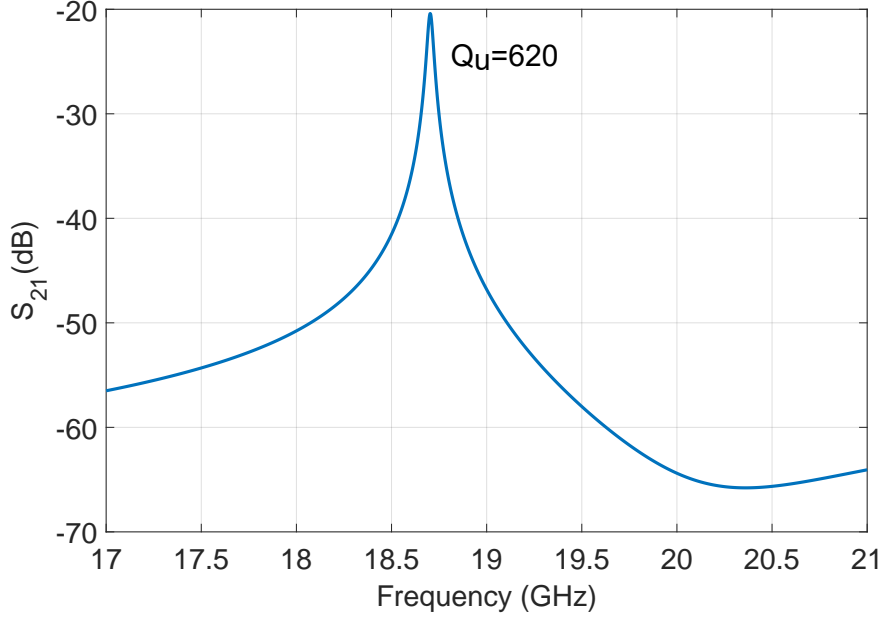
Figure 3.15: S21 parameter of the Ka-band coaxial SIW resonator with 4 non-plated via holes in Rogers RT Duroid 5880 to estimate its Q_u value.

Once the Q_u value of the employed technology is estimated using full-wave EM simulations, this parameter is included in the circuit coupling schemes of the channel filters in the manifold diplexer model.

The synthesized scheme of the Ka-band manifold diplexer is shown in Figure 3.16. The waveguide sections of the model, for the operating frequencies of the diplexer, correspond to standard WR-51 waveguides. Its dimension are 12.954 mm of width and 6.477 mm of height. The channel filters are synthesized using the coupling scheme of Figure 3.10 and considering a Q-factor of 620.

Following the design process detailed in the previous section 3.4, the next step consists on connecting the channel filters (coupling schemes) to the manifold diplexer model. All the initial lengths of the waveguide sections are set to $\lambda_g/2$, with the exception of the one terminated in short circuit, which is initialized as $\lambda_g/4$ (H-plane). Then, an optimization process can be started. After the optimization process of this diplexer model, the lengths for each waveguide section are shown in Figure 3.16. The diplexer response with the corresponding optimized dimensions is shown in Figure 3.17.
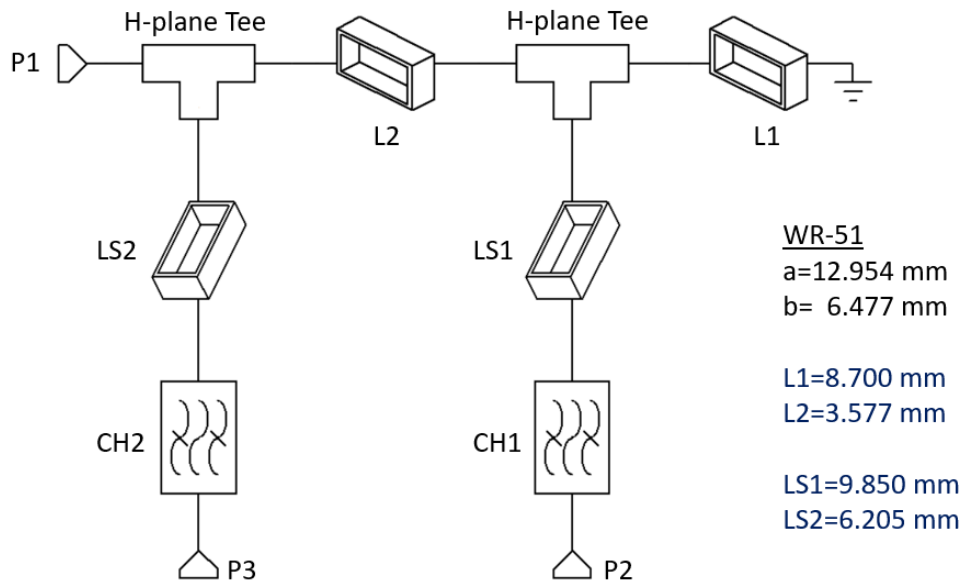
Figure 3.16: Synthesized model of the Ka-band manifold diplexer.
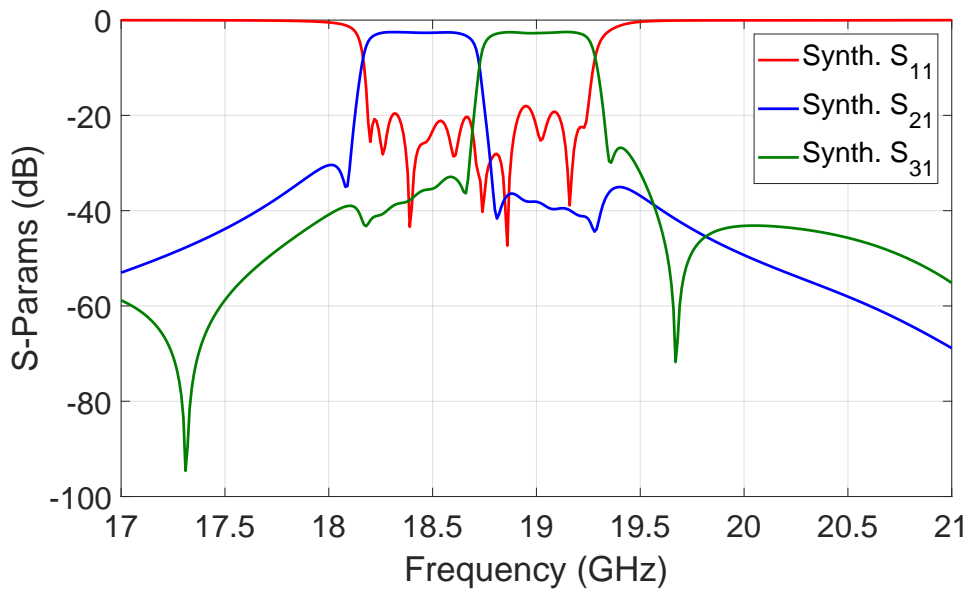
Figure 3.17: S-Parameters results of the synthesis of the Ka-band manifold diplexer.

From the obtained results in the synthesis process (see Figures 3.17, 3.18 and 3.19), we can see that all the specifications are met, except for flatness levels at the passband edges of both filters.
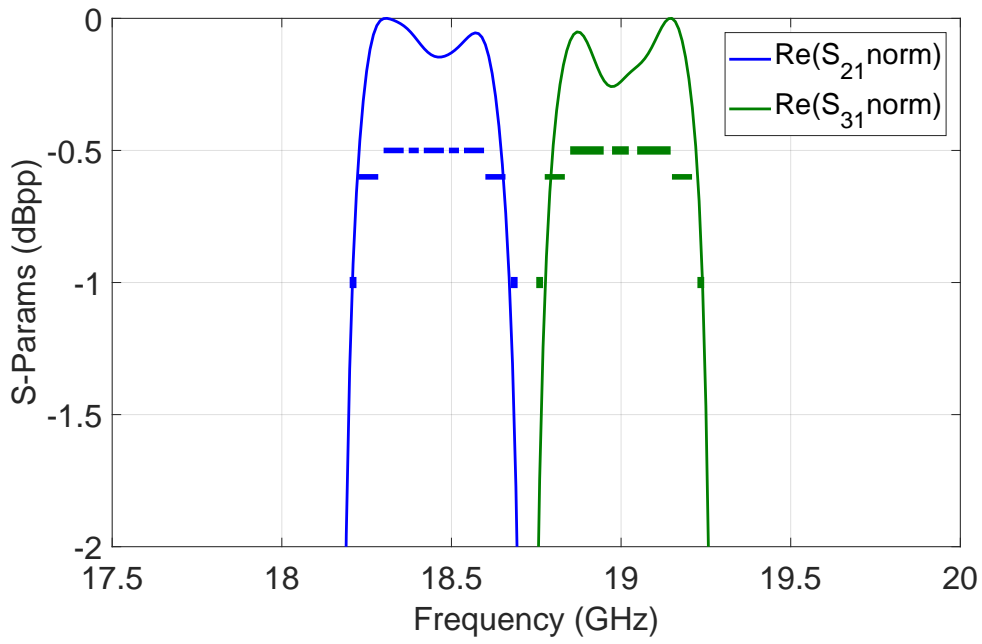
Figure 3.18: Passband flatness evaluation for the channels of the Ka-band manifold diplexer.
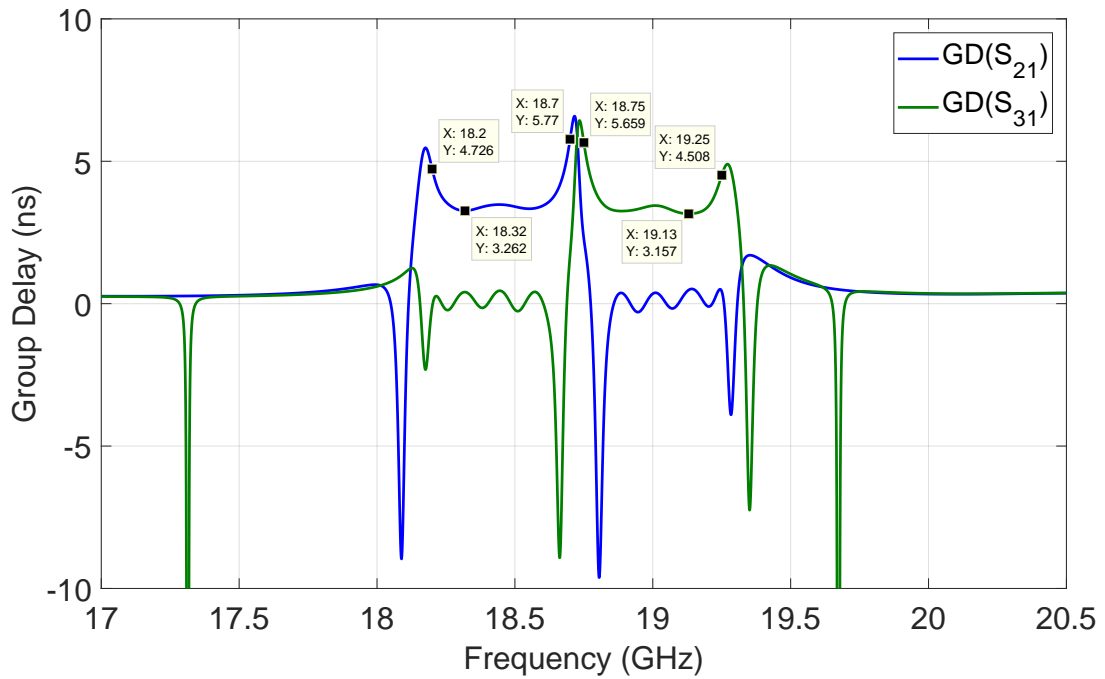
Figure 3.19: Group delay results of the synthesis of the Ka-band manifold diplexer.

3.5.3   Diplexer Design

The design phase consists in characterizing and designing each section of the diplexer model employing full-wave EM simulations. In this way, the design of the manifold lengths are selected to be optimized first.

Thus, the initial diplexer section to be designed is the one shown in Figure 3.20. Its synthesized S-parameter response is plotted in dotted lines in Figure 3.22. For this step, the waveguide model has to be transformed to SIW technology. This can be done in a simple way, just dividing dimensions by $\sqrt{\epsilon_r}$, being ϵ_r the permittivity of the substrate that we are going to use (Rogers RT/Duroid 5880, $\epsilon_r = 2.2$). In this way, the final dimensions obtained are:

$$W_{SIW} = 8.85 \text{ mm; L1} = 5.81 \text{ mm; L2} = 2.49 \text{ mm.}$$

The SIW structure designed is shown in Figure 3.21, where each of its design parameters can be appreciated. Lastly, due to the SMA interface requirement, it is necessary to perform a SIW to CPWG (Coplanar Waveguide with Lower Ground Plane) transition on the common port (P1) in order to properly connectorize the device. A comparison of the full-wave EM simulated response of the optimized SIW structure with the theoretical response of the waveguide-based model is presented in Figure 3.22.
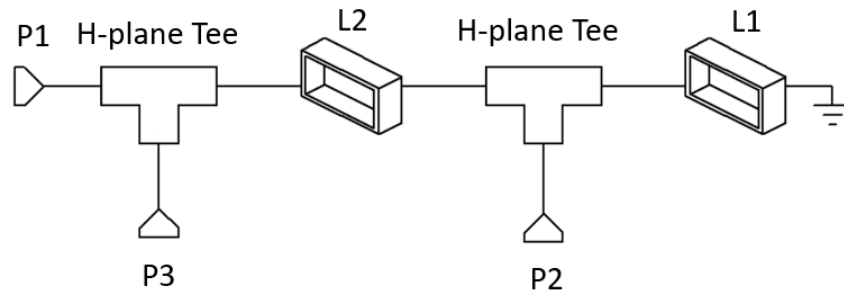
Figure 3.20: Manifold lengths of the synthesized diplexer model to be designed.

As we can see (Figure 3.22), the EM simulation and synthesis responses are not perfectly fitted. That is why, if we now substitute the waveguide sections in the synthesized diplexer model for the EM response of the SIW manifold lengths designed, as shown in Figure 3.23, some synthesis of the model parameters need to be readjusted to recover a response that meet specifications.

Thus, the LS1 and LS2 lengths of the model are modified being now of 9.026 mm and 15.19 mm, respectively, thus obtaining a response like the one depicted in Figure 3.24.
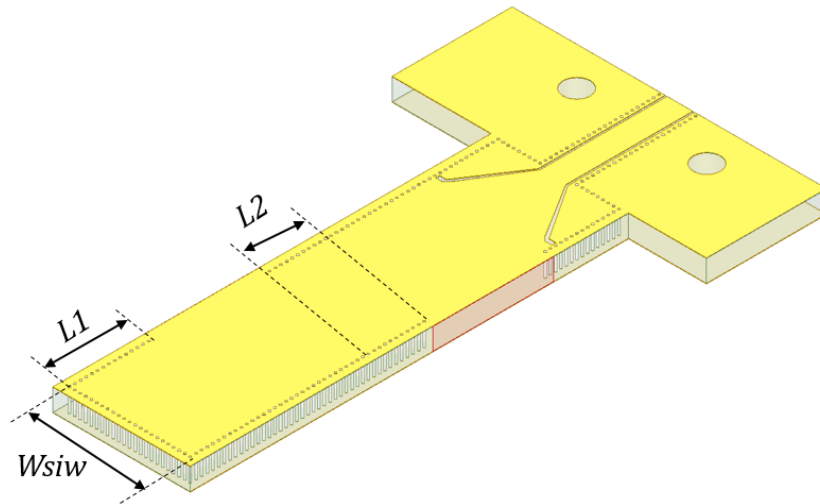
Figure 3.21: 3D-EM layout of the manifold diplexer lengths in SIW.
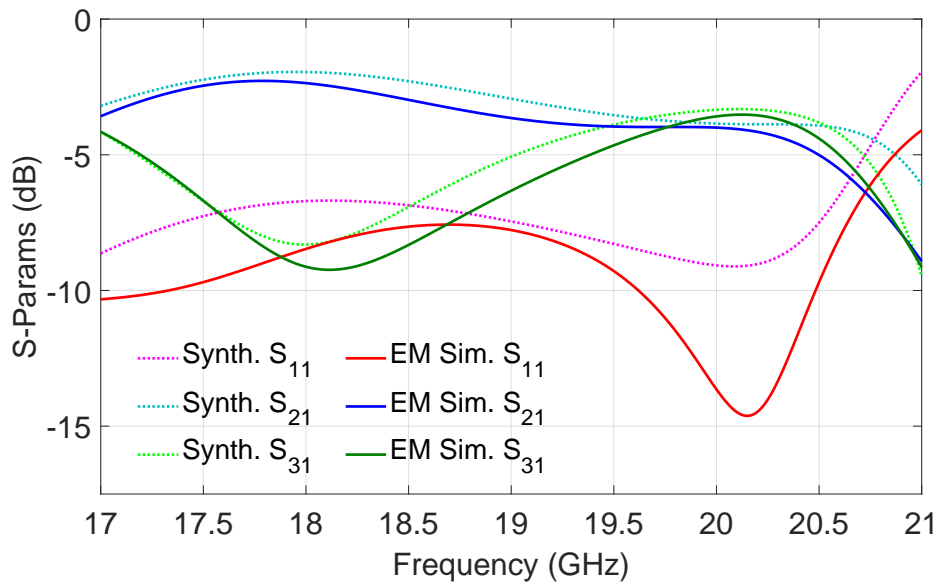
Figure 3.22: Synthesis response versus EM simulations of the manifold lengths of the diplexer.

After refining the initial model, including more details of the final real design, the synthesis of both channel filters has to be modified as well. The synthesis results of both filters within the model of Figure 3.23 are shown in Figure 3.25 for channel 1, and in Figure 3.26 for channel 2. In Figures 3.27 and 3.28, we can see the isolated synthesis response of each filter, within the diplexer structure, to obtain a response like the one in Figure 3.24.
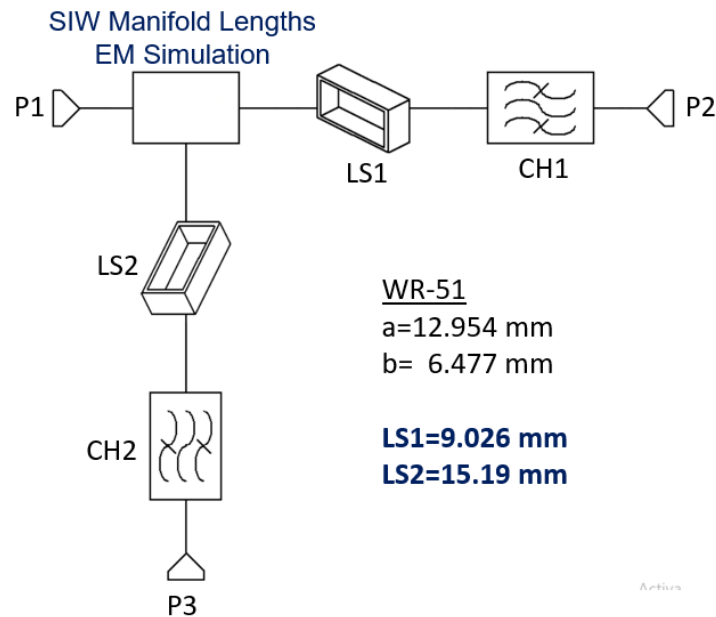
Figure 3.23: Refined model scheme of the Ka-band manifold diplexer.
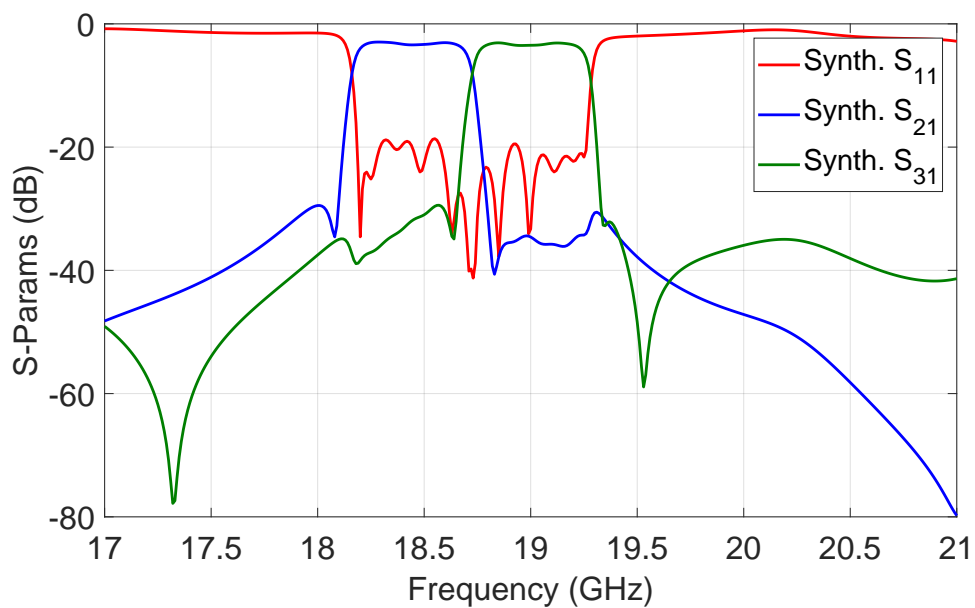
Figure 3.24: S-parameters response of the refined model of the Ka-band manifold diplexer.

The remaining parts to be analyzed with a full-wave EM simulator are the channel filters including the lengths LS1 and LS2 in each case. Since the channel filters will be implemented in coaxial SIW technology, which is more compact than the standard

b=0.0093   f$_0$=18.45 GHz   Q=620   C=(b / ω_0)   L=1/(ω_0^2C)
J01=0.01034   J34=0.0001368   J67=0.01648   B1=-3.328e-05   B4=-2.376e-06
J12=0.0001836   J45=0.0001609   J16=-2.697e-05 B2=5.036e-06   B5=-1.333e-05
J23=0.0001491   J56=0.0002249   J25=2.914e-05 B3=1.095e-06   B6=-5.233e-06
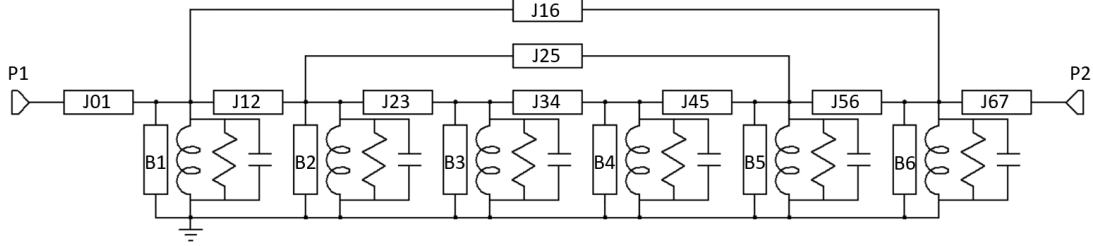
Figure 3.25: Circuit schematic of the synthesized CH1 within the manifold diplexer.

b=0.0091   f$_0$=19 GHz   Q=620   C=(b / ω_0)   L=1/(ω_0^2C)
J01=0.02617   J34=0.0001441   J67=0.01626   B1=-0.0002526   B4=1.035e-05
J12=0.0001865   J45=0.0001558   J16=-3.768e-05 B2=1.599e-08   B5=4.071e-05
J23=0.0001379   J56=0.0002280   J25=1.949e-05 B3=-4.105e-06   B6=5.598e-05
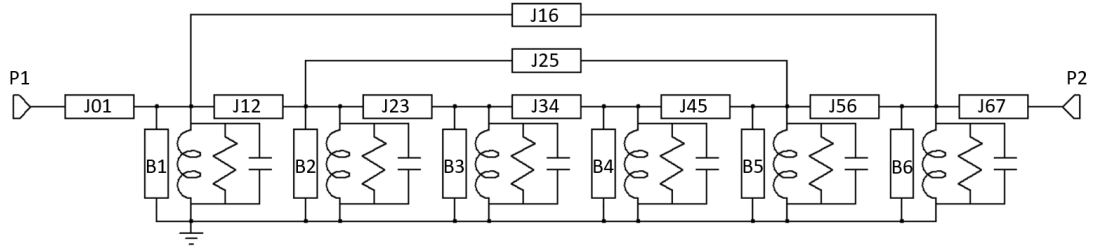
Figure 3.26: Circuit schematic of the synthesized CH2 within the manifold diplexer.

SIW technology employed to implement the manifold lengths, it will be necessary to design a SIW to coaxial SIW transition to couple properly the channel filters to the diplexer manifold structure. In this way, the part of the synthesized scheme model of the diplexer in hybrid technology that we are going to design is the one shown in Figure 3.29, corresponding to CH1. The equivalent 3D structure and their SIW design parameters are shown in Figure 3.30. In Figure 3.31, the main design parameters for the channel filters are summarized.

In Figure 3.31, the resonator distribution is specified by the numbers in white. The w_{ij} parameter refers to the iris width used to couple two cavities, varying the ij sufix in each particular case. As we can see in the top view of the channel filters structure, all the inter-resonator couplings are implemented by means of an iris, except for the 1-6 cross-coupling used for introducing TZs in the response, implemented with a CPW line.
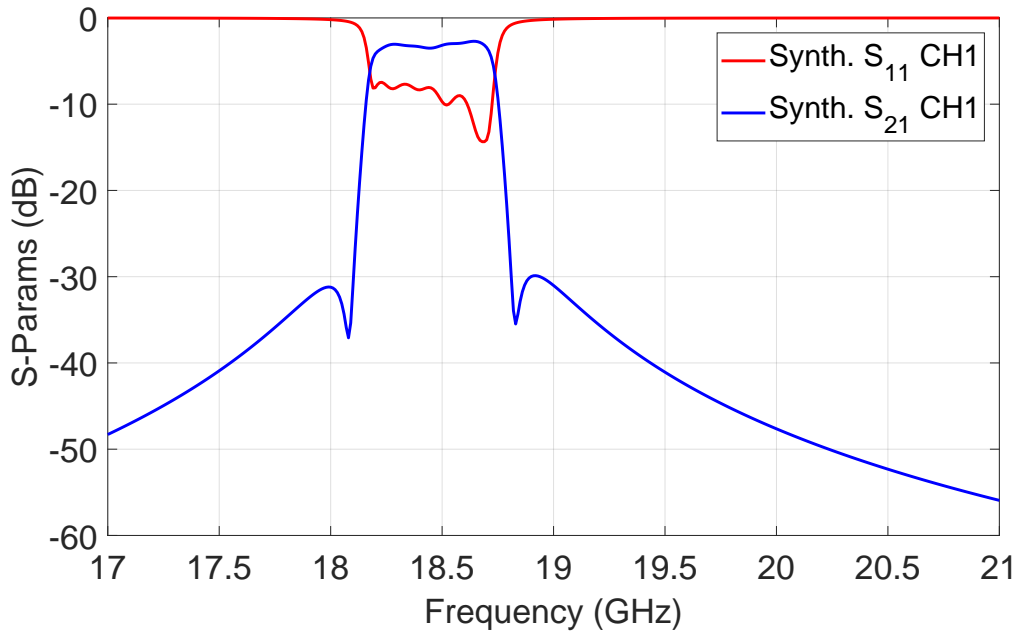
Figure 3.27: S-parameters response of the synthesized CH1 within the manifold diplexer.
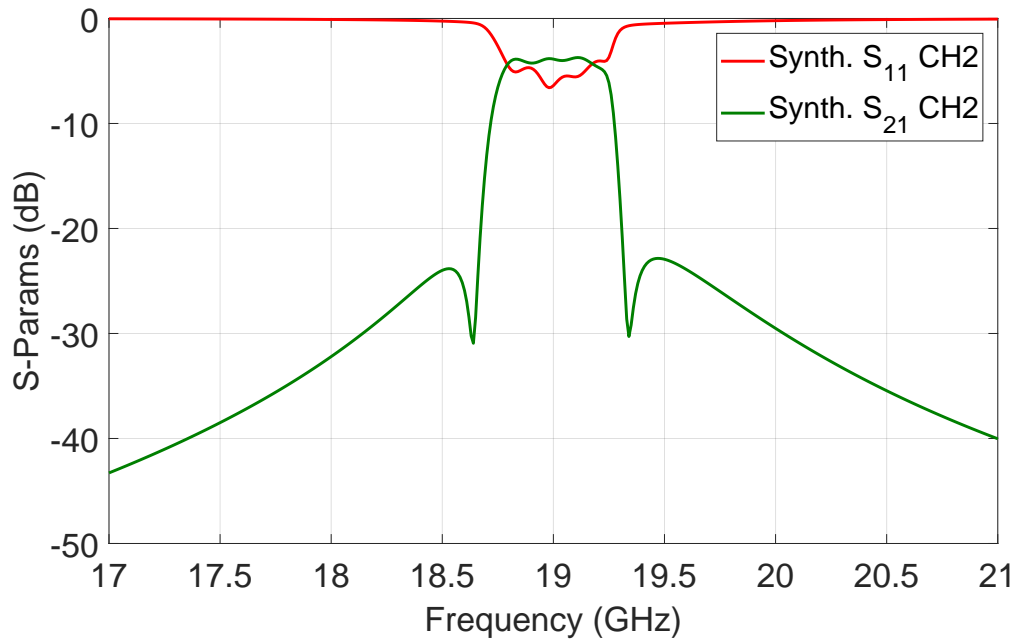
Figure 3.28: S-parameters response of the synthesized CH2 within the manifold diplexer.

For defining this CPW line, its width (w_{16}) is specified and, instead of its total length, the distance between the patch and the line (that is the penetration inside each resonator, p_{16} in Figure 3.31, which is symmetrical in both affected cavities, is used. Both w_{16} and p_{16} are design parameters.
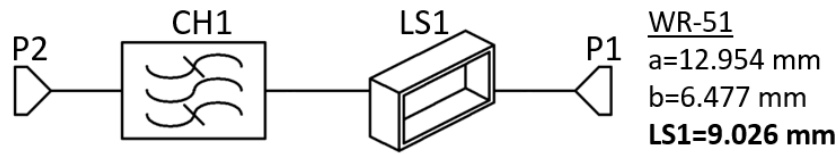
Figure 3.29: Section of the synthesis diplexer model to be designed, corresponding to LS1 + CH1.
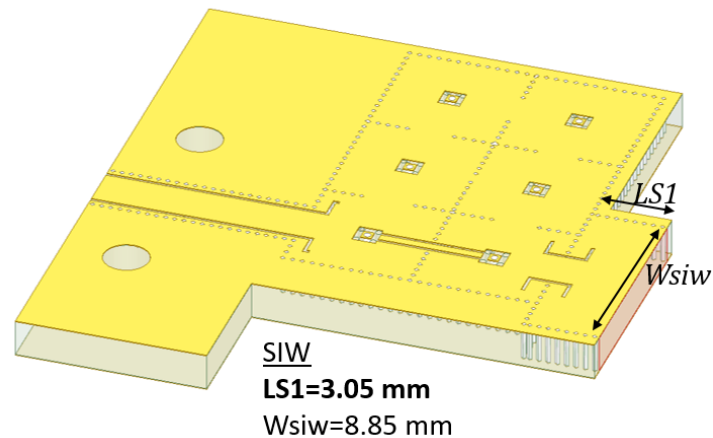
Figure 3.30: 3D-EM layout of the CH1 filter in coaxial SIW and LS1 length in SIW.

Additionally, both Figures 3.30 and 3.31, the required transitions in both ports can be seen. At the output port for terminating with an SMA interface, and at the input port for enabling the proper connection between the SIW manifold lengths and the coaxial SIW cavities. Both transitions are made using a CPW probe. In the input transition, besides the iris, it is neccesary the introduction of the CPW probe to reach the proper external coupling level. This fact leads to the need of adjusting not only the magnitudes of the S-parameter responses of the real and synthesized model filters, but also to consider the phase responses of the filters together with the LS1 section values, since the introduction of the CPW probe prevents a direct correlation between the LS1 length values in both models (the ones used in the synthesis and design stages). Proceeding in this way, we start getting close of the correct values for the phase and external coupling through the SIW LS1 length and the input CPW probe, and then, with the rest of the design parameters of the filter, finely adjust both, the magnitude and phase of responses on the synthesis and design models. After completing this desgn process, we obtain the optimized dimensions of all design variables for the LS1 length plus CH1 filter shown in Figure 3.30.
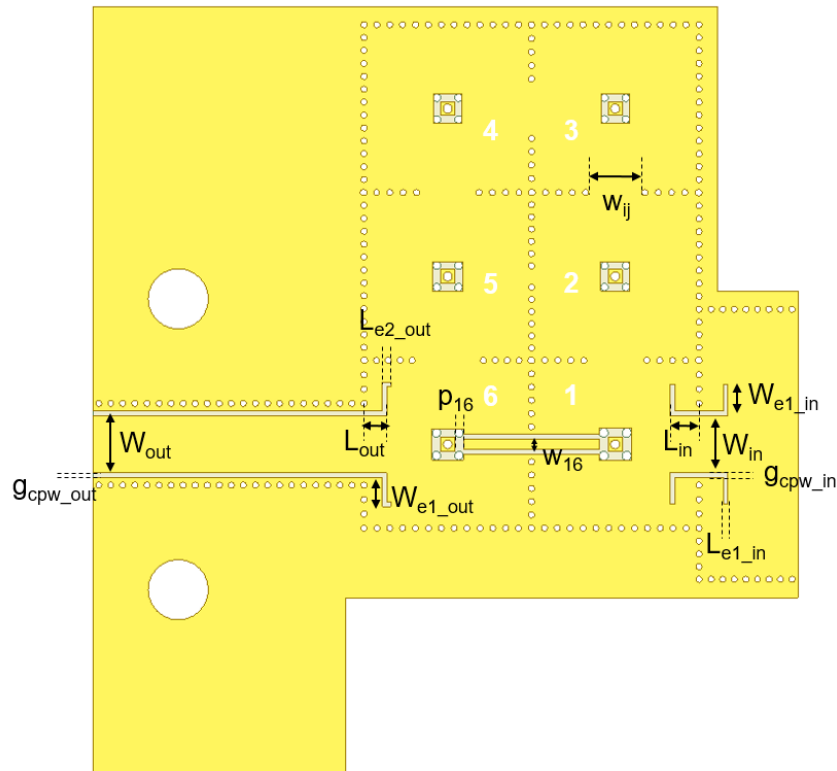
Figure 3.31: General nomenclature of the design parameters for the diplexer channel filters.

Comparisons of the magnitudes and phases of the S-parameter responses of the synthesized diplexer model, and of the full-wave EM simulations of the real structure, can be seen in Figures 3.32 and 3.33. In this case, the EM and theoretical responses are in very good agreement.

Proceeding similarly for the section of the diplexer model corresponding to the LS2 length and channel 2 (Figure 3.34), we obtain the following good fitting between the responses of the synthesized and design models for their phase and S-paremeter responses (see Figures 3.35 and 3.36).

Next, once we have completed the design of all parts of the synthesized model, we proceed to design the full diplexer structure. The initial starting point is the one obtained in the previous cascaded design process. The dimensions of this starting point are collected in Table 3.2. The complete structure layout of the diplexer can be seen in Figure 3.37. Running an EM simulation of this structure with the dimensions of Table 3.2, we obtain the response shown in Figure 3.38. As we can see, the obtained S-parameters response using the explained design method is quite close to the synthesized model response.
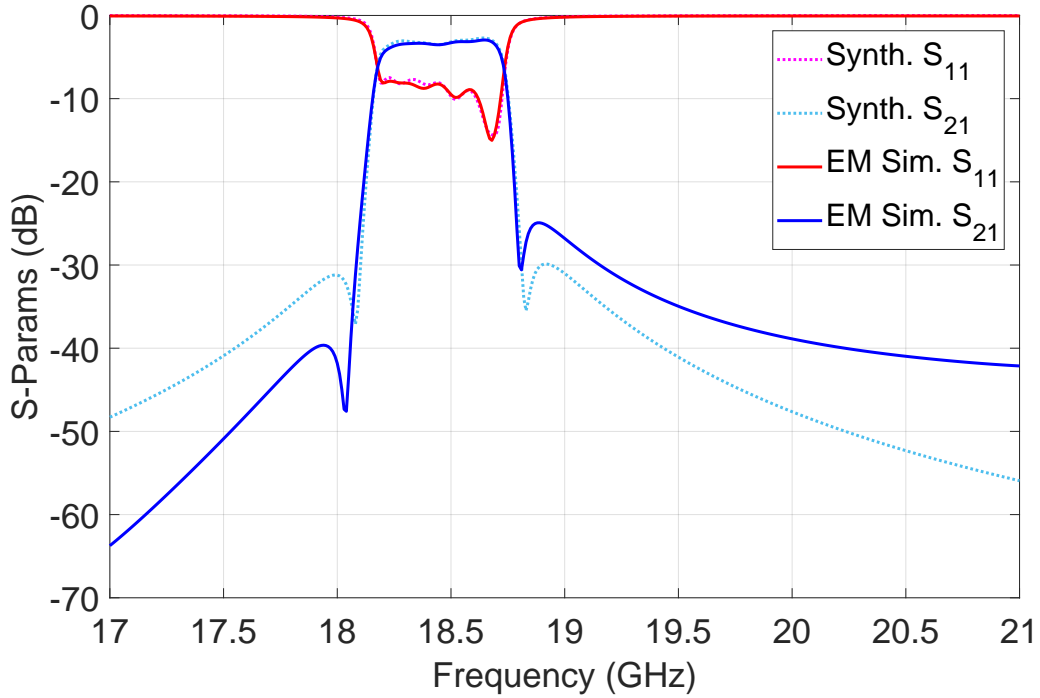
Figure 3.32: Comparison of the magnitudes of the S-parameters for the synthesized and design models of LS1 + CH1 in the manifold diplexer.

At this point, an optimization process is performed for a final adjustment of the response, considering the entire real structure. After this process, the results shown in Figures 3.39, 3.40 and 3.41 are obtained. The final optimized dimensions of the diplexer structure are listed in Table 3.3, where only the modified variables have been updated. In table 3.4, a Statement of Compliance (SoC) of the designed diplexer, with regard to the considered specifications, is included.

Evaluating the EM simulation results of the designed diplexer and compared with respect to the initial specifications, we see that the RL in the whole diplexer bandwidth are better than 17 dB (Figure 3.39), while a value of 18 dB was set in the requirements. The IL values at the center frequency in each channel are fulfilling the specifications, since they are lower than 5 dB. However, in the 500 MHz-bandwidth of each channel filter, the IL values do exceed 5 dB, being lower than 5.63 dB in the entire passband of the channel 1, and lower than 5.53 dB in the passband of channel 2. Regarding the narrow-band isolation, the 20 dB requirement level is met in both channels. However, the 30 dB attenuation required in $f_0 \pm 100\%$BW is only fully achieved at the lower stopband; obtaining, in the case of the channel 1, an attenuation at the upper stopband greater than 25 dB, and in the case of channel 2, a rejection higher than 28 dB.
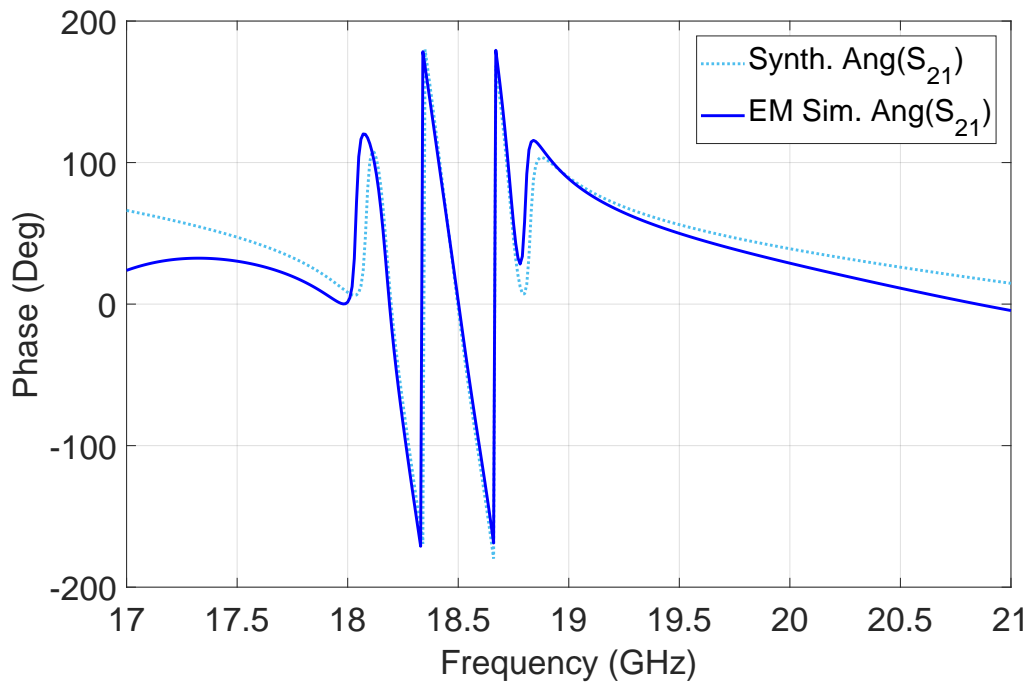
Figure 3.33: Comparison of the S_{21} phases for the synthesized and designed models of LS1 + CH1 in the manifold diplexer.
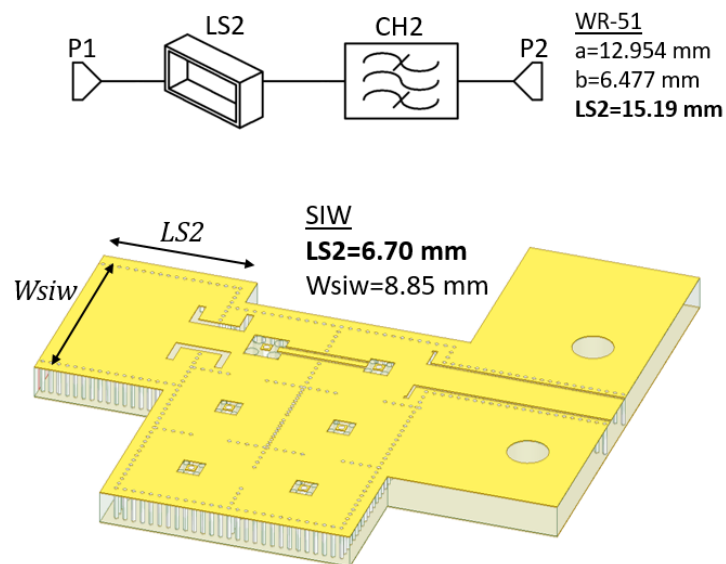
Figure 3.34: Top: Section of the synthesis diplexer model to be designed, corresponding to LS2 + CH2. Bottom: 3D-EM layout design of the CH2 filter in coaxial SIW and LS2 length in SIW.
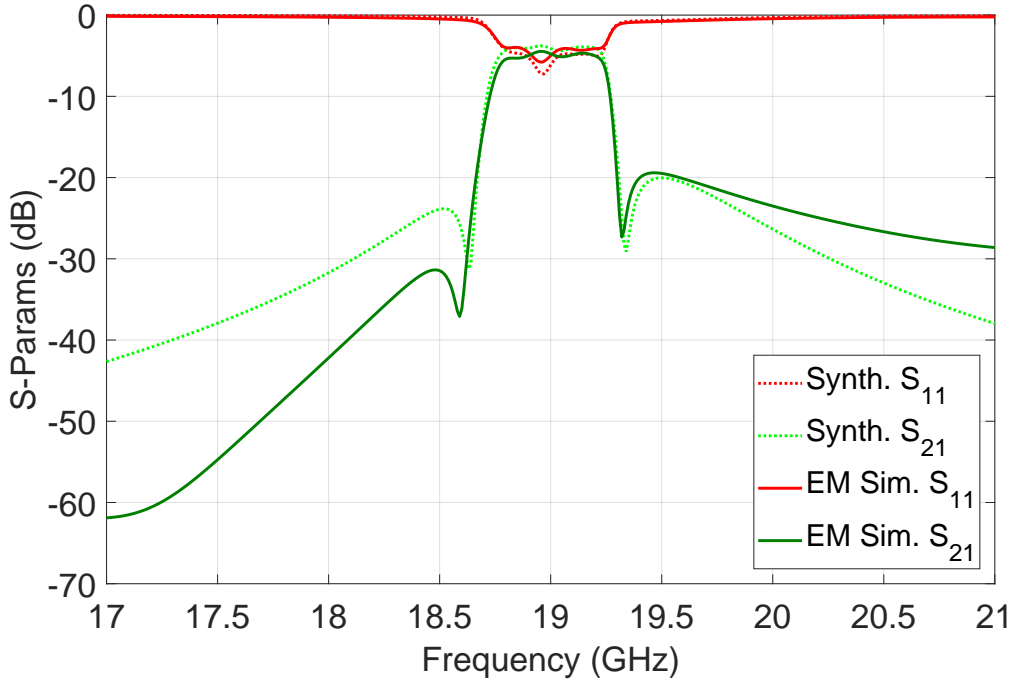
Figure 3.35: Comparison of the magnitudes of the S-parameters for the synthesized and design models of LS2 + CH2 in the manifold diplexer.

With regard of the planarity results in full-wave EM simulations, as previously foreseen during the synthesis phase, the related specifications continue to be unfulfilled. In particular, the channel 2 planarity is even deteriorated more in the full-wave EM simulated results.

Finally, analyzing the group delay results obtained from EM simulations, we can see from the marker values in Figure 3.41, that the variations of the group delay required in the specified frequency ranges would be perfectly fulfilled, being even lower in the range of $f_0 \pm 50\%$BW than 1.6 nspp for channel 1, and lower than 1.7 nspp for channel 2.

To conclude, it is interesting to note that the results achieved in this section are trying to get the best performance of the SIW coaxial technology, using a dielectric material with very good characteristics, but still improvable by using other materials with lower losses and better performance. Even so, despite of not complying 100 % with all the required specifications, the achieved solution has met reasonably and satisfactorily many of them, keeping close to meet those not fully complied.

Several options and alternatives that would allow a re-design of the diplexer in order to meet the set specifications, such as the use of a better material (quartz, alumina) or the application of lossy techniques to flatten the passband with lower Q requirements, are outside the scope of this thesis. However, in the following chapter we will delve into some of the mentioned options and their application in coxial SIW technology.
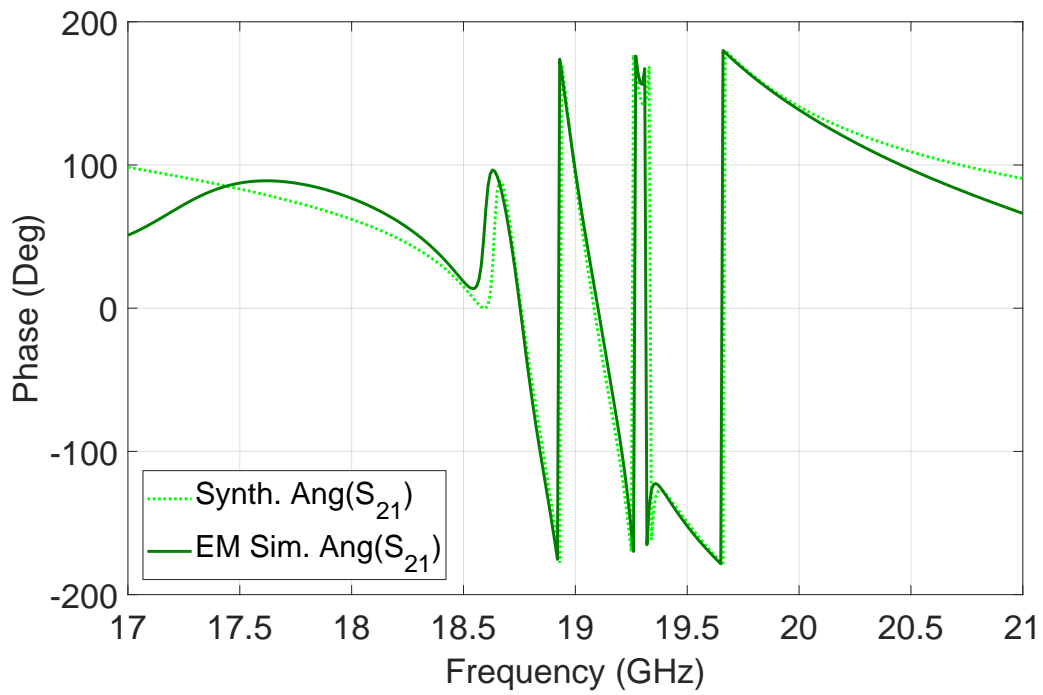
Figure 3.36: Comparison of the S_{21} phases for the synthesized and design models of LS2 + CH2 in the manifold diplexer.
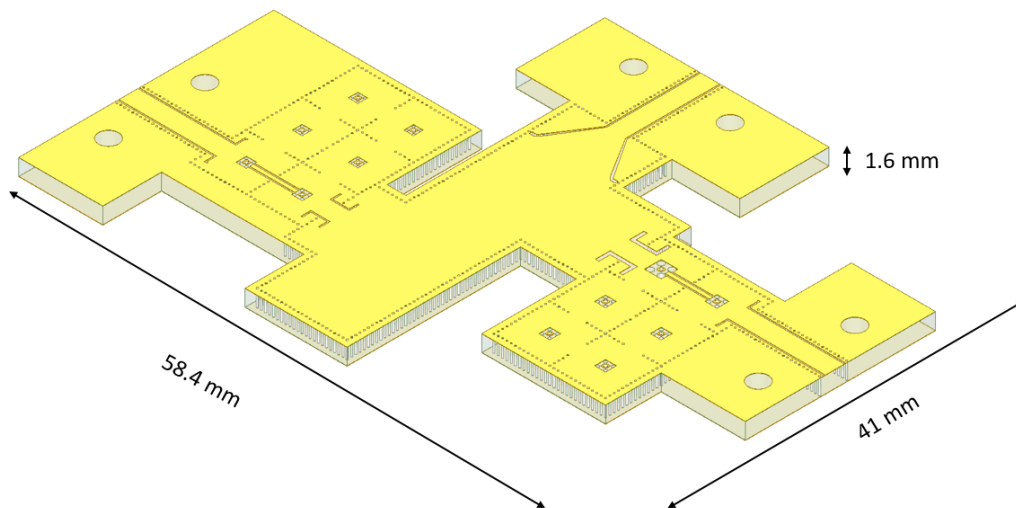
Figure 3.37: Final layout of the Ka-band diplexer including SMA connector interfaces.

Param.	Value		Param.	Value	
				CH1	CH2
W_{SIW}	8.85		w_{34}	1.745	1.74
L1	5.81		w_{45}	1.85	1.78
L2	2.49		w_{56}	2.145	2.22
LS1	3.05		w_{25}	0.5	0.25
LS2	6.7		p_{16}	0.302	0.35
$W_{CSIW} = L_{CSIW}$	5.5		w_{16}	0.35	0.35
d_v	0.3		L_{in}	0.8	1
r_p	0.46		W_{in}	2.478	2.878
s_{p1}	CH1	CH2	W_{e1_in}	0.87	1.12
	0.301	0.62	L_{e1_in}	0.15	0.35
s_{p2}	0.2445	0.302	g_{cpw_in}	0.15	0.35
s_{p3}	0.243	0.310	L_{out}	0.6	0.6
s_{p4}	0.246	0.308	W_{out}	1.878	1.878
s_{p5}	0.255	0.314	W_{e1_out}	0.8	0.9
s_{p6}	0.2845	0.359	L_{e2_out}	0.13	0.1
w_{12}	1.865	1.75	g_{cpw_out}	0.15	0.15
w_{23}	1.75	1.67	g_{cpw_16}	0.15	0.15

Table 3.2: Dimensions (in mm) of the starting point of the Ka-band diplexer structure.
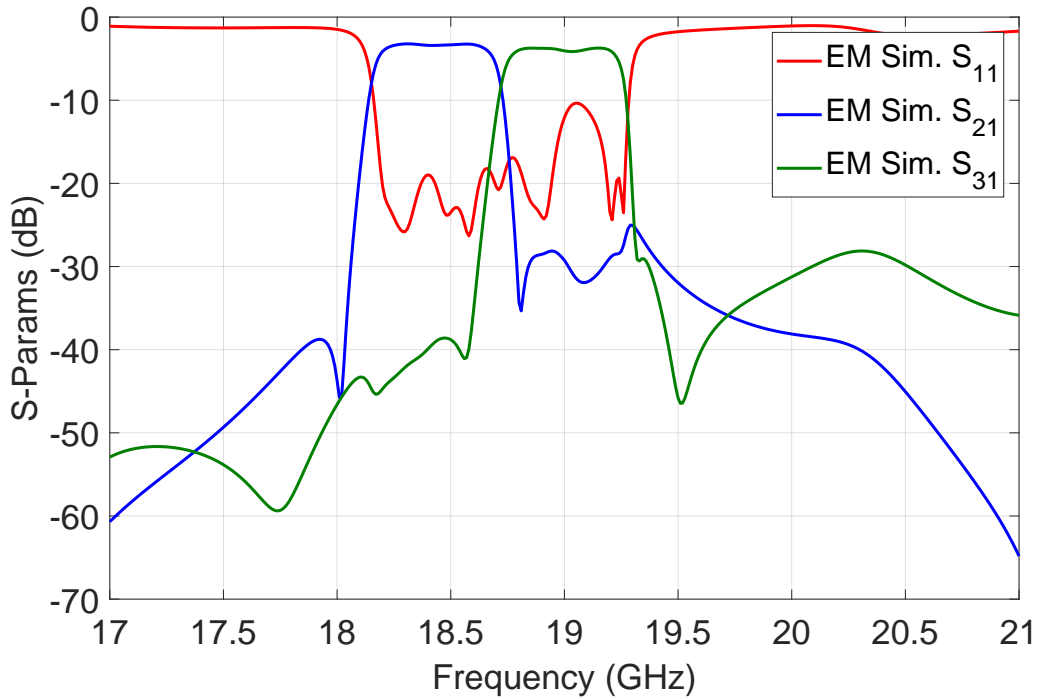
Figure 3.38: Initial EM response of the whole Ka-band diplexer structure after the cascaded design procedure explained (starting point with dimensions of Table 3.2).
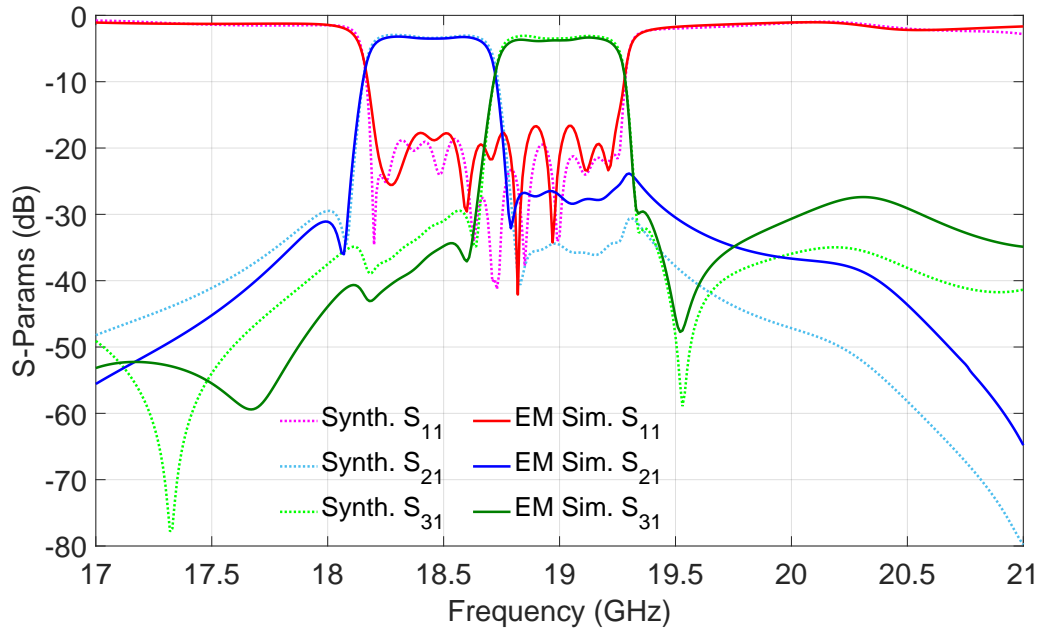
Figure 3.39: S-parameter results of the synthesized diplexer model and of the full-wave EM simulation of the finally designed real structure.
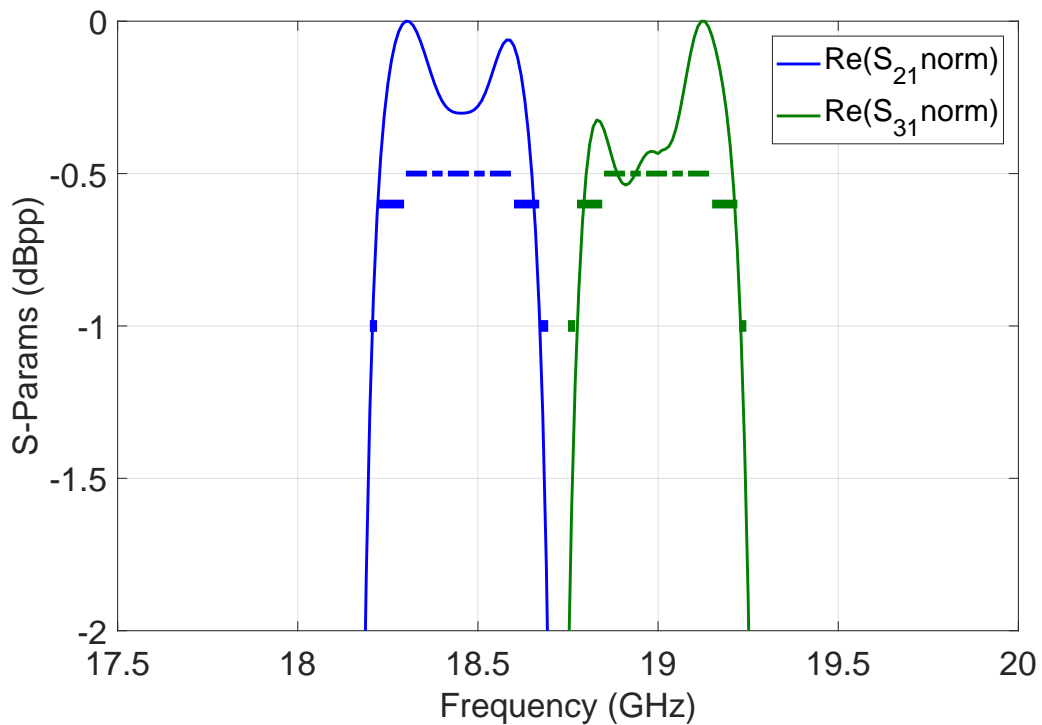
Figure 3.40: IL Flatness results of the full-wave EM simulation of the designed Ka-band diplexer.
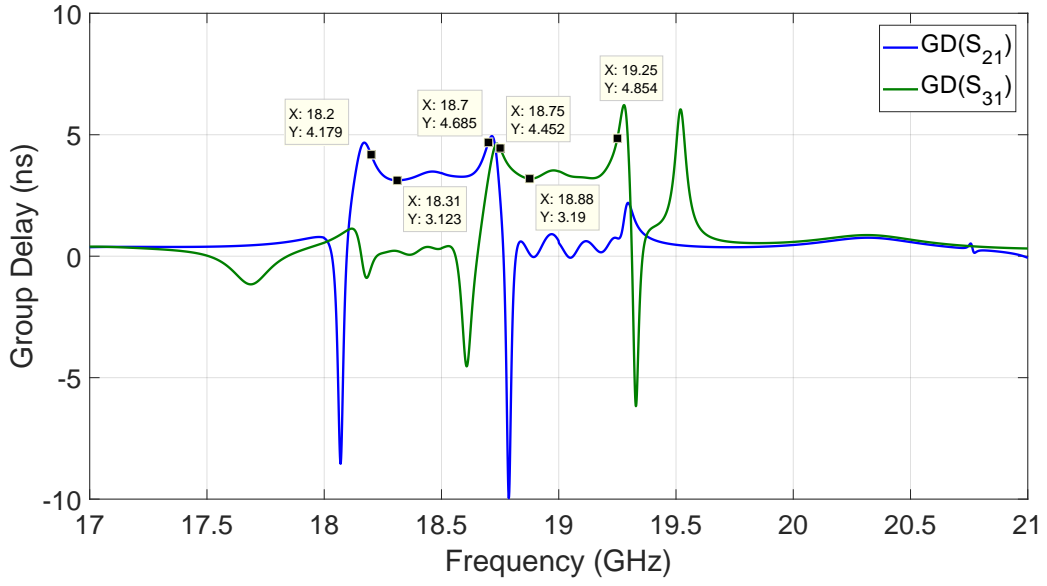
Figure 3.41: Group delay results of the full-wave EM simulation of the designed Ka-band diplexer.

Param.	Value	
	CH1	CH2
s_{p1}	0.303	0.605
s_{p2}	0.245	0.307
s_{p3}	0.243	0.309
s_{p4}	0.246	0.3115
s_{p5}	0.255	0.3202
s_{p6}	0.285	0.358
w_{12}	1.85	1.755
w_{23}	1.74	1.67
w_{34}	1.745	1.74
w_{45}	1.85	1.7853
w_{56}	2.145	2.2
w_{25}	0.4	0.4
p_{16}	0.285	0.335
W_{e1_in}	0.85	1.1
L_{e2_out}	0.13	0.07

Table 3.3: Final dimensions (in mm) of the optimized design parameters of the Ka-band diplexer structure.

Specification	SOC
Manifold Topology in SIW and coaxial SIW technologies	C
f_0 CH1: 18.45 GHz f_0 CH2: 19 GHz	C
Channel BW: 500 MHz	C
IL at f_0 <5 dB	C
IL Flatness: $f_0 \pm 30\%$ BW <0.5 dBpp $f_0 \pm 45\%$ BW <0.6 dBpp $f_0 \pm 50\%$ BW <1 dBpp	NC
Narrowband Isolation: $f_0 \pm 65\%$ BW >20 dB $f_0 \pm 100\%$ BW >30 dB	C NC
Group Delay Variation: $f_0 \pm 30\%$ BW <2 nspp $f_0 \pm 45\%$ BW <3 nspp $f_0 \pm 50\%$ BW <6 nspp	C
Input and Output RL >18 dB	NC
Footprint and Mass: To be minimized	C
Interface SMA	C

Table 3.4: Statement of Compliance (SoC) of the Ka-band manifold diplexer designed: C: compliant; NC: non-compliant.

<div align="right">

Chapter 4

</div>

Filter Design with Improved Passband Flatness

In this chapter, the coaxial SIW resonator will be studied with the goal of obtaining filters with improved in-band flatness. Having a sharp and highly selective filter, as well as a flat frequency response in the passband, are the main requirements of a microwave filter, regardless of its application. These filtering properties will be pursued exploiting the design flexibility of the coaxial SIW topology together with the application of lossy techniques. Finally, several filter examples will be designed applying the proposed techniques showing their flatness improvements achieved.

4.1 Q-Factor Control in Coaxial SIW Resonators

Coaxial SIW resonators provide several degrees of freedom in the design process, all of them related to the different geometrical parameters involved in the structure. Although resonant frequency control and size miniaturization are usually the most relevant ones [81], these resonators provide also the possibility of a fine Q-factor control.

The general structure of a coaxial SIW resonator with its main design parameters is shown in Figure 4.1. As it can be observed, the substrate thickness th_{sub} plays a very important role for the physical and electrical performance, providing both miniaturization and higher unloaded Q-factor with larger thicknesses. However, the substrate thickness does not provide much flexibility to adapt the resonator Q-factor during the design process, as it is fixed and constant for all resonators of a particular topology.

Other geometrical parameters are usually employed for controlling the resonant frequency, such as the capacitive gap s_P or the resonator admittance given by the cavity size,(given by the product of W_{CSIW} and L_{CSIW}). However, the inner via hole diameter d_V and specially the patch size r_P, they allow a fine and constant control of the resonator Q by modulating the introduction of resistive losses associated to the loading capacitance.
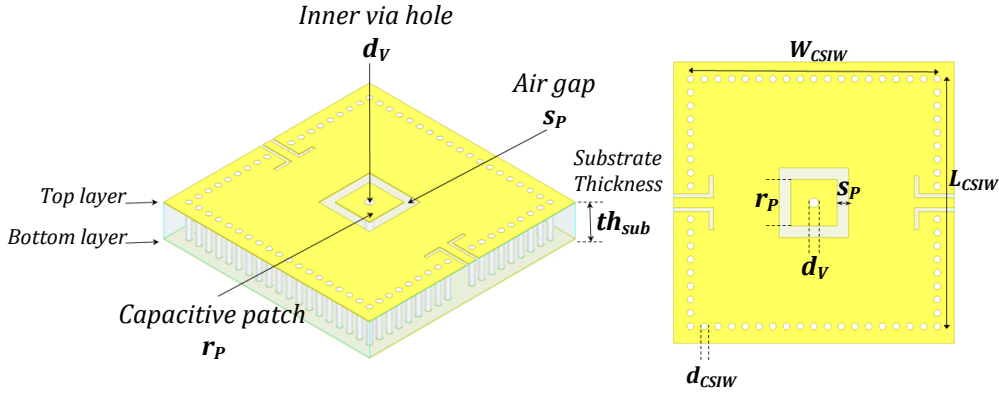
Figure 4.1: 3D and top view of the coaxial SIW resonator.

As it is shown in Figures 4.2 and 4.3, the simulated unloaded Q-factor Q_u changes with both d_V and r_P . However, it is evident from the graphs that r_P provides a wider range of variation of Q_u values, while d_V has a minor effect being related to the inductive part of the resonator. As it is shown, the bigger r_P , the smaller the Q_u, being possible a reduction of Q_u of more than 80%. On the contrary, increasing d_V provides an enhancement of Q_u, but when it is necessary to have a larger patch to place the inner via, the effects of a bigger r_P, produces a higher Q_u reduction than the Q_u improvement of a bigger d_V.

The main parameters of the resonator used in the study of the graphs are: $W_{CSIW} = L_{CSIW} = 10$ mm, $th_{sub} = 1.524$ mm-thick for a Rogers RO4003C substrate ($\epsilon_r = 3.55$, tan $\delta = 2.7 \cdot 10^{-3}$) with a finishing of 35 μm copper and 5 μm of Ni-Au.

With the aim to validate these concepts, two different resonators operating at X-band (i.e. f_0=10 GHz) have been manufactured, one with a small patch (r_P=0.6 mm; $W_{CSIW} = L_{CSIW}$=10 mm; d_V=0.3 mm; s_P=0.23 mm) to reach higher Q_u values, and the other one with a large patch (r_P=3.872 mm, $W_{CSIW} = L_{CSIW}$=10 mm, d_V=2 mm; s_P=0.677 mm) to reach lower Q_u values. In Figure 4.4, a photo of the manufactured resonators is presented. Their correspondent transmission responses are shown in Figure 4.5. For the coaxial SIW resonator with a large patch, the Q_u measured is 53, while for the resonator with small patch the extracted Q_u is 270. These measurements prove the wide range of possible Q_u values that can be obtained, at practically the same resonant frequency, with coaxial SIW resonators of the same cavity size.
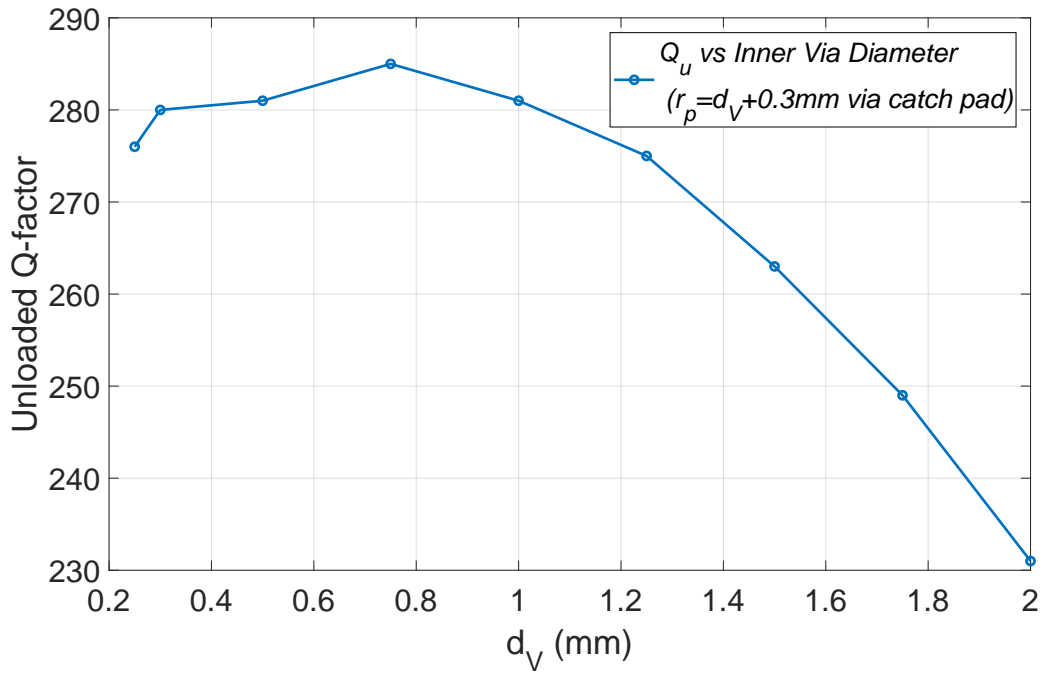
Figure 4.2: Q_u-factor study of the coaxial SIW resonator versus the diameter of the inner via hole d_V.
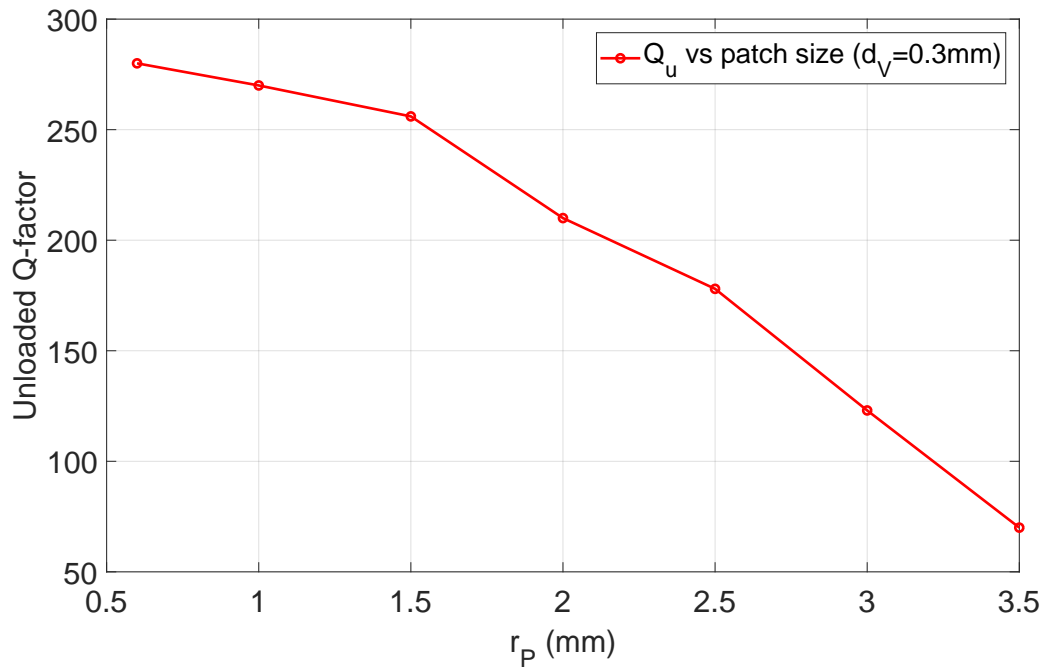
Figure 4.3: Q_u-factor study of the coaxial SIW resonator versus the size of the capacitive patch (dimension r_P).
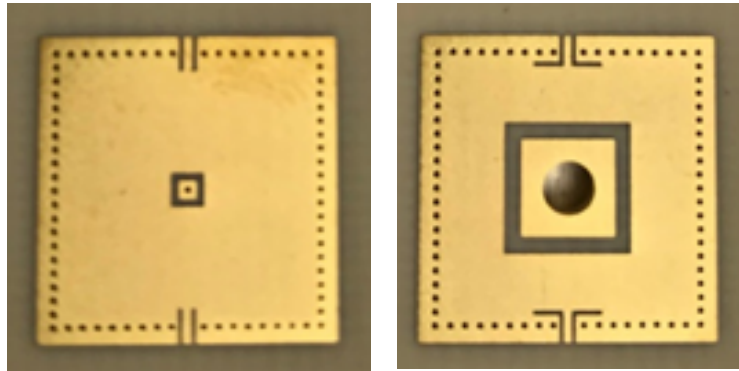
Figure 4.4: Photographs of the manufactured X-band coaxial SIW resonators.
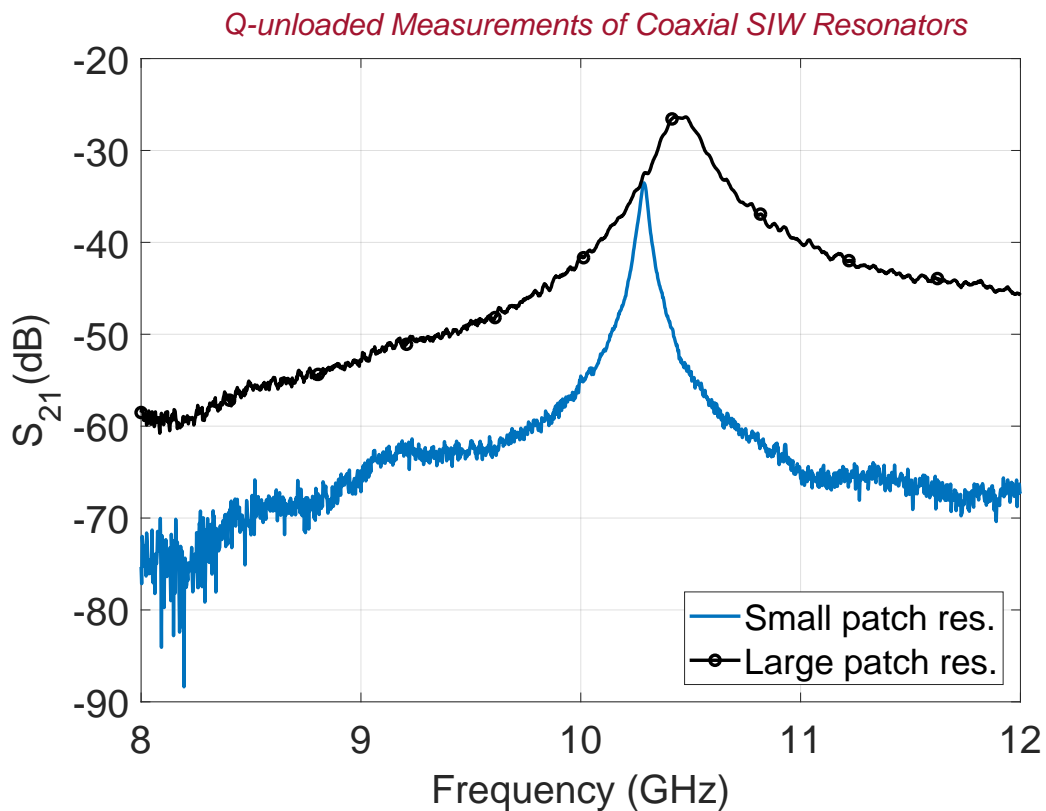
Figure 4.5: Q_u measurements of the manufactured X-band coaxial SIW resonators.

It is interesting to highligth that this ability to control the unloaded Q-factor of coaxial SIW resonators within a very wide range, and without the need of using different technologies or introducing resistors, allows the easy implementation of lossy techniques in this technology, thus enabling to optimize the in-band response of the filters designed, reaching higher-performance and more advanced responses.

4.2   Filter Design with Improved Passband Flatness

In-band flatness requirements in high-end applications, such as satellite communications, pose enormous challenges to compact planar filter implementations due to the need of very high Q-factor resonators. Microstrip filter structures cannot usually reach the required flatness and/or rejection levels for narrow-band channel filters, while conventional SIW topologies are still limited by the inherent losses coming from the dielectric, as well as by a larger footprint. Some low-loss implementations as empty SIW [21] or air-filled [22] could be an alternative at millimeter-wave frequencies, where device size is not critical anymore, but they still present evident inherent limitations in terms of batch manufacturing and integrability.

In order to improve the electrical response directly achievable with moderate-to-low Q resonators, one option is the application of the Q-enhancement techniques, as presented in section 3.3 of the previous chapter. That increase of Q, produce a better in-band characteristics due to the lower losses. Nevertheless, that increase of Q without increasing considerably the size, is not as relevant as for sufficiently improving the filter flatness. A good alternative, on the other hand, is the application of lossy filter design techniques. These techniques accomplish a high-Q effective response with low-Q resonators, introducing additional insertion losses within the passband, but obtaining higher in-band planarity. However, the practical implementation is not straightforward, as resistors must be introduced at the required locations to obtain the requested losses or to provide the Q-control for the different values needed. This is not always feasible without employing solutions based on hybrid technologies, which are usually of difficult implmentation and integration.

In this section, we will study the planarity achieved with three different filters using coaxial SIW resonators. The first one will consist on a classical-conventional uniform Q filter. The second one will be designed applying a Q-enhancement technique, using slots in the topology (as proposed in section 3.3). And the third one will be designed using the lossy technique based on non-uniform Q-factor resonators (see section 4.1).

The specifications for the proposed filters are:

- Topology: Coaxial SIW.
- Center frequency, f_0 : 10 GHz (X-band).
- Bandwidth (BW) = 280 MHz.
- Insertion Losses at $f_0 < 5$ dB.
- Narrow-band Isolation: $f_0 \pm 90\%$ BW > 20 dB
- Input and Output Return Losses: $f_0 \pm 50\%$ BW > 18 dB
- Footprint: To be minimized.
- Interface: SMA.

All designs will be implemented in a 1.524 mm-thick Rogers RO4003C substrate ($\epsilon_r = 3.55$, $\tan \delta = 2.7 \cdot 10^{-3}$) with a finishing of 35 μm copper and 5 μm of Ni-Au.

4.2.1 Filter with Uniform Q using Best-Q-Designed Coaxial SIW Resonators

As we presented in the previous section of this chapter, in SIW coaxial topology (considering the technological limits associated to the structure and the material used), we can control the Q-factor of a cavity in its design phase. From the graphs of the study performed in section 4.1 (see Figures 4.2 and 4.3), elaborated with the same substrate material employed now for designing the considered filter, it is extracted that the smaller r_P, the higher the Q-factor of the resonator, obtaining a maximum Q value in this substrate of 270. Therefore, setting this value as the best-Q factor reachable for the coaxial SIW resonator in this substrate, the response is synthesized for accomplishing the target specifications.

A fourth-order Chebyshev filter with RL of 18 dB has been designed; introducing a cross-coupling between resonators 1-4 in order to fulfill the narrow-band isolation requirement. Figure 4.6 shows the coupling scheme used to synthesize the filter, and Figure 4.7 exhibits the layout structure of the designed filter. Its synthesis parameters and layout values are reported in Table 4.1. Expressions for the synthesis of the capacitors and inductors used in Figure 4.6 are:

$$C = \frac{b}{\omega_0}; \quad L = \frac{1}{\omega_0^2 C} \tag{4.1}$$

For the remaining parameters modelling the coaxial SIW resonators, more information can be found in [82].
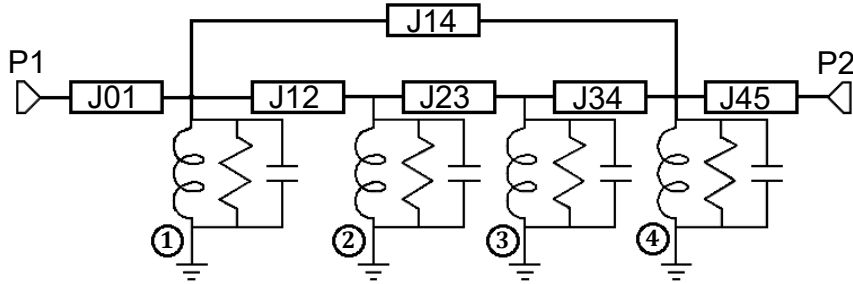
Figure 4.6: Coupling scheme of the best-Q designed coaxial SIW filter.

The S-parameter responses of the synthesized coupling scheme are compared, in Figure 4.8, with the full-wave EM simulated data of the designed filter structure. As can be seen, both responses are in very good agreement. In the full-wave EM simulation response, it can be appreciated a resonance at 11.48 GHz, due to the length of the line
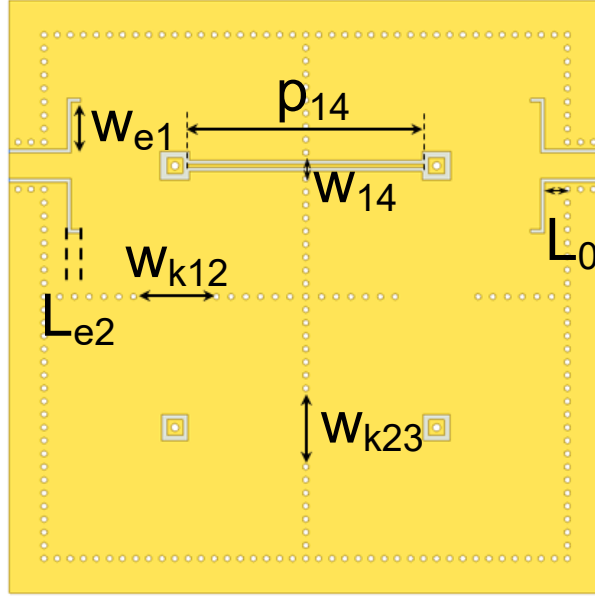
Figure 4.7: Structure of the best-Q designed coaxial SIW filter with its main layout design parameters.

Synthesis Values	Layout Dimensions [in mm]
$J_{01}=J_{45}=0.002827$	$L_0=1$; $w_{e1}=1.8$; $L_{e2}=0.38$
$J_{12}=J_{34}=0.0003479$	$w_{k12}=2.92$
$J_{23}=0.0003204$	$w_{k23}=2.75$
$J_{14}=-0.00007717$	$p_{14}=9$; $w_{14}=0.15$
Resonators 1 and 4 $Q_u=270$; $b=0.0146$; $Z_0=114$ Ω; $\theta_0=34.5°$	Resonators 1 and 4 $L_{CSIW}=W_{CSIW}=10$; $s_P=0.255$; $r_P=0.6$; $d_V=0.3$
Resonators 2 and 3 $Q_u=270$; $b=0.0146$; $Z_0=114$ Ω; $\theta_0=34.5°$	Resonators 2 and 3 $L_{CSIW}=W_{CSIW}=10$; $s_P=0.204$; $r_P=0.6$; $d_V=0.3$

Table 4.1: Values of the synthesis and design parameters of the uniform best-Q-designed coaxial SIW filter.

used to implement the cross-coupling between resonators 1 and 4 for introducing the TZs. This line, as reported in Table 4.1 is of 9 mm length, which corresponds to $\lambda/2$ at the cited frequency (i.e. 11.48 GHz). The insertion losses at f_0 are 2.42 dB. The return loss specification within the bandwidth is met; and the narrow-band isolation for $f_0\pm90\%BW$, with the introduction of the TZs located at 9.567 GHz and 10.278 GHz, is higher than the proposed specification of 20 dB.

Figure 4.8: S-Parameter responses for the synthesized coupling scheme and structure (EM simulation) of the best-Q designed coaxial SIW filter.

4.2.2 Filter with Uniform Q using Q-Enhancement Techniques in Coaxial SIW Topology

To compare and evaluate the proposed Q-enhancement techniques for coaxial SIW resonators (see section 3.3), we are going to design the same filter but introducing slots of air in the capacitive gap (are defined by s_P in Figure 4.1). The coupling scheme shown in Figure 4.6 is totally applicable in this case, but considering now a Q value slightly greater than before for the synthesized model. The maximum estimated value of Q_u through simulations of the coaxial SIW resonator with slots, using the specified 1.524 mm-thick Rogers RO4003C substrate and its metallization, is about 310.

The designed layout structure is displayed in Figure 4.9. Proceeding similarly, its synthesis parameters and layout values are summarized in Table 4.2.

The S-parameters of the synthesized and full-wave EM simulated responses of the of the new designed filter are compared, in Figure 4.10. As before, the results fit almost perfectly with the expected ones, appearing also in the EM simulations the resonance caused by the length of the line used for introducing the cross-coupling, and therefore the TZs. In this case, because of the minor value of the length needed (8.8 mm in this
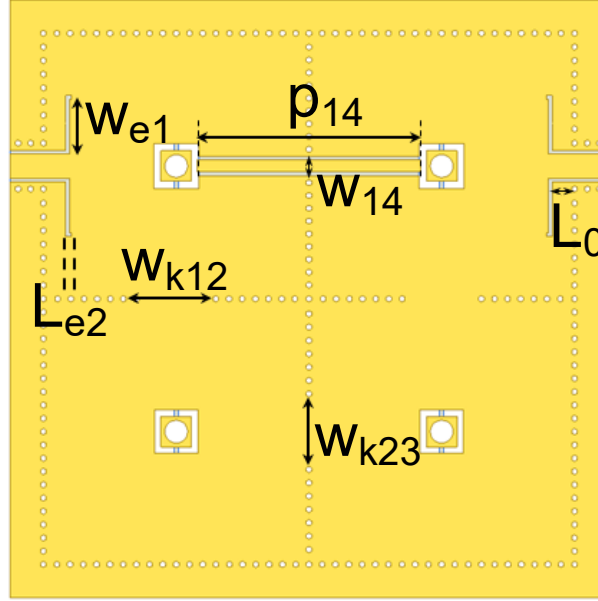
Figure 4.9: Structure of the enhanced-Q coaxial SIW filter using slots together with its main layout design parameters.

Synthesis Values	Layout Dimensions [in mm]
J_{01}=J_{45}=0.003465	L_0=1; w_{e1}=2; L_{e2}=0.085
J_{12}=J_{34}=0.0005076	w_{k12}=2.87
J_{23}=0.0004626	w_{k23}=2.725
J_{14}=−0.0001141	p_{14}=8.8; w_{14}=0.465
Resonators 1 and 4 Q_u=310; b=0.0207; Z_0=80.5 Ω; θ_0=34.5°	Resonators 1 and 4 L_{CSIW}=W_{CSIW}=10.45; s_P=0.288; r_P=1.2; d_V=0.9
Resonators 2 and 3 Q_u=310; b=0.0207; Z_0=80.5 Ω; θ_0=34.5°	Resonators 2 and 3 L_{CSIW}=W_{CSIW}=10.45; s_P=0.25; r_P=1.2; d_V=0.9

Table 4.2: Values of the synthesis and design parameters of the enhanced-Q coaxial SIW filter using slots.

case), the resonance is shown at 11.65 GHz. The insertion losses at f_0 demonstrate the Q-improvement, being in this design of 2.12 dB (whereas in the previous example was of 2.42 dB). The return losses within the passband are better than 19 dB, and the rejections reached with the introduction of the TZs located at 9.575 GHz and 10.272 GHz are higher than 25 dB for $f_0 \pm 90\% BW$.
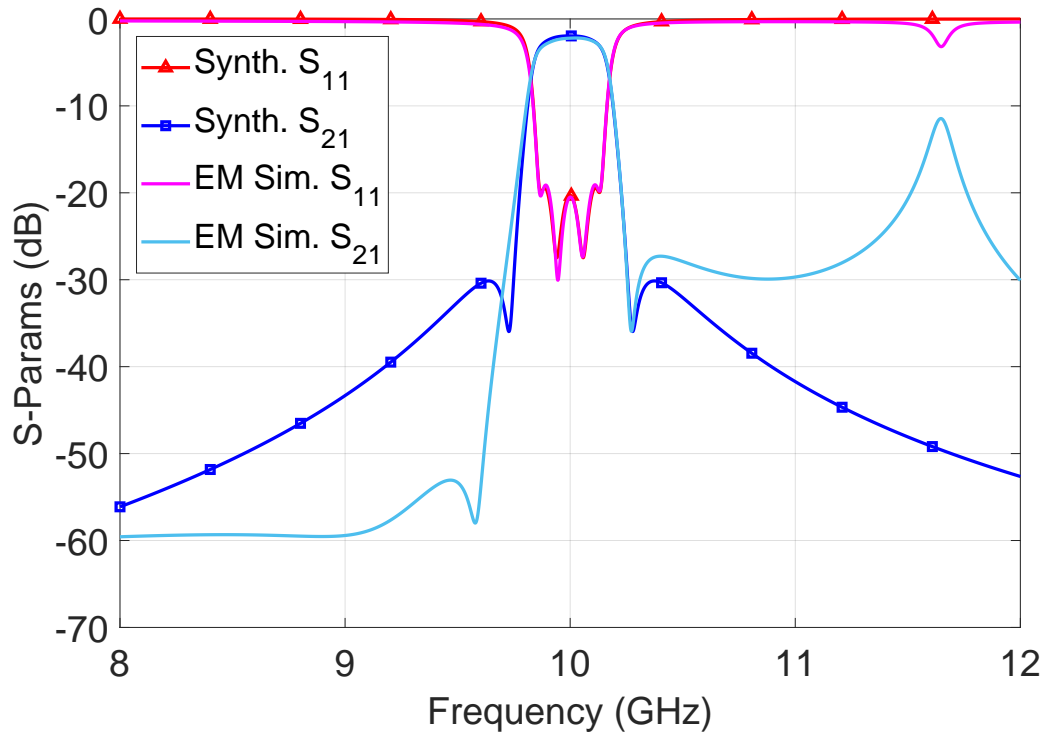
Figure 4.10: S-parameter responses for the synthesized coupling scheme and structure (EM simulation) of the enhanced-Q coaxial SIW filter using slots.

4.2.3   Lossy Filter with Non-Uniform Q using Coaxial SIW Resonators

By last, taking advantage of the Q-factor control feature of the coaxial SIW technology described in section 4.1, the design of a lossy filter with non-uniform distribution of Q-factors among resonators is proposed to improve the in-band characteristics of the X-band filter addressed.

In this manner, initially, the former fourth-order coupling scheme with a cross-coupling between resonators 1 and 4 is considered. Then, by applying lossy techniques for the distribution of losses among the resonators [36], an equivalent circuit has been synthesized by optimization. This process has taken into account the attainable low and high Q values. Thus, the high Q factor for inner resonators is optimized and limited to 270 (as seen in the study of section 4.1 for the proposed material, due to intrinsic dielectric and conductor losses), while the lower Q factor for the first and last resonator is optimized to reach an in-band flatness better than 0.8 dBpp. Figure 4.11 shows the circuit scheme and the structure of the designed filter, where its synthesis parameters and layout values are listed in Table 4.3.
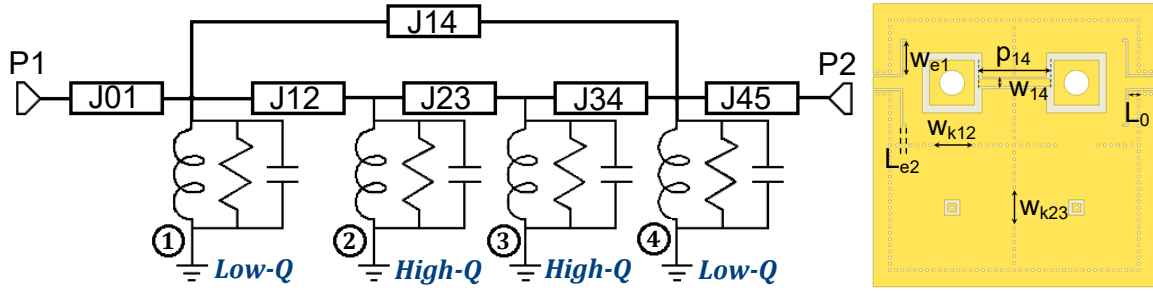
Figure 4.11: Coupling scheme and structure of the non-uniform Q lossy filter using coaxial SIW resonators.

Synthesis Values	Layout Dimensions [in mm]
$J_{01}=J_{45}=0.005616$	$L_0=1$; $w_{e1}=2.7$; $L_{e2}=0.293$
$J_{12}=J_{34}=0.0006206$	$w_{k12}=3.215$
$J_{23}=0.0004025$	$w_{k23}=2.994$
$J_{14}=-0.0003646$	$p_{14}=5.75$; $w_{14}=0.6$
Low-Q Resonators (1 and 4) $Q_u=82$; $b=0.0311$; $Z_0=53.7$ Ω; $\theta_0=34.5°$	Low-Q Resonators (1 and 4) $L_{SIW}=W_{SIW}=10$; $s_P=0.6$; $r_P=3.59$; $d_V=2$
High-Q Resonators (2 and 3) $Q_u=266$; $b=0.0146$; $Z_0=114$ Ω; $\theta_0=34.5°$	High-Q Resonators (2 and 3) $L_{SIW}=W_{SIW}=10$; $s_P=0.268$; $r_P=0.69$; $d_V=0.3$

Table 4.3: Values of the synthesis and design parameters of the non-uniform Q coaxial SIW filter.

The theoretical and EM simulated S-parameter responses are compared in Figure 4.12. As can be checked in the graph both responses are in very good agreement. The insertion losses at f_0 in this case are 3 dB. As could be expected, the resulting insertion losses in this filter are higher than the former examples, owing to the intended additional losses introduced in the first and last resonators. The return losses and flatness requirements are met; and the narrow-band isolation for $f_0 \pm 100\% BW$, with the introduction of the TZs located at 9.58 GHz and 10.28 GHz, is higher than 20 dB. It is worth mentioning that in this filter, the requested length for the line introducing the TZs is shorter (it is just of 5.75 mm, as can be seen in Table 4.3). Therefore, the related resonance is moved up in frequency, and this is why it can not be seen in the results for this case (Figure 4.12).

In order to demonstrate the proposed approach, the designed filter has been manufactured. The fabricated prototype is shown in Figure 4.13, and its measured results and EM simulations are plotted in Figure 4.14. The final dimensions are 2.3 x 2.3 cm².
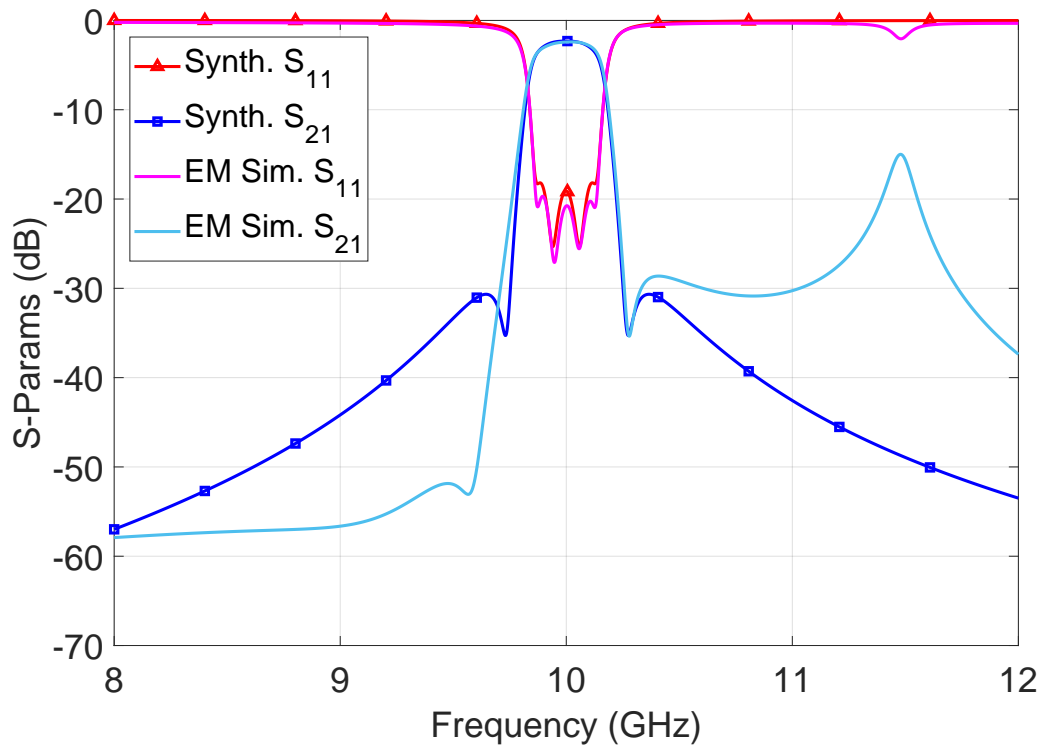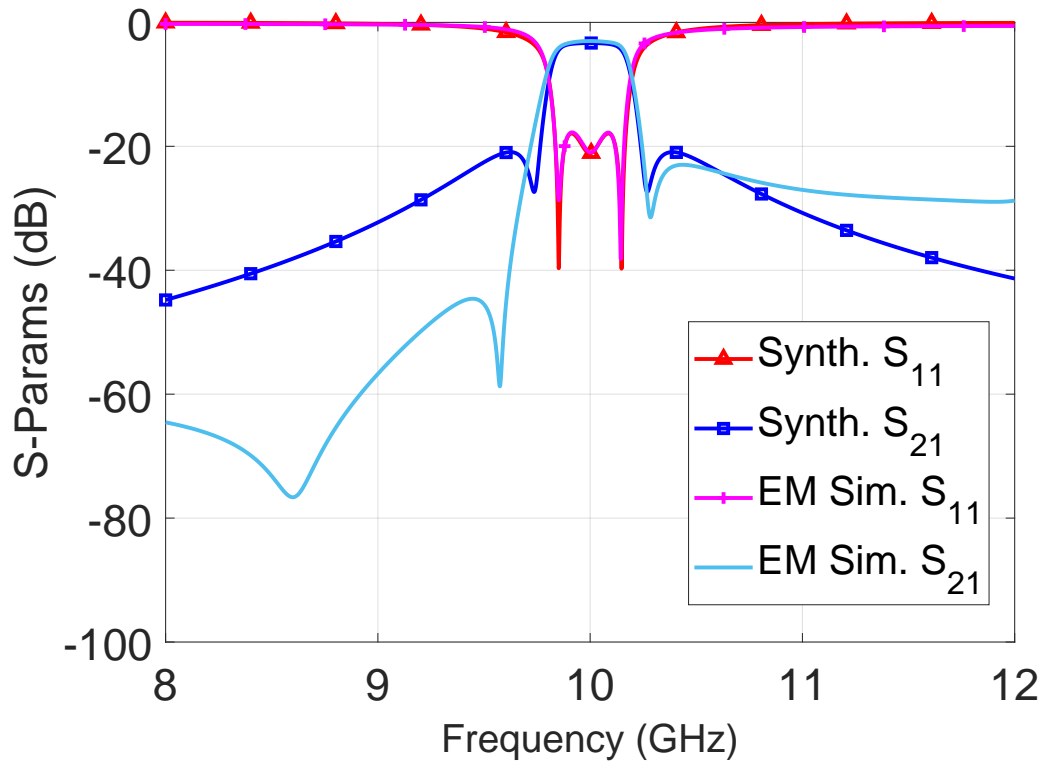
Figure 4.12: S-parameter responses for the synthesized coupling scheme and structure (EM simulation) of the non-uniform Q lossy coaxial SIW filter.

The measured 3 dB bandwidth has a small variation of about 40 MHz compared to the simulated one, while the measured and simulated frequency rejections are in a good agreement. The measured insertion loss value at f_0 is 3.25 dB, which is slightly higher than the 3 dB obtained in simulation. It can be easily appreciated that the flatness is considerably improved from a coaxial SIW filter with uniform Q resonators, but with a slight variation from the simulated values, reaching 1 dBpp in the passband, instead of the aimed value of 0.8 dBpp. With these results the flatness level achieved is equivalent to the one of a uniform Q filter with a Q value of 600.
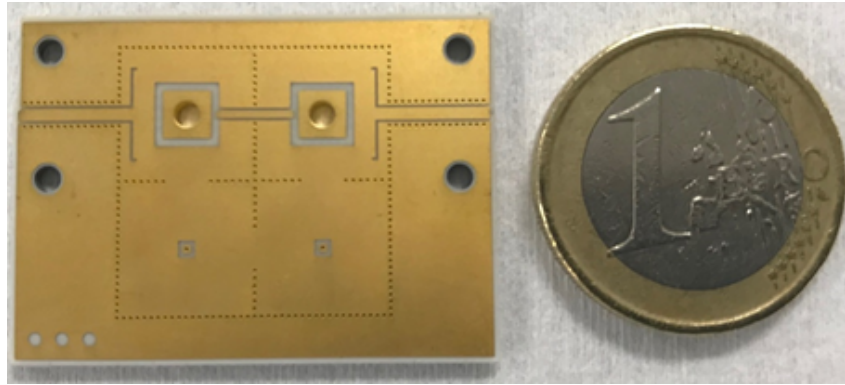
Figure 4.13: Photograph of the fabricated non-uniform Q lossy coaxial SIW filter prototype.
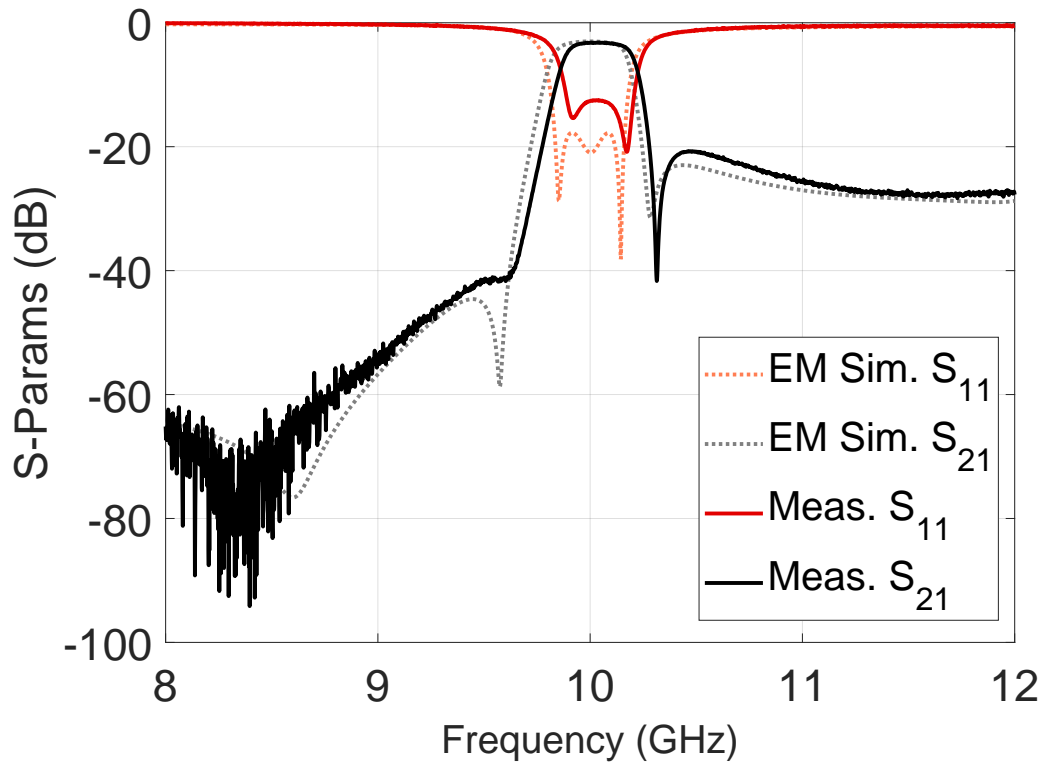
Figure 4.14: Measurements versus EM simulations of the fabricated non-uniform Q lossy coaxial SIW filter prototype.

Once the three filters have been designed, we are going to analyze the achievements of the techniques used for improving the passband characteristics, by comparing the EM simulated three passbands shapes in more detail (see Figure 4.15).
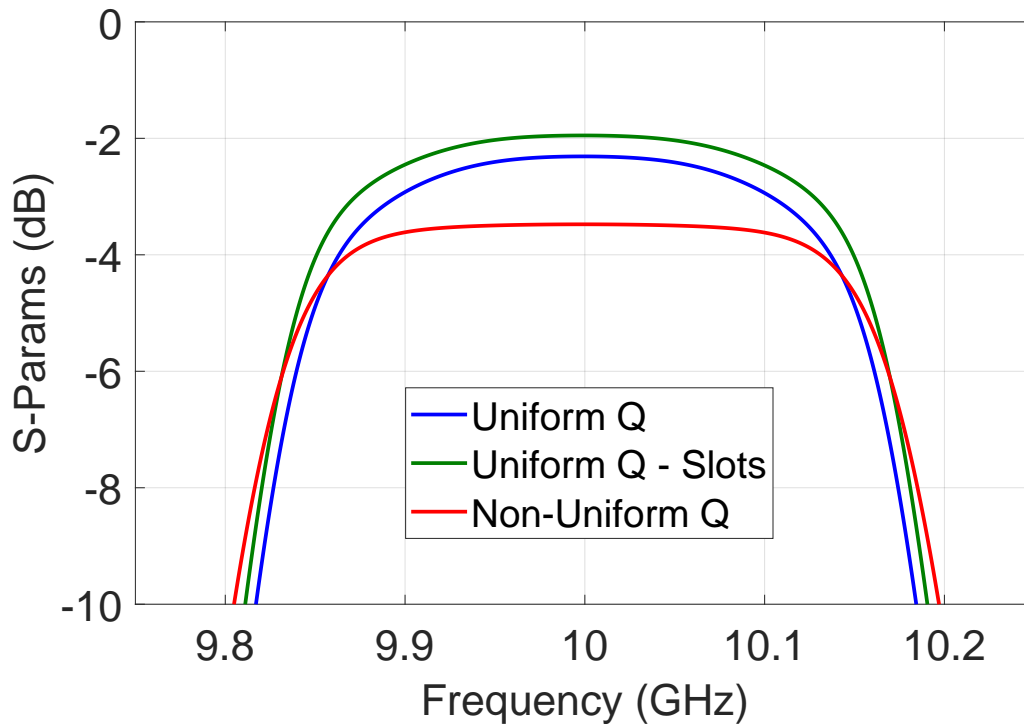
Figure 4.15: Comparison of the transmission responses within the passband of the three filters designed.

As can be observed in Figure 4.15, the two responses with uniform Q can be easily distinguished of the lossy one. Moreover, in this detailed view of the passbands, it is better appreciated the effect of using slots in the considered resonator (thus providing an enhnaced Q-value) when compared to the classical coaxial SIW structure. Therefore, the design of a band-pass fitler with very flat response using non-uniform Q resonators is considered and demonstrated. The main advantage of this approach is that the proper Q-factor values required after the synthesis of the desired response can be implemented. The structure is based on the ability to control the unloaded Q-factor of coaxial SIW resonators within a very wide range, and without the need of using different technologies or introducing resistors. The obtained results show that this approach could be of promising application for filters with very demanding responses (in terms of in-band planarity), while keeping low-cost manufacturing, high integrability and very compact size.

<div align="right">Chapter 5</div>

Conclusions and Future Work

5.1 Conclusions

In this doctoral thesis, we have presented various advances in the area of microwave filters in planar and hybrid technologies, discussing new and simple design methodologies to enhance the features and performances of the filtering responses that can be achieved in current practical implementations. The previous achievements are aimed to be reached by keeping (or even improving) the intrinsic benefits and strengths of both technological solutions, such as its compact size, low-cost and easy integration, must be preserved.

First, we have presented an original technique for the introduction of transmission zeros in filtering responses. The technique is general, applicable to different filter solutions (independently of the considered topology), as it has been demostrated with several examples. The proposed scheme is based on the addition of simple networks as terminations of the filter, capable of achieving independent and controllable transmission zeros that improve the selectivity and/or the out-of-band response of any filter. Furthermore, thanks to the proposed solutions, the transmission zeros originated can be easily and arbitrarily distributed at the lower or at the upper filter stopband. Likewise, equations for the synthesis of TZs have been developed, which allow theoretically estimating the values for the elements of these cells from known design parameters.

The way to implement these networks can be diverse. This thesis has mainly addressed the realization by means of lumped and quasi-lumped elements, with the intention of avoiding possible complications in the design procedure and following a clear and systematic methodology. In addition, the low cost and the small size of the proposed solutions have an additional positive impact. However, not all the implementations of the networks presented have been carried out with lumped elements. For the practical implementation of some terminating netowrks, a hybrid solution based on lumped and distributed elements has also been proposed.

On the other hand, different application examples of the proposed cells have been studied. Depending on the application, the approach for solving the problem has changed, but the fundamental method for introducing the TZs has been maintained.

The first application seeks to improve the rejection bands of planar filters, extending them as much as possible in frequency through the cancellation of their spurious responses. The strategy followed consists of using the described sections, concretely, the lowpass termination through its implementation with lumped elements including also their parasitics. In this way, it has been possible to introduce up to 2 independent and controllable TZs for each cell added to the filter. On this occasion, it has been designed a strongly loaded combline filter centered at 1 GHz that, incorporating two cells, one at the input and one at the output, achieves an ultra-wide spurious-free band with a rejection greater than 22 dB up to $10 \cdot f_0$. The results obtained are in good agreement with those of the full-wave EM simulation, verifying in this way the proposed design solution. For this application, the use of lumped elements is especially convenient and interesting since, in addition to take advantage of a normally undesired phenomenon such as the self-resonance of components, it has allowed to significantly improve the performance of the filter with a negligible increase in the size of the final device.

In the second application example, it is intended to achieve selective microwave filtering responses, so that the positions of the TZs are placed close to the passband. In this case, 4 filters have been designed and manufactured, each of them with a different distribution of the TZs. The structure of the filter, however, has been the same one for 3 of them and corresponds to a bandpass filter centered at 4 GHz, based on parallel coupled-lines in microstrip technology. And finally, demonstrating the flexibility of the proposed technique, that can be applied independently of the filtering structure, a combline filter with no-capacitive loading, locating the TZs even closer to the passband, has been designed. The results obtained are satisfactory, as all designed filters have measured responses quite similar to those estimated with full-wave EM simulations. From the analysis of the results for the designed filters, we can approximate the attenuation improvement achieved when the TZs are introduced, in comparison to the case without TZs, to be of 20 - 30 dB.

Next, the use of these cells has been successfully applied to a different microwave front-ends, describing the design of a dual-band filter for Software Defined Radio and fifth generation (5G) systems with improved out of band rejection levels. This is an additional example where it is demonstrated, through the results shown, that the proposed technique for introducing TZs is effective to achieve the desired specifications in all the considered scenarios.

In the second part of this thesis, several techniques have been studied to achieve advanced, high performance and improved responses in compact filters. For these purposes, after evaluating different technologies, it has been decided to consider one based on coaxial SIW resonators; due to its high level of compaction, integrability, low cost, flexibility in design and high Q values when compared to classical planar solutions. The coaxial SIW technology is a good compromise solution for all desired features, with great potential applicability in modern microwave filtering devices.

Inspired by the developed techniques to improve the Q-factor in SIW structures, exposed in the state of the art, two simple techniques have been proposed for the Q-improvement in coaxial SIW technology. In both cases, air is introduced in the SIW coaxial resonator and, therefore, the losses associated with the dielectric are reduced in a simple (and easy to manufacture) way, without involving a large increase in terms of size. The introduction of air is carried out by means of a series of air drills or slots, perform from top to bottom in the capacitive gap area of the SIW coaxial resonator. The solution based on air slots, since they provide a greater reduction of lossy dielectric material, provides a greater improvement of the Q-factor. Nevertheless, these two techniques do usually provide a slight enhancement of the Q-factor, which can not be enough for achieving the required specifications of certain applications.

The design of a novel Ka-band manifold diplexer, with very demanding specifications for space applications, has been performed using a hybrid solution based on SIW and coaxial SIW technologies. The introduction of air-drills in the capacitive gap area of the coaxial SIW cavities to enhance the Q-factor, has allowed to reach the compliance of most of the provided hard specifications. Potential solutions for enhancing the achieved in-band planarity are also given. Additionally, a design and optimization technique, which allows a faster and easier design of multiplexers and complex filtering structures has been provided. The success of the proposed technique has been verified with the design of the considererd Ka-band diplexer, where the difficulty of integrating different technologies with a lot of vias, which involve full-wave EM simulations with large computational times, was overcome and reduced by the application of the described design method.

Finally, to cope with hard specifications in terms of in-band planarity response, as it is the case of the considered Ka-band diplexer, the particular strengths of the coaxial SIW technology have been investigated and exploited. In particular, the degrees of freedom and flexibility in the design process of the SIW coaxial technology are considered, developing a technique which allows the control of the Q-factor of the coaxial cavity during its design process. An important variation rate of the unloaded Q-factor can be obtained by adequately controlling several of the coaxial SIW layout parameters, thus enabling to optimize the in-band response achieved in the design of a filter, by applying lossy techniques. The approach is based on the use of non-uniform-Q resonators implemented in coaxial SIW technology without requiring any extra component, thus facilitating its design, manufacture and practical implementation. In this respect, a resistorless lossy filter with non-uniform Q values using coaxial SIW resonators is proposed, designed and manufactured. It has been compared with two other filters of uniform Q-values, based on coaxial SIW resonators with standard and enhanced Q-factors, showing a significant improvement in terms of insertion loss flatness in all cases.

In conclusion, all the main goals initially proposed for this PhD thesis have been accomplished successfully. As a result, this thesis has generated international publications in relevant journals and conferences dedicated to microwave engineering, as it is summarized in Appendix A. Additionally, the designed Ka-band diplexer (detailed in section 3.5) was developed under a project funded by the European Space Agency (ESA) and is currently being manufactured.

5.2 Future work

The results of this thesis can be used as the initial steps for future investigations, or can be extended for their application of other kind of filter solutions in planar and hybrid technologies. In the next paragraphs, we outline some of the possible future works that could be further researched from the presented results, and that will also help to the progress in the microwave filter design field. Among them we can cite:

- Study of the viability and derivation of design expressions to introduce multiple transmission zeros per terminating cell. Any filter is benefited with the introduction of TZs, that allow to improve the out-of-band rejection and selectivity, reaching a response closer to the ideal one. The potential and broad use of these termination sections make them suitable for various applications. These circumstances encourage us to continue exploiting these structures to achieve more optimal designs, in terms of number of generated transmission zeros, for different filter topologies.

- Design of terminating cells with switchable or adjustable transmission zeros. Due to the flexibility of the presented technique for introducing TZs, independently of the filter topology, the tuning capacity can be easily developed. This reconfiguration feature is very promising and attractive for new applications (e.g. 5G, LTE, satellite payloads), that demand the integration and co-existence of multi-standard and/or multi-band operations in a single device, thus offering higher functionality, efficiency and flexibility in terms of frequency spectrum usage.

- Further investigations to exploit the Q-enhancement techniques proposed in coaxial SIW topology. After manufacturing the Ka-band diplexer, we will be able to evaluate, with experimental results, the actual improvement of the Q-factor due to the use of air-drills with the conventional coaxial SIW structures. Additionally, going deeper on the technique of employing slots, which provides higher Q values with a negligible increase in size, it will be also of great interest; due to its easy practical fabrication, as well as to the time savings during its full-wave EM simulation when compared to the inclusion of additional metal vias.

- Implementation of these compact filter structures with a higher quality factor. To do this, the implementation of miniaturized coaxial SIW filters in LTCC (Low-Temperature Co-fired Ceramics) technology will be investigated; with the aim of improving also the degree of miniaturization of the implemented structures, taking advantage of the integration of cavities at multiple layers. In addition, the study of new materials (such as quartz or sapphire) that can potentially increase the Q factor to be reached into a greater extent must be addressed.

- Design of the considered Ka-band diplexer applying the described lossy techniques based on coaxial SIW resontors with a non-uniform Q distribution, in order to meet the related flatness specifications imposed. The simple and easy application of lossy techniques using coaxial SIW resonators, will allow the attainment of these demanding requirements, typical of space communications payloads. As a consequence, in scenarios where waveguide solutions are traditionally employed (such as space applications), this promising, low-cost and compact technology (based on coaxial SIW resonators) must be considered a very good solution offering high performance.

Appendix A

Publications list

The main and novel results of this doctoral thesis have resulted into a total number of 5 scientific publications, which are distributed as 2 journal papers, 1 contribution to an international conference, 1 contribution to a national conference and 1 presented in an international workshop, as follows:

- A.1 Journal publications
  - S. Marín, J. D. Martínez, C. I. Valero and V. E. Boria, "Microstrip Filters With Enhanced Stopband Based on Lumped Bisected Pi-Sections With Parasitics," in *IEEE Microwave and Wireless Components Letters*, vol. 27, no. 1, pp. 19-21, Jan. 2017, doi: 10.1109/LMWC.2016.2630841.
  - S. Marín, J. D. Martínez and V. E. Boria, "Implementing Quasi-Elliptic Microstrip Filters Using Terminating Half Sections," in *IEEE Microwave and Wireless Components Letters*, vol. 28, no. 9, pp. 783-785, Sept. 2018, doi: 10.1109/LMWC.2018.2855562.
- A.2 International Conference publications
  - S. Marín, J. D. Martínez and V. E. Boria, "Realization of filters with improved selectivity using lumped and quasi-lumped terminating half sections," *2017 47th European Microwave Conference (EuMC)*, 2017, pp. 636-639, doi: 10.23919/EuMC.2017.8230928.

- A.3 International Workshop publications
  - S. Marín, J. D. Martínez and V. E. Boria, "Resistorless Implementation of Lossy Filters Using Coaxial SIW Resonators With Non-uniform Q," *2021 1st International Microwave Filter Workshop*, Perugia, Italy, Nov. 2021.
- A.4 National Conference publications
  - S. Marín, J.D. Martínez, C.I. Valero, and V.E. Boria, "Microstrip Filter with Wide Stopband Using m-Derived Terminations", in *Proc. of 31st Spanish URSI*, Madrid, Sep. 2016.

Bibliography

[1] J.-S. Hong and M. Lancaster, "Design of highly selective microstrip bandpass filters with a single pair of attenuation poles at finite frequencies," *IEEE Transactions on Microwave Theory and Techniques*, vol. 48, no. 7, pp. 1098–1107, 2000.

[2] Y. Singh and N. Kumar, "Compact stub-loaded open-loop BPF with enhanced stopband by introducing extra transmission zeros," *Electronics Letters*, vol. 51, no. 2, pp. 164–166, 2015.

[3] V. Miraftab and M. Yu, "Generalized lossy microwave filter coupling matrix synthesis and design using mixed technologies," *IEEE Transactions on Microwave Theory and Techniques*, vol. 56, no. 12, pp. 3016–3027, 2008.

[4] D. G. Swanson, "Narrow-band microwave filter design," *IEEE Microwave Magazine*, vol. 8, no. 5, pp. 105–114, 2007.

[5] C. Quendo, E. Rius, C. Person, and M. Ney, "Integration of optimized low-pass filters in a bandpass filter for out-of-band improvement," *IEEE Transactions on Microwave Theory and Techniques*, vol. 49, no. 12, pp. 2376–2383, 2001.

[6] T.-N. Kuo, W.-C. Li, C.-H. Wang, and C. H. Chen, "Wide-stopband microstrip bandpass filters using quarter-wavelength stepped-impedance resonators and bandstop embedded resonators," *IEEE Microwave and Wireless Components Letters*, vol. 18, no. 6, pp. 389–391, 2008.

[7] T. Lopetegi, M. Laso, F. Falcone, F. Martin, J. Bonache, J. Garcia, L. Perez-Cuevas, M. Sorolla, and M. Guglielmi, "Microstrip "wiggly-line" bandpass filters with multispurious rejection," *IEEE Microwave and Wireless Components Letters*, vol. 14, no. 11, pp. 531–533, 2004.

[8] W. Fathelbab and M. Steer, "Parallel-coupled line filters with enhanced stopband performances," *IEEE Transactions on Microwave Theory and Techniques*, vol. 53, no. 12, pp. 3774–3781, 2005.

[9] K.-W. Hsu, M.-J. Tsou, Y.-H. Tseng, and W.-H. Tu, "Wide-stopband bandpass filter with symmetrical loaded-stub resonators," in *2011 Asia-Pacific Microwave Conference*, 2011, pp. 1043–1046.

[10] J. Xu, Y.-X. Ji, W. Wu, and C. Miao, "Design of miniaturized microstrip LPF and wideband BPF with ultra-wide stopband," *IEEE Microwave and Wireless Components Letters*, vol. 23, no. 8, pp. 397–399, 2013.

[11] L. Hepburn and J. Hong, "Compact integrated lumped element LCP filter," *IEEE Microwave and Wireless Components Letters*, vol. 26, no. 1, pp. 19–21, 2016.

[12] R. Levy, "Filters with single transmission zeros at real or imaginary frequencies," *IEEE Transactions on Microwave Theory and Techniques*, vol. 24, no. 4, pp. 172–181, 1976.

[13] J.-S. Hong and M. Lancaster, "Design of highly selective microstrip bandpass filters with a single pair of attenuation poles at finite frequencies," *IEEE Transactions on Microwave Theory and Techniques*, vol. 48, no. 7, pp. 1098–1107, 2000.

[14] L. Zhou, Z. Long, H. Li, T. Zhang, and M. Qiao, "A novel configuration for compact HTS CQ structure linear phase filter design," *IEEE Transactions on Applied Superconductivity*, vol. 28, no. 8, pp. 1–8, 2018.

[15] K. Yeo and M. Lancaster, "The design of microstrip six-pole quasi-elliptic filter with linear phase response using extracted-pole technique," *IEEE Transactions on Microwave Theory and Techniques*, vol. 49, no. 2, pp. 321–327, 2001.

[16] U. Rosenberg and S. Amari, "Novel coupling schemes for microwave resonator filters," in *2002 IEEE MTT-S International Microwave Symposium Digest*, vol. 3, 2002, pp. 1605–1608.

[17] D. Rebenaque, F. Pereira, J. Garcia, A. Melcon, and M. Guglielmi, "Two compact configurations for implementing transmission zeros in microstrip filters," *IEEE Microwave and Wireless Components Letters*, vol. 14, no. 10, pp. 475–477, 2004.

[18] M. Sánchez-Renedo, R. Gómez-Garcia, and R. Loeches-Sánchez, "Microstrip filters with selectivity improvement using the new concept of signal-interference source/load coupling," in *2013 IEEE MTT-S International Microwave Symposium Digest*, 2013, pp. 1–4.

[19] E. Fourn, E. Rius, G. Tanne, A. Manchec, and C. Quendo, "Frequency variations improvement of a bandwidth and central frequency reconfigurable DBR filter," in *2006 European Microwave Conference*, 2006, pp. 1139–1142.

[20] S. Chen, L.-F. Shi, G.-X. Liu, and J.-H. Xun, "An alternate circuit for narrow-bandpass elliptic microstrip filter design," *IEEE Microwave and Wireless Components Letters*, vol. 27, no. 7, pp. 624–626, 2017.

[21] A. L. Borja, A. Belenguer, H. Esteban, and V. E. Boria, "Design and performance of a high-Q narrow bandwidth bandpass filter in empty substrate integrated coaxial line at k_u -band," *IEEE Microwave and Wireless Components Letters*, vol. 27, no. 11, pp. 977–979, 2017.

[22] F. Parment, A. Ghiotto, T.-P. Vuong, J.-M. Duchamp, and K. Wu, "Low-loss air-filled substrate integrated waveguide (SIW) band-pass filter with inductive posts," in *2015 European Microwave Conference*, 2015, pp. 761–764.

[23] F. Grine, T. Djerafi, M. T. Benhabiles, K. Wu, and M. L. Riabi, "High-Q substrate integrated waveguide resonator filter with dielectric loading," *IEEE Access*, vol. 5, pp. 12 526–12 532, 2017.

[24] A. Coves, G. Torregrosa, A. San-Blas, M. Sanchez-Soriano, A. Martellosio, E. Bronchalo, and M. Bozzi, "A novel band-pass filter based on a periodically drilled SIW structure," *Radio Science*, vol. 51, no. 4, pp. 328–336, 2016.

[25] A. Romano and R. Mansour, "Enhanced-Q microstrip bandpass filter with coupled negative resistors," in *1997 IEEE MTT-S International Microwave Symposium Digest*, vol. 2, 1997, pp. 709–712.

[26] T.-H. Le, X.-W. Zhu, C. Ge, and T.-V. Duong, "A novel diplexer integrated with a shielding case using high Q-factor hybrid resonator bandpass filters," *IEEE Microwave and Wireless Components Letters*, vol. 28, no. 3, pp. 215–217, 2018.

[27] D. Psychogiou, R. Gómez-García, R. Loeches-Sánchez, and D. Peroulis, "Hybrid acoustic-wave-lumped-element resonators (AWLRS) for high-Q bandpass filters with quasi-elliptic frequency response," *IEEE Transactions on Microwave Theory and Techniques*, vol. 63, no. 7, pp. 2233–2244, 2015.

[28] J. Li, C. Guo, L. Mao, and J. Xu, "Compact high-Q hemispherical resonators for 3-D printed bandpass filter applications," in *2017 IEEE MTT-S International Microwave Symposium Digest*, 2017, pp. 1591–1594.

[29] K. Zhao and D. Psychogiou, "A monolithic vertical integration concept for compact coaxial-resonator-based bandpass filters using additive manufacturing," *IEEE Microwave and Wireless Components Letters*, vol. 31, no. 6, pp. 689–692, 2021.

[30] M. Dishal, "Design of dissipative band-pass filters producing desired exact amplitude-frequency characteristics," *Proceedings of the IRE*, vol. 37, no. 9, pp. 1050–1069, 1949.

[31] A. Williams, W. Bush, and R. Bonetti, "Predistortion techniques for multicoupled resonator filters," in *1984 IEEE MTT-S International Microwave Symposium Digest*, 1984, pp. 290–291.

[32] M. Yu, W.-C. Tang, A. Malarky, V. Dokas, R. Cameron, and Y. Wang, "Predistortion technique for cross-coupled filters and its application to satellite communication systems," *IEEE Transactions on Microwave Theory and Techniques*, vol. 51, no. 12, pp. 2505–2515, 2003.

[33] M. Yu, R. Cameron, D. Smith, V. Dokas, and Y. Wang, "Symmetrical realization for predistorted microwave filters," in *2005 IEEE International Microwave Symposium Digest*, 2005, pp. 245–248.

[34] X.-P. Chen, L. Han, and K. Wu, "Synthesis and design of substrate integrated waveguide filter using predistortion technique," in *2007 Asia-Pacific Microwave Conference*, 2007, pp. 1–4.

[35] A. P. Díaz, *Synthesis and Design of Dissipative Filters with Improved Performance*. Universitat Politècnica de Catalunya, 2015.

[36] A. Guyette, I. Hunter, and R. Pollard, "The design of microwave bandpass filters using resonators with nonuniform Q," *IEEE Transactions on Microwave Theory and Techniques*, vol. 54, no. 11, pp. 3914–3922, 2006.

[37] M. Meng, I. C. Hunter, and J. D. Rhodes, "The design of parallel connected filter networks with nonuniform Q resonators," *IEEE Transactions on Microwave Theory and Techniques*, vol. 61, no. 1, pp. 372–381, 2013.

[38] J. Mateu, A. Padilla, C. Collado, M. Martinez-Mendoza, E. Rocas, C. Ernst, and J. M. O'Callaghan, "Synthesis of 4th order lossy filters with uniform Q distribution," in *2010 IEEE MTT-S International Microwave Symposium*, 2010, pp. 1–1.

[39] A. Basti, A. Périgaud, S. Bila, S. Verdeyme, L. Estagerie, and H. Leblond, "Design of microstrip lossy filters for receivers in satellite transponders," *IEEE Transactions on Microwave Theory and Techniques*, vol. 62, no. 9, pp. 2014–2024, 2014.

[40] J. Ni, W. Tang, J. Hong, and R. H. Geschke, "Design of microstrip lossy filter using an extended doublet topology," *IEEE Microwave and Wireless Components Letters*, vol. 24, no. 5, pp. 318–320, 2014.

[41] L. Szydlowski, A. Lamecki, and M. Mrozowski, "Design of microwave lossy filter based on substrate integrated waveguide (SIW)," *IEEE Microwave and Wireless Components Letters*, vol. 21, no. 5, pp. 249–251, 2011.

[42] L. Szydlowski, A. Lamecki, and M. Mrozowski, "Synthesis of coupled-lossy resonator filters," *IEEE Microwave and Wireless Components Letters*, vol. 20, no. 7, pp. 366–368, 2010.

[43] B. Gao, L.-S. Wu, and J.-F. Mao, "Lossy substrate integrated waveguide filter with flat passband," in *2016 IEEE MTT-S International Wireless Symposium*, 2016, pp. 1–4.

[44] V. Miraftab and M. Yu, "Advanced coupling matrix and admittance function synthesis techniques for dissipative microwave filters," *IEEE Transactions on Microwave Theory and Techniques*, vol. 57, no. 10, pp. 2429–2438, 2009.

[45] M. Oldoni, G. Macchiarella, G. G. Gentili, and C. Ernst, "A new approach to the synthesis of microwave lossy filters," *IEEE Transactions on Microwave Theory and Techniques*, vol. 58, no. 5, pp. 1222–1229, 2010.

[46] C. M. Kudsia, R. J. Cameron and R. R. Mansour, *Microwave Filters for Communication Systems*. Wiley, 2007.

[47] H. Hu, K.-L. Wu, and R. J. Cameron, "Stepped circular waveguide dual-mode filters for broadband contiguous multiplexers," *IEEE Transactions on Microwave Theory and Techniques*, vol. 61, no. 1, pp. 139–145, 2013.

[48] T. Kojima, A. Gonzalez, S. Asayama and Y. Uzawa, "Design and development of a hybrid-coupled waveguide multiplexer for a multiband receiver," *IEEE Transactions on Terahertz Science and Technology*, vol. 7, no. 1, pp. 10–19, 2017.

[49] H. Hu and K.-L. Wu, "A deterministic EM design technique for general waveguide dual-mode bandpass filters," *IEEE Transactions on Microwave Theory and Techniques*, vol. 61, no. 2, pp. 800–807, 2013.

[50] S. Cogollos, P. Soto, V. E. Boria, M. Guglielmi, M. Brumos, B. Gimeno, and D. Raboso, "Efficient design of waveguide manifold multiplexers based on low-order EM distributed models," *IEEE Transactions on Microwave Theory and Techniques*, vol. 63, no. 8, pp. 2540–2549, 2015.

[51] J.-K. Xiao, M. Zhu, Y. Li, L. Tian, and J.-G. Ma, "High selective microstrip band-pass filter and diplexer with mixed electromagnetic coupling," *IEEE Microwave and Wireless Components Letters*, vol. 25, no. 12, pp. 781–783, 2015.

[52] H. Liu, W. Xu, Z. Zhang, and X. Guan, "Compact diplexer using slotline stepped impedance resonator," *IEEE Microwave and Wireless Components Letters*, vol. 23, no. 2, pp.75–77, 2013.

[53] C.-W. Tang and S.-F. You, "Design methodologies of LTCC bandpass filters, diplexer, and triplexer with transmission zeros," *IEEE Transactions on Microwave Theory and Techniques*, vol. 54, no. 2, pp. 717–723, 2006.

[54] M.-I. Lai and S.-K. Jeng, "A microstrip three-port and four channel multiplexer for WLAN and UWB coexistence," *IEEE Transactions on Microwave Theory and Techniques*, vol. 53, no. 10, pp. 3244–3250, 2005.

[55] S.-J. Zeng, J.-Y. Wu, and W.-H. Tu, "Compact and high-isolation quadruplexer using distributed coupling technique," *IEEE Microwave and Wireless Components Letters*, vol. 21, no. 4, pp.197–199, 2011.

[56] C.-F. Chen, T.-Y. Huang, C.-P. Chou and R.-B Wu, "Microstrip diplexers design with common resonator sections for compact size but high isolation," *IEEE Transactions on Microwave Theory and Techniques*, vol. 54, no. 5, pp. 1945–1952, 2006.

[57] C.-F. Chen, T.-M. Shen, T.-Y. Huang and R.-B Wu, "Design of multimode net-type resonators and their applications to filters and multiplexers," *IEEE Transactions on Microwave Theory and Techniques*, vol. 59, no. 4, pp. 848–856, 2011.

[58] S. Hong and K. Chang, "A 10-35-GHz six-channel microstrip multiplexer for wide-band communication systems," *IEEE Transactions on Microwave Theory and Techniques*, vol. 54, no. 4, pp. 1370–1378, 2006.

[59] Z.-C. Hao, X.-P. Huo, W.-Q. Ding, and W. Hong, "Efficient design of compact contiguous-channel SIW multiplexers using the space-mapping method," *IEEE Transactions on Microwave Theory and Techniques*, vol. 63, no. 11, pp. 3651–3662, 2015.

[60] H. J. Tang, W. Hong, J.-X. Chen, G. Q. Luo, and K. Wu, "Development of millimeter-wave planar diplexers based on complementary characters of dual-mode substrate integrated waveguide filters with circular and elliptic cavities," *IEEE Transactions on Microwave Theory and Techniques*, vol. 55, no. 4, pp. 776–782, 2007.

[61] F. Cheng, X. Lin, K. Song, Y. Jiang, and Y. Fan, "Compact diplexer with high isolation using the dual-mode substrate integrated waveguide resonator," *IEEE Microwave and Wireless Components Letters*, vol. 23, no. 9, pp. 459–461, 2013.

[62] Y. Dong and T. Itoh, "Substrate integrated waveguide loaded by complementary split-ring resonators for miniaturized diplexer design," *IEEE Microwave and Wireless Components Letters*, vol. 21, no. 1, pp. 10–12, 2011.

[63] A. García-Lampérez, M. Salazar-Palma, and S. H. Yeung, "Siw compact diplexer," in *2014 IEEE MTT-S International Microwave Symposium*, 2014, pp. 1–4.

[64] S. Sirci, J. D. Martínez, J. Vague, and V. E. Boria, "Substrate integrated waveguide diplexer based on circular triplet combline filters," *IEEE Microwave and Wireless Components Letters*, vol. 25, no. 7, pp. 430–432, 2015.

[65] J.-S. Hong and M. J. Lancaster, *Microstrip Filters for RF/Microwave Applications*, 1st ed. Wiley, 2001.

[66] R. Kurzrok, "General four-resonator filters at microwave frequencies (correspondence)," *IEEE Transactions on Microwave Theory and Techniques*, vol. 14, no. 6, pp. 295–296, 1966.

[67] C.-C. Chen, Y.-R. Chen, and C.-Y. Chang, "Miniaturized microstrip cross-coupled filters using quarter-wave or quasi-quarter-wave resonators," *IEEE Transactions on Microwave Theory and Techniques*, vol. 51, no. 1, pp. 120–131, 2003.

[68] M. Guglielmi, P. Jarry, E. Kerherve, O. Roquebrun, and D. Schmitt, "A new family of all-inductive dual-mode filters," *IEEE Transactions on Microwave Theory and Techniques*, vol. 49, no. 10, pp. 1764–1769, 2001.

[69] C.-K. Liao and C.-Y. Chang, "Design of microstrip quadruplet filters with source-load coupling," *IEEE Transactions on Microwave Theory and Techniques*, vol. 53, no. 7, pp. 2302–2308, 2005.

[70] H. Shaman and J.-S. Hong, "Input and output cross-coupled wideband bandpass filter," *IEEE Transactions on Microwave Theory and Techniques*, vol. 55, no. 12, pp. 2562–2568, 2007.

[71] C.-M. Tsai, S.-Y. Lee, and C.-C. Tsai, "Hairpin filters with tunable transmission zeros," in *2001 IEEE MTT-S International Microwave Sympsoium Digest*, vol. 3, 2001, pp. 2175–2178.

[72] L.-H. Hsieh and K. Chang, "Tunable microstrip bandpass filters with two transmission zeros," *IEEE Transactions on Microwave Theory and Techniques*, vol. 51, no. 2, pp. 520–525, 2003.

[73] J. Rhodes and R. Cameron, "General extracted pole synthesis technique with applications to low-loss TE_{011} mode filters," *IEEE Transactions on Microwave Theory and Techniques*, vol. 28, no. 9, pp. 1018–1028, 1980.

[74] I. Bahl, *Fundamentals of RF and Microwave Transistor Amplifiers*. USA: Wiley-Interscience, 2009.

[75] T. Iida, *Satellite Communications – System and Its Design Technology*. Amsterdam: IOS Press, 2000.

[76] J. Ness, "A unified approach to the design, measurement, and tuning of coupled-resonator filters," *IEEE Transactions on Microwave Theory and Techniques*, vol. 46, no. 4, pp. 343–351, 1998.

[77] Y.-H. Cho, H.-I. Baek, H.-S. Lee, and S.-W. Yun, "A dual-band combline bandpass filter loaded by lumped series resonators," *IEEE Microwave and Wireless Components Letters*, vol. 19, no. 10, pp. 626–628, 2009.

[78] L.-S. Wu, L. Zhou, X.-L. Zhou, and W.-Y. Yin, "Bandpass filter using substrate integrated waveguide cavity loaded with dielectric rod," *IEEE Microwave and Wireless Components Letters*, vol. 19, no. 8, pp. 491–493, 2009.

[79] N. Delmonte, M. Bozzi, L. Perregrini, and C. Tomassoni, "Miniaturization and quality-factor in substrate integrated waveguide cavities," in *2018 IEEE MTT-S International Conference on Numerical Electromagnetic and Multiphysics Modeling and Optimization*, 2018, pp. 1–4.

[80] J. D. Martínez, M. Taroncher, and V. E. Boria, "Capacitively loaded resonator for compact substrate integrated waveguide filters," in *2010 European Microwave Conference*, 2010, pp. 192–195.

[81] J. D. Martinez, S. Sirci, V. E. Boria, and M. A. Sanchez-Soriano, "When compactness meets flexibility: Basic coaxial SIW filter topology for device miniaturization, design flexibility, advanced filtering responses, and implementation of tunable filters," *IEEE Microwave Magazine*, vol. 21, no. 6, pp. 58–78, 2020.

[82] J. D. Martinez, S. Sirci, M. Taroncher, and V. E. Boria, "Compact CPW-fed combline filter in substrate integrated waveguide technology," *IEEE Microwave and Wireless Components Letters*, vol. 22, no. 1, pp. 7–9, 2012.